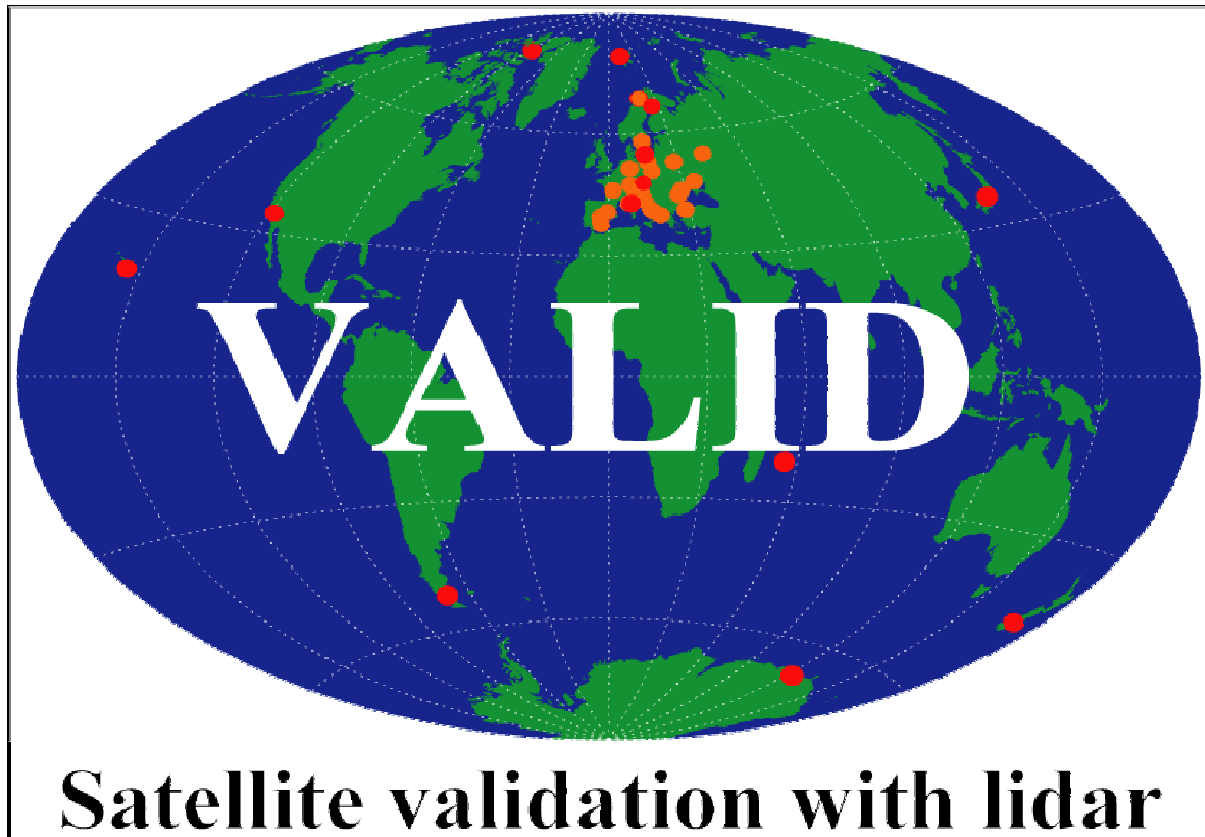


Final Report

2008-2010



Prepared by: Anne van Gijssel (RIVM/KNMI), Lucia Mona (CNR-IMAA),
Gelsomina Pappalardo (CNR-IMAA) and Daan Swart (RIVM)
Reviewed by: Ewa Kwiatkowska (ESA) and Thorsten Fehr (ESA)
Issued on: 11-07-2011
Contract no: 18193/04/NL/AR

Table of Contents

1	Summary.....	4
1.1	Organisation of this document	7
2	Introduction.....	8
2.1	Ozone and temperature profiles	8
2.1.1	DIAL ozone measurement technique and design	9
2.1.2	Rayleigh temperature measurement technique and design.....	9
2.2	Aerosol and cloud lidar data.....	9
2.2.1	EARLINET database	11
3	LIDAR Data.....	14
3.1	Ozone and temperature lidar – status per site	14
4	Data availability and validation approach.....	18
4.1	ENVISAT data availability	18
4.2	Identification of satellite-derived aerosol and cloud products for validation and climatological studies.....	19
4.2.1	CALIPSO	19
4.2.2	MODIS	19
4.2.3	OMI.....	19
4.2.4	MISR.....	20
4.2.5	SYNAER	20
4.3	Validation approach.....	20
4.3.1	Strategies for validation of ozone and temperature profiles derived from satellite measurements	21
4.3.2	Strategies for validation of cloud and aerosol products from satellite measurements	21
4.3.3	Software development	21
5	SCIAMACHY	23
6	MIPAS.....	25
7	GOMOS.....	27
8	ACE FTS.....	33
9	CALIPSO.....	37
10	MODIS	40
11	MISR.....	49
12	OMI.....	51
13	SYNAER	52
14	VALID-related presentations and publications	53
15	Conclusions	53
16	References.....	55
17	Appendix 1: Overview of submission statistics - tables.....	61
18	Appendix 2: EARLINET AOD data	70
19	Appendix 3: Comparison of Multi-TASTE and VALID validation strategies.....	73
20	Appendix 4: Validation of GOMOS high resolution temperature profiles using sonde and lidar measurements.....	77

1 Summary

This is the final report of the VALID-1 project. During its three year-term, lidar profiles of ozone, aerosol and cloud properties and temperature have been gathered, quality-checked and been made available for validation purposes. The high quality lidar measurements have been used to support and perform the quality assessment of ozone and temperature profiles retrieved from ENVISAT data and ACE FTS. This part of the project was coordinated by RIVM and is a direct multi-mission continuation of the EQUAL projects. These activities are to be continued in the VALID-2 project (2011-2012). CNR-IMAA coordinated the comparison of operational cloud and aerosol products from satellites with measurements performed by ground-based lidars in EARLINET. This report therefore contains two main components: (1) validation of stratospheric ozone and stratospheric/mesospheric temperature profiles and (2) comparison satellite-lidar-derived cloud and aerosol properties (focussing on the troposphere).

4883 ozone profiles and 5568 temperature profiles measured in the period 2002 to 2010 have been submitted so far (March 2011).

The operational GOMOS level 2 processor continues to be IPF 5.00 which corresponds to GOPR 6.0. The GOMOS ozone profiles obtained with this version continue to show an excellent agreement with validation data with a bias within 2% between altitudes of 20-40 km. More detailed analyses were published in the special issue in ACP (Keckhut et al., 2010; van Gijssels et al., 2010b).

During the course of the project, various new test algorithms (GOPR 7.0 ab-de) were compared with ground-based observations, together with the same data processed with GOPR 6.0cf (very similar to IPF 5.00). Results with respect to the ground-based measurements are very similar for versions 6 and 7, with the new processor showing improvement in terms of a reduction in the number of outlier profiles.

The comparison of high-resolution temperature product (HRTP) of IPF 5.00 with sonde and lidar profiles shows that a further maturation of the GOMOS retrieval algorithm is needed.

In 2009 we also assisted in the validation of ozone profiles obtained with the GOMOS bright limb processor (version 2.0 (Tukiainen et al., 2010)). Results showed a great improvement in comparison to bright limb measurements processed with the operational processor. Nevertheless, a dependency of the data quality on the solar zenith angle was found. The results were reported to ESA together with the satellite comparisons (GOMOS dark limb operational retrievals, OSIRIS, MIPAS and SCIAMACHY) and NO₂ validation results (Hassinen et al., 2010). A more quantitative analysis using multiple years and a large set of collocations will be carried out in the follow-up project. GOMOS reprocessing with the operational processor version 6 is expected to be completed in the summer of 2011.

MIPAS optimised resolution (OR) had no operational level 2 data processing in the first of years of the project. In that period, we focused our analysis on scientific data produced by Oxford University (MORSE version 1.02). Selected datasets of temperature and ozone from August 2002 to July 2009 were tested. The MORSE data were not corrected for the incorrect altitude determination, leading to a variable shift of the profiles, making the comparison with the validation data complicated.

Mean maximum ozone concentrations appear to be a little overestimated. Some outliers are found at higher altitudes (tropics and polar regions) and at the bottom of the profiles (tropics and mid-latitudes).

Temperature profiles from version 1.02 were compared with sonde and lidar data. A deviation with a peculiar shape is seen around 30 km where we shift from lidar+sonde to comparison with lidar data only, but for most altitudes, data match within one to two Kelvin.

In 2010 MIPAS ORM 1 and 2 (corresponding to IPF version 5.04) ozone and temperature profiles became available. Data were provided with averaging kernels and a corrected altitude grid together with the engineering altitudes. As the averaging kernel for the ozone retrieval is on the corrected altitude grid, we have been able to perform the analysis on this grid. The validation data were convolved by interpolating the averaging kernel to the validation instrument's altitude grid. The convolved data were subsequently checked for unrealistic values. This removed about one third of the data and especially affected the comparison with sonde measurements where the altitude range is limited and thus application of the averaging kernel is not always successful (part of the kernel may have a contribution from altitudes where no sonde data are available).

For ozone, MIPAS showed in both ORM versions 1 and 2 an overestimation below the ozone maximum and at high altitudes (above 60 km) at all latitudes. In between the MIPAS ORM data match the verification instruments quite well (within a few percent), with a somewhat more negative bias towards the poles. The peak seen between 15 and 20 km for the tropics was thought to possibly be related to the presence of sub-visual cirrus.

Compared to the lidar data alone, differences are within a few percent, with an excellent match between 20 to 35 km in the polar region, 25 to 30 km in the mid-latitudes and 25 to 40 km in the tropics. Above the mentioned upper altitudes MIPAS is overestimating the ozone concentrations except in the polar region.

For temperature, the averaging kernel is on the pressure grid and has therefore not been applied. The observed bias in the MIPAS ORM temperature data with respect to the verification instruments is within the -6 K to +2 K extremes and mostly within 1 to 2 K from lidar. No best altitude axis (engineering/corrected) can be identified from the verification results.

Reprocessing of the entire MIPAS catalogue with the level 2 IPF version 5.04 should be completed by February 2011.

In the duration of the project, SCIAMACHY ozone profiles have been compared for various versions (operational processor version 3.01, test versions for 4 and 5) and the scientific algorithm from IUP Bremen (Stratozone 2.0-2.2). For an initial assessment of version 5.01, a partial reprocessing was created. For this dataset, a positive bias (5 to 23%) could be seen in the SCIAMACHY data in the tropics over the altitude range 15 to 40 km. In the polar region, the SCIAMACHY profiles reasonably match the validation instruments, with a variable bias ranging between -10% and +7% in the altitude range 15 to 35 km, with the bias increasing above, with the strength depending on the validation instrument. The best performance is seen in the mid-latitudes, where data are within 5% up to an altitude of 38 km. All observations match those identified in the testing+verification phase, pointing at an adequate data selection. When considering the four profiles retrieved during one state (scan angle dependence), the Eastern profiles often have a more negative bias than the Western profiles.

SCIAMACHY reprocessing with version 5 should be completed by the second half of 2011.

ACE FTS version 2.2 (ozone update) ozone and temperature profiles have also been compared to ground/balloon-based observations. Although the dataset is not very large, very reasonable results were obtained for temperature (bias within -2K to +2K). For ozone, a small positive bias (mostly within 5%) was found, which increases from 30 km to reach a maximum around 52 km for sunrise measurements and from about 40 km reaching a maximum at 50 km for sunset observations after which the bias starts to reduce becoming negative at 60 km for sunrise measurements and at 55 km for sunset measurements. At low altitudes (below 15 km), the sunrise measurements still seem to provide relatively very good profiles (median error within 10% above 6 km) whereas the sunset measurements also give reasonable values (median error within 20% above 6 km) although outlier profiles are found with both modes (leading to a larger mean error). No dependence on the beta angle or hemisphere could be seen.

CNR-IMAA coordinates activities related to the comparison of operational cloud and aerosol products from satellites with measurements performed by ground-based lidars in EARLINET.

The involvement of EARLINET in the VALID activities concerns the analysis and the report of the quality of the aerosol and clouds measurements of ESA's and third-party atmospheric sensors (e.g., CALIPSO, ADM-AEOLUS, EarthCARE).

The main activity of CNR-IMAA during the third year of the project was to enlarge comparison and methodology developed in the previous years to more EARLINET stations and different satellite sensors. A big effort was also paid to the investigation of possible causes of large discrepancies observed between MODIS and Thessaloniki EARLINET data. In particular, a detailed analysis of instrumental modification allowed identifying the uncorrected overlap function as the most suitable reason of those discrepancies (see Appendix 2: EARLINET AOD data). Thessaloniki data were reanalysed after this investigation. Final comparison between MODIS and EARLINET data are included in this report, together with overall network comparisons with MISR, OMI and daily aerosol optical depth as provided by a synergic use of AATSR and SCIAMACHY.

In addition, comparison and correlative study for CALIPSO aerosol and clouds products are performed as well mainly based on another ESA project (ESTEC contract 21487/08/NL/HE). After first promising results obtained on both Level 1 and level 2 data, there was a new release of CALIPSO data in June 2010. The software developed for the systematic EARLINET versus CALIPSO comparison was properly modified in order to take into account new variables, new resolution and extended covered vertical range included in version 3 of the data. An example of comparison between EARLINET and CALIPSO versions 2 and 3 of the data is given.

The comparison with MODIS is significantly improved by identification of an overlap problem in Thessaloniki data. Even though within the errors, MODIS annual averaged AOD is typically slightly higher than AOD measured by EARLINET stations. This is mainly to be due to the large uncertainty in this kind of comparison related to the wavelength scaling between 550 nm (MODIS) and 355 nm (EARLINET). For measurements performed on the same day, count distributions of the differences between MODIS and EARLINET AOD are well fitted by a Gaussian distribution centred at zero for all the stations.

The distribution of MISR vs EARLINET differences is similarly well fitted by a Gaussian distribution centered on 0.08 with a standard deviation of 0.17. A slight underestimation within the errors is observed in MISR data if compared to EARLINET and MODIS data.

An overestimation is found in OMI data of 0.06 with a standard deviation of 0.24 in comparison to seven EARLINET sites. However, an underestimation is seen for comparisons with Athens. For this sensor, the correlation with the Gaussian fitting curve for the probability distribution function is significantly lower than those obtained for MODIS and MISR. This could be the signature of anomalous behaviour of retrieved OMI AOD for specific situations that would need further investigations.

Aerosol Optical depth resulting from the synergistic use of AATSR + SCIAMACHY measurements (SYNAER) underestimates the measured AOD of about 0.15 with a standard deviation of 0.09 (Gaussian fit) in comparison to the three EARLINET sites L'Aquila, Napoli and Potenza. A total of 123 coincident measurements were identified. Thus, it is clear that the database available for the comparison is insufficient for a thorough assessment of the SYNAER aerosol load characterization capability.

1.1 Organisation of this document

Section 3 provides an overview of the available measurements that were submitted to the calibration/validation database NADIR (with tables for each year listed in Appendix 1). Section 4 describes the validation approach and satellite data availability. Sections 5, 6 and 7 the present the validation results for SCIAMACHY, MIPAS and GOMOS respectively, whereas section 8 present the comparison with ACE FTS data, section 9 is dedicated to CALIPSO and section 10 to MODIS, chapter 11 presents the studies with MISR, 12 shows the results for OMI and finally section 13 presents an initial comparison for SYNAER (AATRS+SCIAMACHY) AODs. The conclusions are presented in section 15. Complementary data, figures and methodologies are provided in the four appendices.

2 Introduction

This is the final report of the *Satellite validation with lidar* (VALID) project led by the Dutch National Institute for Public Health and the Environment (RIVM) with a sub-contract to the Italian National Research Council – Institute of Methodologies for Environmental Analysis (CNR-IMAA). The objectives of this project have been to provide the European Space Agency (ESA) with adequate support for the assessment and reporting on the product quality of temperature and ozone profiles retrieved from ENVISAT data in the period 2008-2010 and secondly, to study the possibilities of using EARLINET lidar data for the validation of aerosol and cloud products from satellite-borne sensors.

2.1 Ozone and temperature profiles

In order to fulfil the first objective, temperature and ozone profiles obtained with stratospheric lidars from a total of 13 stations (see Figure 2-1 and Table 3-1) have been collected and made accessible for comparison.

Lidar systems used in the long-term validation of ENVISAT ozone/temperature profiles

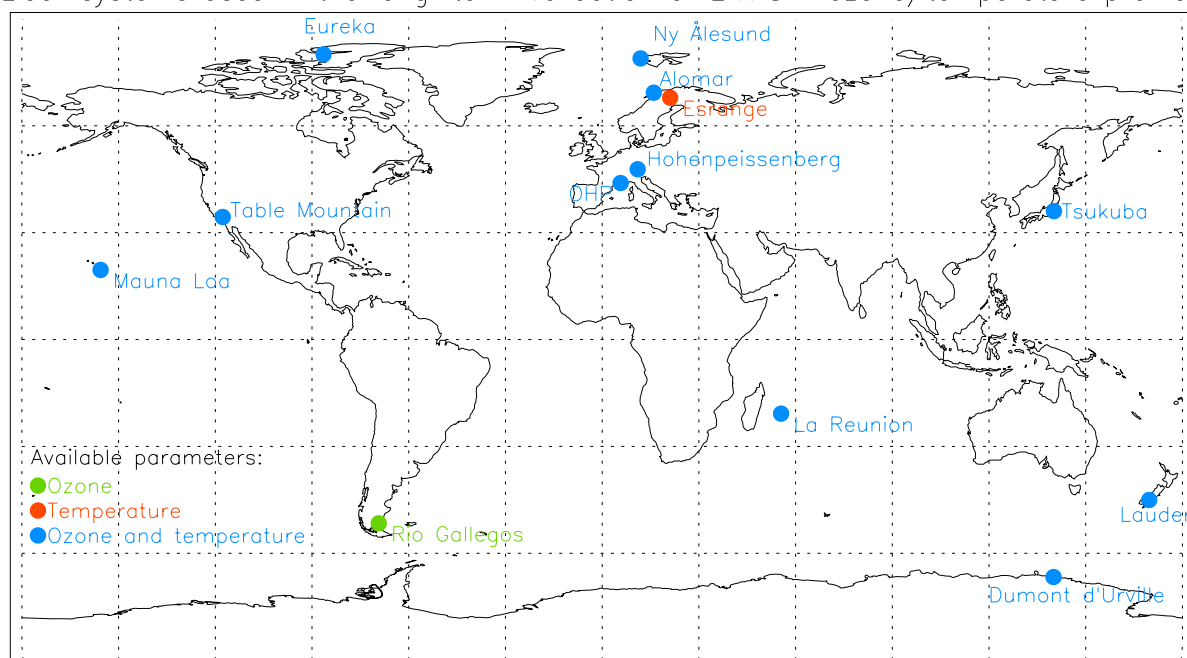


Figure 2-1: Station locations of the lidar instruments used in the VALID project for validation of ozone/temperature profiles.

All lidar sites, except Esrange, are part of the international Network for the Detection of Atmospheric Composition Change (NDACC). NDACC is composed of more than 70 high-quality, remote-sensing research stations for observing and understanding the physical and chemical state of the stratosphere and upper troposphere and for assessing the impact of stratosphere changes on the underlying troposphere and on global climate.

While the NDACC continues monitoring changes in the stratosphere with an emphasis on the long-term evolution of the ozone layer, its priorities have broadened considerably to encompass issues such as the detection of trends in overall atmospheric composition and understanding their impacts on the stratosphere and troposphere, and establishing links between climate change and atmospheric composition.

As part of this network, more than twenty groundbased Lidar (Light Detection And Ranging) instruments deployed worldwide from Pole to Pole are monitoring atmospheric ozone, temperature, aerosols, water vapour, and polar stratospheric clouds. This laser-based active

remote sensing technique has been used widely for several decades in environmental science and chemistry, and has contributed significantly to the validation of space-based measurements.

To ensure quality and consistency of the NDACC lidars operation and products, a number of protocols have been formulated covering such topics as validation, measurements and instruments intercomparisons, and theory and analysis. The members of the NDACC Lidar Working Group (LWG) are committed to follow the principles of these protocols, and the LWG meets every two years to review and coordinate the activities necessary to the valuable contribution of the lidars to NDACC.

2.1.1 DIAL ozone measurement technique and design

The Differential Absorption Lidar (DIAL) technique uses the absorption properties of a given atmospheric constituent to deduce its atmospheric concentration. Laser beams at two different wavelengths are sent into the atmosphere. The wavelengths are chosen so that one of them is sensitively more absorbed (wavelength “ON”) than the other (wavelength “OFF”). The difference in the absorption along the beam path causes the returned lidar signals to yield a different altitude dependence. Knowing from laboratory work the absorption cross-sections of the constituent at both wavelengths, the atmospheric number density of this constituent can be deduced from the ratio of the slope of the logarithm of the signals at the two wavelengths. This technique does not require any calibration. Today, the most common DIAL systems are dedicated to the measurement of ozone, but some systems were also designed for the measurement of water vapour, methane, and carbon dioxide.

The systems in VALID are dedicated to the measurement of stratospheric ozone (10-45 to 50 km). For detection in the stratosphere where ozone is very abundant, typical wavelengths used are 308 nm (“ON”) and 355 nm (“OFF”). The NDACC stratospheric ozone DIAL systems typically have an overall error ranging from 3% near the ozone concentration peak to 10 and 30% in the lowermost and uppermost stratosphere (limited by ozone abundance and/or signal-to-noise ratio).

2.1.2 Rayleigh temperature measurement technique and design

The Rayleigh temperature lidar technique uses the backscattering properties of the air molecules, and the hydrostatic and ideal gas properties of the atmosphere. In the absence of particles such as aerosols and clouds (typically above 30 km), the number of photons collected on the lidar telescope is proportional to the number of backscattering air molecules. After various corrections and normalization to a concurrent pressure or density profile, the lidar number density profile is integrated downward from the top of the profile, allowing, for typical existing Rayleigh lidars, the retrieval of atmospheric temperature between 30 and 80 km. A similar method applied to the lidar signals returned from vibrational Raman scattering by atmospheric Nitrogen (insensitive to particles) allows to extend temperature retrieval below 30 km. Rayleigh/Raman temperature lidar systems typically have a temperature error ranging from less than 0.5 K in the stratosphere to 15 K in the upper mesosphere (limited by signal-to-noise ratio and initialization).

More information can be found on www.ndacc-lidar.org.

2.2 Aerosol and cloud lidar data

Aerosol and cloud lidar profiles have been added to the project in 2008 with the participation of EARLINET to VALID activities. EARLINET (<http://www.earlinet.org/>), the European Aerosol Research Lidar Network, is the first aerosol lidar network, established in 2000, with the main goal to provide a comprehensive, quantitative, and statistically significant data base for the aerosol distribution on a continental scale. In March 2006, the 5-year EC Project EARLINET-ASOS (Advanced Sustainable Observation System) started on the base of the EARLINET infrastructure. The main objective is the improvement of the EARLINET infrastructure,

resulting in a better spatial and temporal coverage of the observations, continuous quality control for the complete observation system, and fast availability of standardised data products.

Currently, EARLINET is a coordinated network of 25 lidar stations (see Figure 2-2), distributed over Europe, using advanced lidar methods for the vertical profiling of aerosols. As reported in Figure 2-2, different capabilities are available at the EARLINET stations. In particular, 7 EARLINET stations are equipped with simple backscatter lidars, 9 are UV elastic/Raman lidar stations and finally 9 are multi-wavelength elastic/Raman lidar stations.

Different equipments lead to different possibilities from an observational point of view. Namely, the simply backscatter lidar technique allows the determination of reliable aerosol backscatter coefficient profiles based on assumption about the extinction to backscatter ratio (the so called lidar ratio) profile (Fernald, 1984; Klett, 1985; di Girolamo et al., 1999).

Elastic/Raman technique instead allows the independent measurement of aerosol extinction and backscatter profiles and in addition allows also to determine the lidar ratio profiles (Ansmann et al., 1992). In particular, the presence, in the detection unit of lidar system, of a receiving channel for the detection at the N_2 Raman shifted signal allows to directly obtain the aerosol (and clouds) extinction profile without significant assumptions (Ansmann et al., 1990). Together with HSRL (High Spectral Resolution Lidar) (Esselborn et al., 2008), Raman lidar technique is currently the only remote sensing technique able to provide vertical resolved measurements of the aerosol extinction coefficient without significant assumptions.

Multi-wavelength lidar allows aerosol extinction and backscatter coefficients to be determined at more than one wavelength through elastic/Raman techniques. This kind of system typically provides aerosol extinction and backscatter coefficient profiles at 355 and 532 nm. An additional detection channel at 1064nm allows obtaining the aerosol backscatter coefficient profile at this wavelength through the elastic lidar technique. In addition, this kind of system is often equipped with receiving channels for the detection of components of backscattered light polarized perpendicular and parallel to the direction of the linearly polarized transmitted laser beam, and therefore allows the linear depolarization ratio profiles measurements, giving information about the orientation of the particles in the atmosphere. Multi-wavelength Raman aerosol lidar techniques have been demonstrated to have the unique ability of providing range-resolved aerosol microphysical properties (Müller et al., 1999; Veselovskii et al., 2002; Ansmann et al., 2005; Böckmann et al., 2005).

Different instruments of the EARLINET network and the different techniques applied in it call for a devoted quality assurance program within the network. Within EARLINET, special care has been taken to assure data quality, both at instrument and algorithm levels. This is a fundamental aspect within a network in order to produce “certified” data that can be considered reliable by the whole network community.

To check the performance and reliability of the individual lidar systems, intercomparison measurements were made comparing the results of two lidar systems located close together and therefore probing nearly the same volume of air (Matthias et al., 2004a). Inter-comparison campaigns devoted to check the performance of the lidar systems are also scheduled in the period 2009 - 2012 with the support of the EC EARLINET-ASOS and the ESA-CEOS projects. To check the algorithms used in the analysis of lidar signals by each group, an algorithm intercomparison has been performed (Böckmann et al., 2004; Pappalardo et al., 2004). Standard routines for quality assurance of lidar instruments and algorithms distributed to all stations ensure that the data products provided by the individual stations are permanently of highest possible quality according to common standards and are thus usable by the research community in a homogenous manner.

EARLINET observations started on May 2000. A specific schedule for measurements plan was established in 2000. All EARLINET stations perform almost simultaneously measurements three times per week: one on Monday around noon, when the boundary layer is usually well developed,

and two night time measurements per week on Monday and Thursday, with low background light, in order to allow performing Raman extinction measurements. These measurements allow one to obtain unbiased data for climatological studies. Only cloud free conditions are considered in order to provide a description of the aerosol content over the stations.

Besides climatological measurements based on the schedule reported above, additional measurements are performed in order to monitor special events such as Saharan dust outbreaks, forest fires, photochemical smog, and volcano eruptions. Finally, a strategy for CALIPSO related correlative measurements has been developed and optimized within EARLINET (Mona et al., 2009; Pappalardo et al., 2010b).

At the present, EARLINET database collected since May 2000 is the most comprehensive collection of high quality data on the aerosol vertical distribution of aerosol extinction and backscatter coefficients. This database is a very powerful tool for the aerosol studies as demonstrated by the large number of high quality publications carried out on the base of single stations data and on the base of EARLINET database (a complete list of EARLINET related publications is available at the EARLINET website: <http://www.earlinet.org/>).

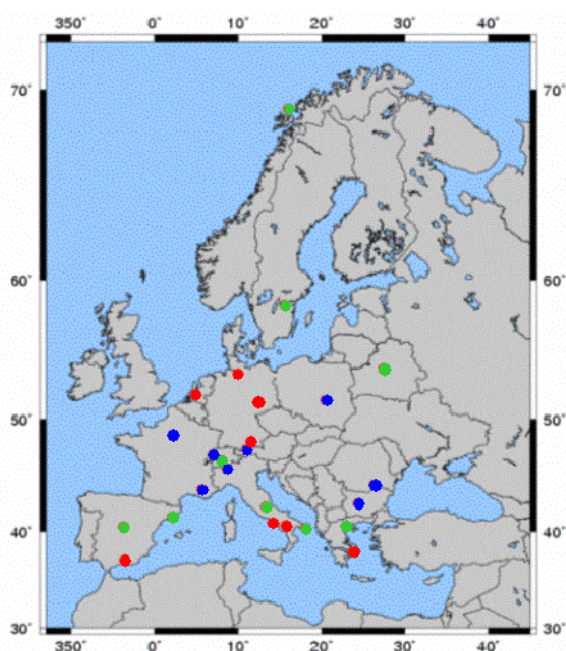


Figure 2-2: Map of Europe with all the EARLINET lidar stations: (red circles) multi-wavelength Raman lidar stations; (blue circles) Raman lidar stations; (green circles) elastic-backscatter lidar stations

2.2.1 EARLINET database

The main products contained in the EARLINET database are the aerosol extinction and backscatter profiles. Together with these quantities, the top altitude of the planetary boundary layer (PBL) + residual layer is provided (Matthias et al., 2004a) and the lidar ratio profile is reported when the aerosol extinction and backscatter profiles are obtained independently. Additional information, as depolarization ratio profiles, is provided when available.

As key parameter for the assessment of the aerosol influence on the radiation budget, the aerosol optical depth is considered in the following. EARLINET database is a vertical profiles database. EARLINET database includes extinction profiles directly measured at Raman lidar stations, without any significant assumptions. Aerosol optical depth (AOD) is not included in there, but it can be simply calculated as integration over the column of extinction profile, as reported in Appendix 2.

Following EARLINET quality assurance (QA) program, two years are needed to completely provide the final EARLINET QA label. This means that at the moment only data until the end

of 2007 are quality assured and therefore open to a public use. In the following studies only quality assured data are used.

Results reported below are obtained using the EARLINET database as it is on November 2009 and using only data until the end of 2007. At that time, EARLINET database consists of more than 22000 aerosol profiles divided into 10 categories:

- Climatological (9224 profiles)
Measurements performed 3 times per week on the base of a fixed time schedule
- Saharan dust (3607)
Measurements performed in correspondence of alerts based on Saharan dust forecasts distributed to all EARLINET stations by the NTUA (National Technical University of Athens) group
- CALIPSO (4993)
Measurements performed following a devoted measurement strategy realized and optimised by the CNR-IMAA group
- Cirrus (994)
Files characterized by the presence of cirrus clouds
- Diurnal cycle (1957)
Coordinated measurements performed in case of stable high pressure conditions in order to study the evolution of diurnal cycle
- Etna (133)
Observations performed during Etna's eruptive periods
- Forest fires (292)
Observations in correspondence of forest fire episodes
- Photosmog (50)
Observation of particular photochemical smog events
- Rural-urban (618)
Measurements performed at a set of relatively nearby stations but with different characteristics (one rural and one urban) during stable atmospheric conditions
- Stratosphere (303)
Measurements vertically extending up to the stratosphere for the stratospheric aerosol layer monitoring.

All available data are considered. EARLINET extinction profiles are available both for regular measurements (twice per week) and for special events observations, in absence of low clouds. In order to improve the temporal coverage of EARLINET data both regular and additional measurements are considered to calculate daily AOD. However, previous studies have shown that the EARLINET scheduling of regular measurements is effective for climatological studies (Mona et al., 2008). On the other hand the inclusion of special event observations in climatological study will obviously bias the results. Therefore, EARLINET AOD values are computed for each day of observation, but only regular measurements are considered for climatological analysis. For coincident measurements comparison instead daily AOD calculated from all available EARLINET data are considered.

In the following only Raman lidar stations are considered because they have the capability to directly measure the extinction profile and therefore the AOD. From Figure 2-2, it is evident that in Central Europe the coverage is very good in terms of aerosol optical depth measurement capability, while only a Raman station is actually operational in Eastern Europe, as a result of the upgrading of the Minsk system from simple backscatter to Raman configuration. Moreover, even if there is a gap in the British Isles, the Cork lidar station (Ireland) is going to join the network.

Starting from the beginning of the network in 2000 until now, a total number of 14 stations have been equipped with at least one Raman channel for aerosol extinction measurements. Table 2-1 reports the list of past and present EARLINET Raman lidar stations considered for this study together with the temporal coverage of aerosol extinction measurements.

Table 2-1. Past and present EARLINET Raman lidar stations considered for this study with the temporal coverage of aerosol extinction measurements.

Site	ID	Altitude a.s.l. (m)	Coordinates	Wavelength (nm)	Temporal coverage
Aberystwith, UK	ab	15	51.86°N, 4.25°W	355	May '00 - Oct. '02
Athens, Greece	at	200	37.96°N, 23.78°E	355	Nov. '00 - Sep. '03 Jan. '05 - Dec. '05
Hamburg, Germany	hh	25	53.57°N, 9.97°E	355	May '00 - Oct. '02
L'Aquila, Italy	la	683	42.38°N, 13.32°E	351	May '01 - Dec. '03 April '06 - Dec. '08
Lecce, Italy	lc	30	40.30°N, 18.10°E	351/355	May '00 - Aug. '02 Feb. '07 - July '08
Leipzig, Germany	le	100	51.35°N, 12.44°E	355 532	May '00 - July '03 June '06 - May '08
Napoli, Italy	na	118	40.84°N, 14.18°E	355 532	Oct. '00 - Aug. '03 Nov. '07 - Sep. '08
Potenza, Italy	po	760	40.60°N, 15.72°E	355 532	May '00 - April '05 May '08 - Nov. '08
Thessaloniki, Greece	th	60	40.63°N, 22.95°E	355	Feb. '01 - June '07

Besides these nine considered stations, the Munich and Madrid stations are also capable of measuring aerosol extinction, but data are not considered here because of the low number of quality assured profiles currently available. In addition, the Bucharest and Minsk stations upgraded their instruments and are providing extinction profiles since 2009. Finally, Kühlungsborn data (May 2000 - October 2002) are not considered here because an extinction retrieval algorithm intercomparison was not performed at that station – which is therefore not yet part of the network.

Taking into account that EARLINET data are finalised after 2 years from the measurements, in the following only data between May 2000 and December 2007 are considered. A strong effort within the network is in progress in order to assure much faster data delivery in the next future.

3 LIDAR Data

For aerosol and cloud properties, data is collected from the EARLINET infrastructure which consists of 25 stations (Figure 2-2). The EARLINET infrastructure represents a unique tool in the VALID activity for the validation of aerosol and cloud optical properties retrieved from satellites.

Thirteen lidar stations in the VALID network are collecting ozone and/or temperature profiles (see Figure 2-1 and Table 3-1). The statistics of the lidar data that have been measured, processed, converted (to HDF) and submitted to the ENVISAT Cal/Val database (maintained by NILU) are shown in Figure 3-1 for the ozone profiles and in Figure 3-2 for the temperature profiles. Each figure presents per month the number of days with lidar measurements. Note that multiple profiles per day are counted as one in this representation. The first set of panels regard the ozone measurements, while the second part concerns the temperature measurements. In each panel title we have indicated with an acronym the station location (see Table 3-1) and the system name which corresponds to the filename in the NILU database (e.g., files with NILU001 in their name contain ozone profile information and NILU002 temperature profile information, and both for the Alomar research facility, Norway).

Table 3-1: Overview of ozone/temperature LIDAR systems: acronyms, locations and parameters					
Ground station	Acro	Lat.	Long.	Parameter	System name
Eureka	EUR	80.05	-86.42	Ozone, temperature	CARE.STB.EC001, CARE.STB.EC002
Ny Ålesund	NYA	78.92	11.93	Ozone*, temperature	AWI001, AWI002
Alomar	ALO	69.30	16.00	Ozone, temperature	NILU001, NILU002
Esrang	ESR	67.88	21.10	Temperature	UBONN003, MISU001
Hohenpeissenberg	HOH	47.80	11.02	Ozone, temperature	DWD001, DWD002
Observatoire Haute Provence	OHP	43.94	5.71	Ozone, temperature	CNRS.SA001, RMR_CNRS.SA001
Tsukuba	TSU	36.05	140.13	Ozone, temperature	NIES001, NIES002
Table Mountain	TMF	34.40	-117.70	Ozone, temperature	NASA.JPL003, NASA.JPL004
Mauna Loa	MLO	19.54	-155.58	Ozone, temperature	NASA.JPL001, NASA.JPL002
La Reunion	LAR	-20.80	55.50	Ozone, temperature	LPA001, LPA002
Lauder	LAU	-45.04	169.68	Ozone, temperature	RIVM002, RIVM003 [#]
Rio Gallegos	RGA	-51.6	-69.3	Ozone	CEILAP001
Dumont d'Urville	DDU	-66.67	140.01	Ozone, temperature	CNRS.SA007 [#] , RMR_CNRS.SA002

* Contrarily to the EQUAL project, in VALID only temperature data are available.
[#] Algorithm is under development and data are not yet available, see also section 3.1 below

3.1 Ozone and temperature lidar – status per site

The section below discusses the data processing and physical status of each ozone/temperature lidar.

At the end of the 2009 Polar Sunrise campaign in **Eureka**, the laser stopped functioning due to a student messing with the system. By the end of 2010 it was still not clear when the lidar will become operational again.

Measurements are very limited for the **Ny Ålesund** site.

The **Alomar** system is in a good condition, but personnel and funding are very limited and a halt to the measurements may come half-way 2011.

Measurements performed with **Esrangle** lidar are on-going.

The lidar at **Hohenpeissenberg** is in a good condition.

The **Observatoire Haute Provence** ozone lidar performs well, the temperature lidar has a severe problem with the electronics chain since September 2010.

The post-doc performing the measurements at **Tsukuba** has informed us that his project may end in March 2011. Communication remains difficult.

The lidar at **Table Mountain** is performing well again after some problems in the beginning of 2010 with the 308 nm channel.

The system at **Mauna Loa** is in a good condition.

The stratospheric ozone lidar at **La Reunion** is still not operational. The temperature lidar is operational, but few measurements were taken in 2010. Data are undergoing validation.

The **Lauder** system is performing well. An intercomparison campaign with the NDACC travelling standard is scheduled for end of April to beginning of May 2011. Retrieved temperatures will be validated and if results are good, data will be submitted covering the period since the beginning of the Envisat mission (although data will be available from April 1995 onwards).

The lidar at **Rio Gallegos** is in a good condition.

The ozone lidar in **Dumont d'Urville** is operational since 2008. Data has been reprocessed again in 2010.

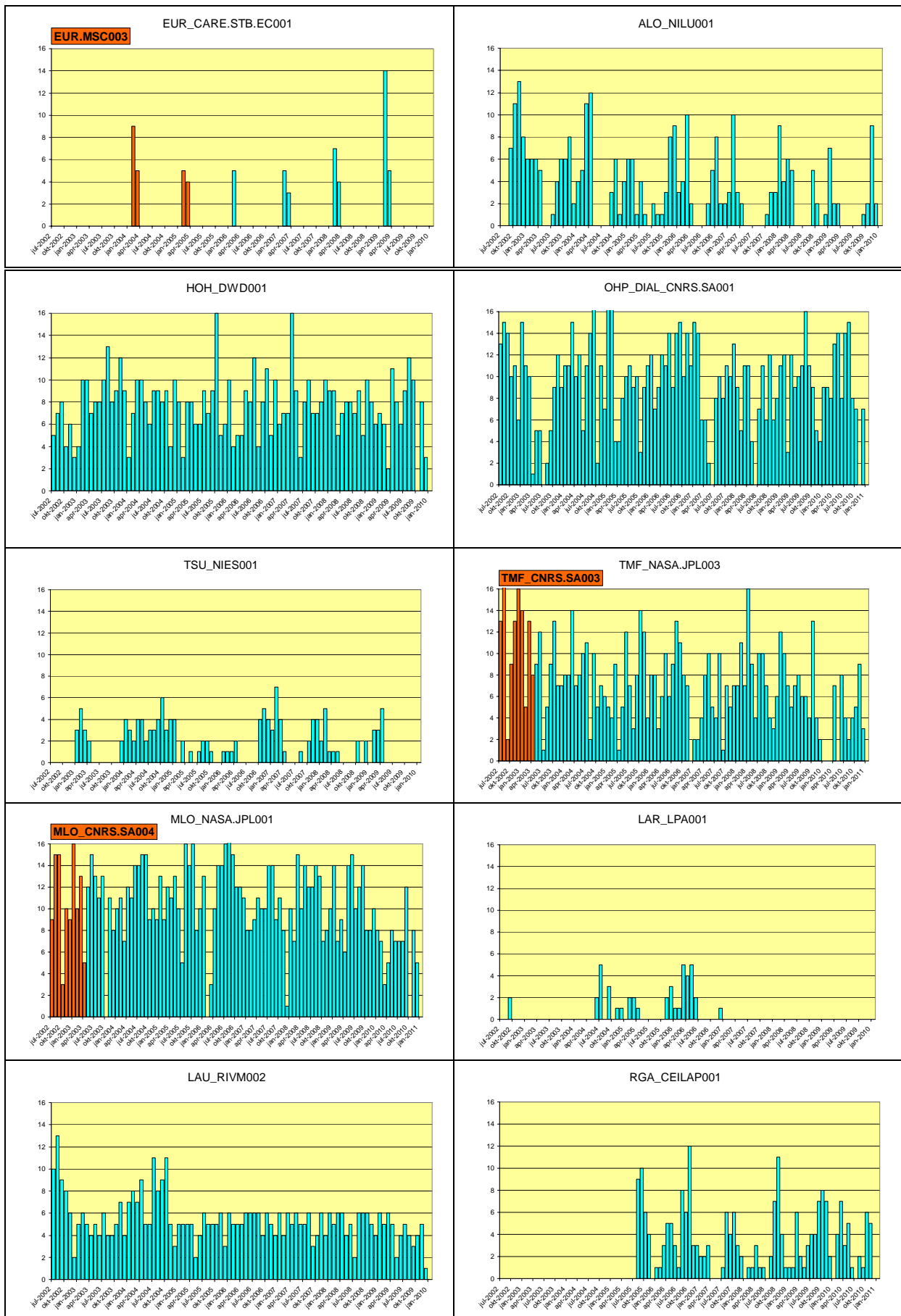
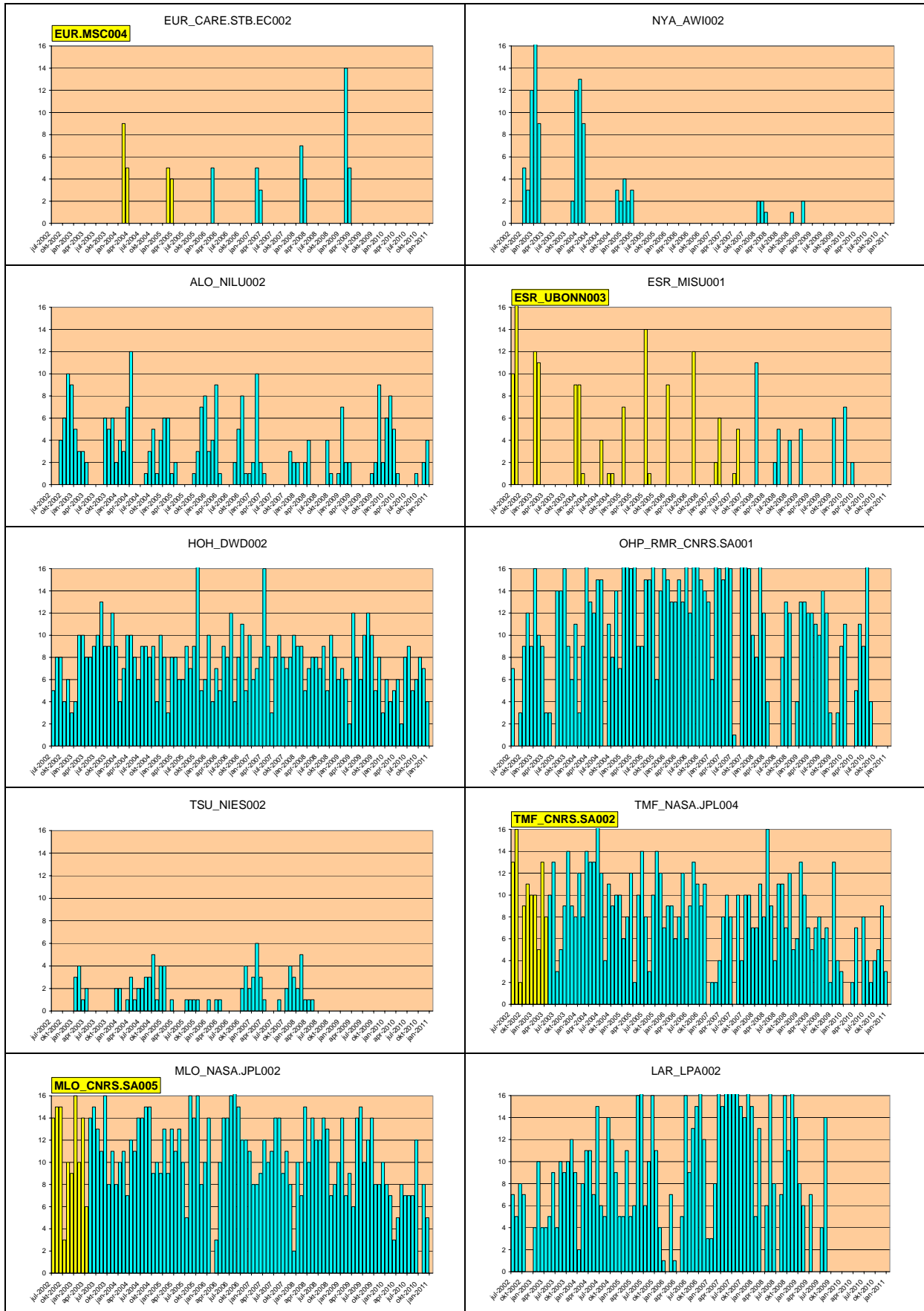


Figure 3-1. Statistics of available OZONE lidar data in the NILU database. Numbers indicate the number of days per month with lidar measurements. Note that the maximum range for the numbers is fixed to 16 and larger numbers are not displayed (see Tables 15-1 to 15-7).



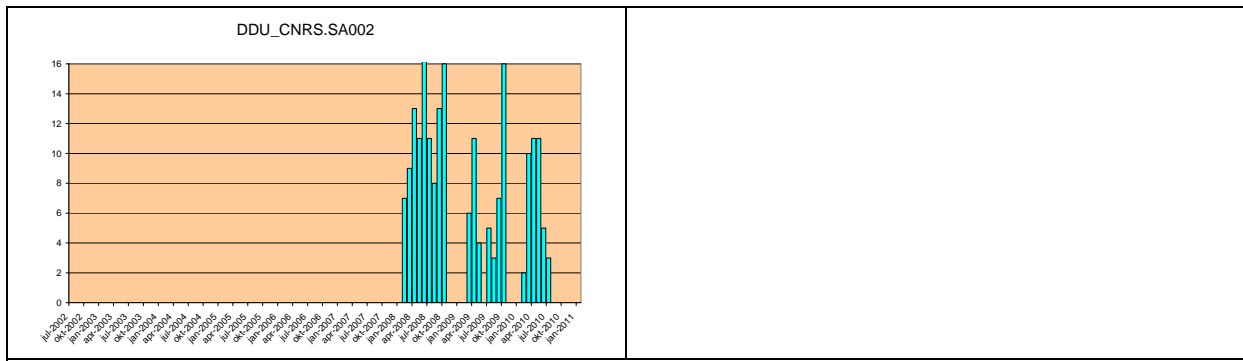


Figure 3-2: Statistics of available TEMPERATURE lidar data in the calibration/validation database. Numbers indicate the number of days per month with lidar measurements. Note that the maximum range for the numbers is fixed to 16 and larger numbers are not displayed (see Tables 15-1 to 15-7 in Appendix 1 for these values).

4 Data availability and validation approach

4.1 ENVISAT data availability

In this section we give an overview of the available ENVISAT data (level 2) for the VALID project (see Table 4-1 and Table 4-2). Note that data might have been (temporarily) available but not acquired within the VALID project. These tables serve as a rough indication and they are not a precise representation of actual data availability.

Legend: ■ = potential data, ■ = available data, ■ = available data for part of the year

Table 4-1: Available ENVISAT Data from IPF Processor

Instrument	20YY									
	2	3	4	5	6	7	8	9	10	
GOMOS	■	■	■	■	■	■	■	■	■	■
MIPAS	■	■	■	■	■	■	■	■	■	■
SCIAMACHY	■	■	■	■	■	■	■	■	■	■

Table 4-2: Available ENVISAT Data from Scientific Institutes

Instrument	20YY									
	2	3	4	5	6	7	8	9	10	
GOMOS *	■	■	■	■	■	■	■	■	■	■
MIPAS	■	■	■	■	■	■	■	■	■	■
SCIAMACHY	■	■	■	■	■	■	■	■	■	■

* This dataset is produced only from GOMOS bright limb profiles

4.2 Identification of satellite-derived aerosol and cloud products for validation and climatological studies

In the previous years of this project, we have identified currently operative satellites that provide measurements of physical quantities, such as the aerosol optical depth, that are directly comparable with Raman lidar measurements. Four satellite instruments were identified as having aerosol products suitable for the comparison with lidar measurements: MODIS, OMI, MISR and CALIPSO. In 2010 a further satellite product was added taking advantage from the synergistic use of AATSR and SCIAMACHY aerosol data: namely the SYNAER/ENV aerosol optical depth. In this chapter a short synthesis of MODIS, OMI, MISR and CALIPSO data used is given. Details about these instruments and aerosol and clouds products are reported in the VALID 2008 and 2009 annual reports. More details are reported here for SYNAER/ENV, because it was not included in the previous annual reports.

4.2.1 CALIPSO

Started on April 2006, the CALIPSO (Cloud-Aerosol Lidar and Infrared Pathfinder Satellite Observations) mission provides for the first time the opportunity to address the 4-dimensional distribution of aerosols and clouds on a global scale. CALIOP (Cloud-Aerosol Lidar with Orthogonal Polarization), the lidar on board CALIPSO, is an elastic backscatter lidar that provides vertical profiles of aerosol and cloud backscatter coefficients at 532 nm and 1064 nm and depolarization ratio profiles at 532 nm. Since June 2006, the first satellite-borne lidar specifically designed for aerosol and cloud study, CALIOP has been providing near-continuous global data set of aerosols and clouds high-resolution vertical profiles (Winker et al., 2007).

4.2.2 MODIS

The MODerate Resolution Imaging Spectroradiometer (MODIS) is a major instrument on the Earth Observing System TERRA (EOS-AM1) and AQUA (EOS-PM1) missions (King et al., 1995). MODIS observes nearly the entire Earth every two days and provides key observations important to studies of the atmosphere, oceans, and land surfaces (Barnes et al., 1998).

Over land, aerosol optical depth is retrieved using the so-called second type method based on the variation in the measured contrast between pixels of the image (King et al., 1992). For comparison with Raman lidar measurements, MODIS aerosol optical depth measured in the blue wavelength region is considered. In particular, daily time series of aerosol optical depth at 550 nm of the collection 5 with a resolution of $1^\circ \times 1^\circ$ data are considered.

4.2.3 OMI

The Ozone Monitoring Instrument (OMI) instrument is a nadir viewing imaging spectrograph onboard the EOS-Aura satellite that measures the solar radiation backscattered by the Earth's atmosphere and surface over the entire wavelength range from 270 to 500 nm.

Aerosol absorption optical depth (AAOD), and the aerosol optical depth (AOD) are obtained with OMAERUV algorithm. The optical depth values at 388 nm are inverted from radiance observations while the 354 and 500 nm results are calculated on the base of aerosol models by conversion of the 388 nm retrievals (National aeronautics and space administration (NASA), 2007). So the reported values at wavelengths other than 388 nm, particularly those at 500 nm, should be considered less reliable (National aeronautics and space administration (NASA), 2007). The OMAERO AOD product is highly promising because it is based on the so-called multi-wavelength aerosol retrieval algorithm. The multi-wavelength algorithm is based on the spectral information in the near UV and the visible between 342.5 nm and 483.5 nm. Including the near UV wavelength range enhances the capability of the retrieval to distinguish between weakly absorbing and strongly absorbing aerosol types. OMAERO is a standard product released in November 2007. First validation studies performed on this product shown that for land scenes, correlation coefficients lower than 0.8 are observed between OMAERO and MODIS AOD.

Strongly site-dependent correlations are reported for comparisons of the AOD from the OMAERO product with ground-based data from various AERONET stations in Europe. The main cause of this relative low correlation coefficient lies in the assumption about the surface albedo (Veihelmann et al., 2009).

Because of the highly promising capability of the multi-wavelength aerosol retrieval algorithm, the OMAERO AOD has been selected for a first OMI validation study to be performed with EARLINET data. In the results reported here, time series of OMAERO aerosol optical depths at 388 nm averaged on a $1^\circ \times 1^\circ$ area are considered.

4.2.4 MISR

The Multi-angle Imaging SpectroRadiometer (MISR) instrument measures upwelling short-wave radiance from Earth in four spectral bands centered at 446, 558, 672, and 866 nm, at nine view angles spread out in the forward and backward directions along the flight path, providing a global coverage about once per week. Its imagery is carefully calibrated to provide accurate measures of the brightness, contrast, and color of reflected sunlight.

The MISR standard aerosol retrieval algorithm retrieves aerosol optical thickness in the operational mode with a horizontal resolution of 17.6 km which allows the determination of aerosol optical depth on a regional basis using an analysis of the view angle variation of contrast, by means of a principal component analysis and using a data base of top-of-atmosphere radiances simulated for the MISR channels, and assumptions on possible aerosol mixtures (Martonchik et al., 1998; Diner et al., 1999; Martonchik et al., 2002).

4.2.5 SYNAER

Daily aerosol parameters (particle mass concentrations, optical depth and type) on a 60×30 km² resolution are retrieved with the new method SYNAER [SYNergetic Aerosol Retrieval] (Holzer-Popp et al., 2000; Holzer-Popp et al., 2002b; Holzer-Popp et al., 2002a) from a synergetic exploitation of two sensors onboard ENVISAT, the spectrometer SCIAMACHY and the radiometer AATSR. The high spectral resolution of SCIAMACHY ideally supplements the high spatial resolution of AATSR. In this method cloud detection is first performed for all 1 km AATSR pixels.

Boundary layer aerosol optical depth (BLAOT) values at 670 nm (over land) and 870 nm (over ocean) are derived for dark AATSR nadir pixels for which the surface albedo can be estimated with good accuracy. BLAOT values over the irregularly distributed dark fields are interpolated to all cloud free AATSR pixels with a distance weighting scheme. The AATSR derived parameters are co-registered to SCIAMACHY pixels and interpolated spatially.

BLAOT and surface albedo calculation is repeated for 40 different aerosol mixtures which are defined by external mixing of five basic aerosol components from an extended OPAC database (Hess et al., 1998). Using the AATSR calculated values of optical depth and surface albedo, SCIAMACHY surface and consecutively top-of-the-atmosphere spectra for the same set of different mixtures are simulated at 10 selected wavelengths. The measured SCIAMACHY spectra are corrected for cloud and ozone influences as well as radiometric errors. A least square fit of the simulated to the measured SCIAMACHY spectrum selects the most plausible type of aerosol and its corresponding BLAOT value at the reference wavelength of 550 nm in a SCIAMACHY pixel. Finally, a quality control and an ambiguity test are applied by comparing the fit error with deviations between different mixtures. This method was further improved in version 2 and evaluated against AERONET data of 2003 and 2005 (Holzer-Popp et al., 2008). The currently most recent version (2.2) was applied to the complete ENVISAT dataset from 2003 and consists of the final optimization of the aerosol type selection algorithm.

4.3 Validation approach

4.3.1 Strategies for validation of ozone and temperature profiles derived from satellite measurements

The validation approach used in this project has been outlined in 'EQUAL Annual Report 2004' (Meijer et al., 2005a), which as a final result provides comparisons of ground- or balloon-based measurements with profiles retrieved by satellite instruments. This comparison comprises lists of collocations with pointers to the measurements and a range of comparison images grouped on specific measurement conditions (for instance star magnitude). The validation approach and target level-2 data quality have also been described in Meijer et al. (2004; 2005b).

Data screening criteria applied in this validation approach have been compared to the screening criteria used in another atmospheric chemistry validation project, Multi-TASTE. Preliminary results and conclusions from these comparisons are given in Appendix 3: Comparison of Multi-TASTE and VALID validation strategies. The effort is driven by the need to harmonize, where possible, and to formulate the protocols used in the validation of atmospheric chemistry satellite measurements.

Note that when different data sources (e.g. sonde plus lidar) have been used, occasionally shifts at the end of the altitude ranges (e.g. top of sonde data at 30 km) can be seen. These do not necessarily indicate a problem with the consistency between the different sources or with the satellite product as they can be an effect of the sampling (spatially or temporally). It is not always possible to separate the potential influences.

4.3.2 Strategies for validation of cloud and aerosol products from satellite measurements

As stated before, one of the reasons for the great uncertainty on the role that aerosol and clouds play on climate is their high variability in time and space (Forster et al., 2007). Studies involving the monitoring of aerosol load during long periods of time can help understand their natural seasonal variability and their variations in the presence of special large scale events (volcanic eruptions, large forest fires etc.). The study of the variation of the aerosol optical depth both from satellite and from a ground based instrument, like the Raman lidar, can help define the spatial scale of this variability.

Based on the amount of Raman lidar data available and on the kind of satellite products available, we identified two types of strategies for performing satellite validation:

- One strategy is to compare quantities in a climatological or statistical sense, which means to perform comparisons on a dataset that spans years of measurements. This kind of validation does not require strictly collocated measurements and allows studying the average correlation between satellite and ground based measurements. This is the strategy that can be used for studying the aerosol optical depth measurements from satellites like MODIS and OMI, for example.
- The other strategy is a point to point validation and requires correlative measurements with the lidar to the overpass of the satellite. This strategy allows a more detailed comparison of the satellite measurements and is the strategy used within EARLINET for the validation of CALIPSO. In particular in the case of CALIPSO the validation allows to compare vertically resolved features within a single profile, for which the time and space correlation is a key requirement.

4.3.3 Software development

The validation software has been extended in 2010 to deal with ACE FTS observations, add an optional smoothing to the validation data and to apply the new averaging kernels provided with the MIPAS data.

Devoted EARLINET measurements are planned for CALIPSO correlative studies starting from high resolution ground-track provided to EARLINET by NASA. The strategy for the correlative measurements has been optimized and realized within the ESA-CALIPSO project (ESTEC contract 21487/08/NL/HE). Within the same project the validation software has been realized. In 2010, the software for validation purposes has been updated in order to make comparisons with the latest release of CALIPSO data. In particular, in the new version of the data, the whole aerosol optical profiles (backscatter and extinction) are available (instead of pieces of profiles related to aerosol layers identified in the previous release). The developed software allows for the comparison on the whole profile and for taking the most of the new resolution available for aerosol profile, that is the same spatial resolution as the aerosol layer products.

As a consequence of the change of host institute for the follow-up of this project and limited possibilities for optimising the working group environment, it was decided to discontinue the website development at RIVM and use the experiences and recommendations gathered by this project for the creation of a new validation portal at KNMI.

In the following sections we will present the validation results.

5 SCIAMACHY

An initial assessment of the SCIAMACHY version 5.01 ozone data was carried out. The ozone profiles were compared with ozone sondes, microwave radiometer and lidar data available with a maximum difference of 20 hours and 800 km. New in this SCIAMACHY processor version is the production of a cloud flag. A peculiarity was identified that not for all profiles a corresponding flag would be available. The available flags had to be linked to the profiles using the data set start (dsr_time) values. The QWG will investigate why there is a different number of cloud flags.

The patterns seen in the verification exercises during the algorithm development are similar, indicating a well chosen dataset for this exercise. A positive bias (5 to 23%) can be seen in the SCIAMACHY data in the tropics over the altitude range 15 to 40 km. In the polar region, the SCIAMACHY profiles reasonably match the validation instruments, with a variable bias ranging between -10% and +7% in the altitude range 15 to 35 km, with the bias increasing above, with the strength depending on the validation instrument. The best performance is seen in the mid-latitudes, where data are within 5% up to an altitude of 38 km (Figure 5-1).

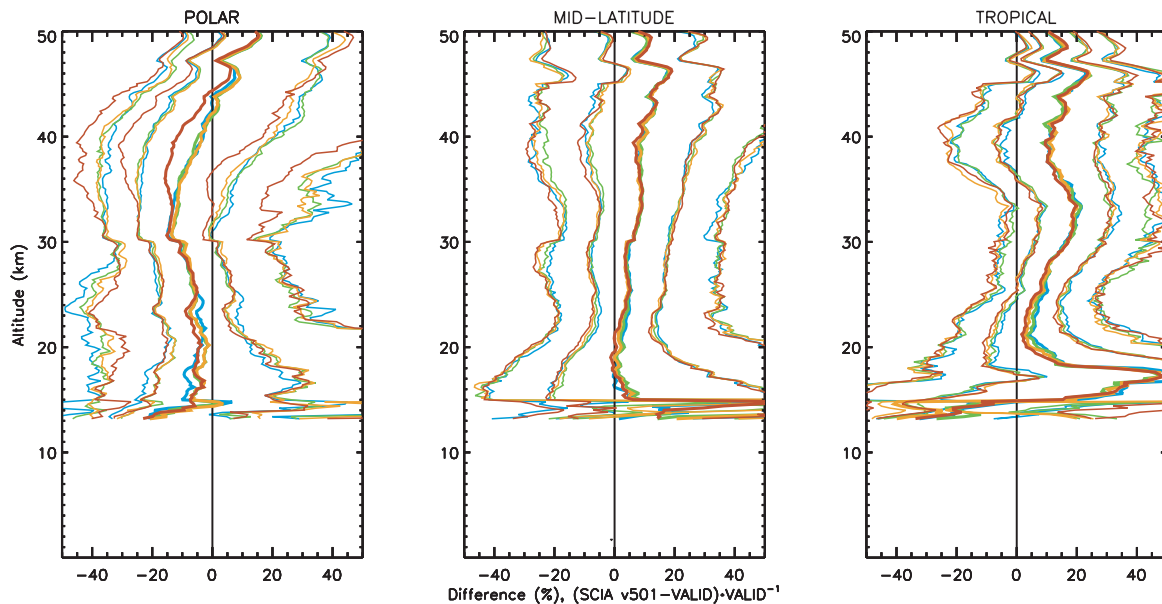


Figure 5-1. Validation results for SCIAMACHY version 5.01 split by latitude as a function of altitude. Left panel: polar regions; middle panels: mid latitudes; right panel: tropics. Colour indicates the state position; red=East, orange=central East; green=central West; blue=West. The thick lines correspond to the median differences, the other lines correspond to the percentile differences as follows: 2.5%, 16% 64% and 97.5%.

Often, cloud free data appear to have a more positive bias (a few percent) compared to the cases disregarding the cloud flags. This is the case especially in the tropics, whereas in the polar region, the bias is slightly more negative for the cloud free data (Figure 5-2).

Finally, when considering the four profiles retrieved during one state, the Eastern profiles overall have a more negative bias than the Western profiles (Figure 5-1). This scan angle dependence is also seen by other groups in other data (SCIAVALIG, Living planet symposium, SCIAMACHY QWG).

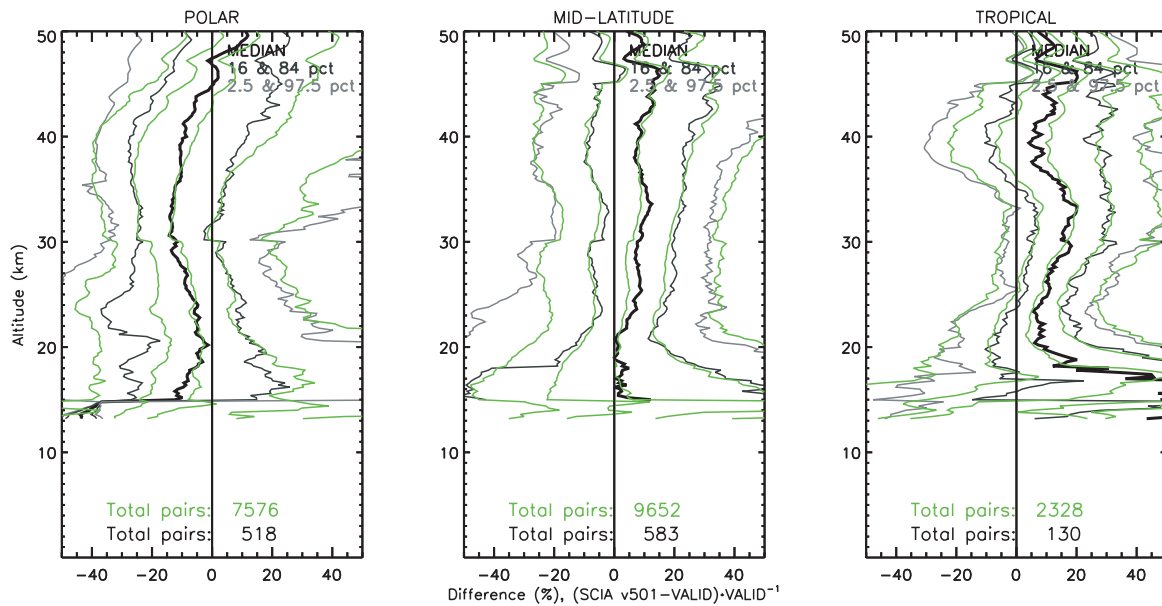


Figure 5-2. Same as Figure 5-1 except that colours indicate cloud flag: green=non-cloud free data; black/blue = cloud free data. The total number of pairs for each case is listed at the bottom of the panels (most data are available with a flag indicating an unknown retrieval or the presence of some type of cloud).

6 MIPAS

In 2010 two prototype tests for IPF version 5.04 became available: ORM 1 and ORM 2. For ozone, these profiles were matched up with lidar, sonde and microwave radiometer data acquired within 800 km and 20 hours (5 hours above 50 km). About 10000 collocating pairs were found for the two versions (somewhat more for ORM 2). MIPAS averaging kernels have been applied for the ozone profile comparison; subsequent filtering on convoluted data to remove outlier values $[0, 10^{19} \text{ molec/m}^3]$ originating from a too short available altitude interval. All data are compared on the corrected altitude axis as no pressure is retrieved by the lidars and the altitudes of the averaging kernel correspond to the corrected altitude grid data. MIPAS data at altitudes with a flag indicating a bad retrieval are not considered.

For temperature, data was restricted to 5 hours and 300 km. Averaging kernels were not applied as these are on the pressure grid. This did allow us to test for dependencies on the two altitude grids (corrected and engineering). Over 2000 collocating pairs were available for these studies.

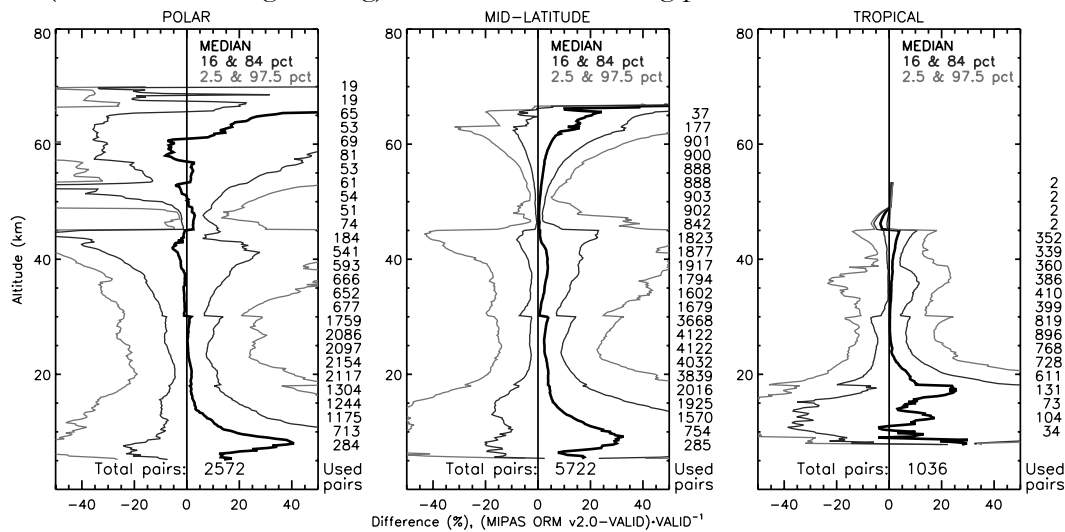


Figure 6-1. Verification results for the MIPAS ORM v2 ozone profiles for three latitude groups: polar regions (left), mid-latitudes (middle) and tropics (right). Shown are the percentiles as before of the percent differences with respect to the verification instruments (MIPAS ORM v2-verification)/verification

For ozone, MIPAS showed in both versions an overestimation below the ozone maximum and at high altitudes (above 60 km) at all latitudes. In between the MIPAS ORM data match the verification instruments quite well, with a somewhat more negative bias towards the poles. The peak seen between 15 and 20 km for the tropics (Figure 6-1) was thought to possibly be related to the presence of sub-visual cirrus.

Compared to the lidar data alone, differences are within a few percent, with an excellent match between 20 to 35 km in the polar region, 25 to 30 km in the mid-latitudes and 25 to 40 km in the tropics. Above the mentioned upper altitudes MIPAS is overestimating the ozone concentrations except in the polar region.

These results appear to be quite consistent with those obtained for the reprocessed data for the period 2005-2010 with IPF 5.04 (Figure 6-2). The polar region is showing a change of sign at higher altitudes, but also displays a very large distribution of values (2.5 and 97.5 percentiles off the plot). Other patterns are very similar.

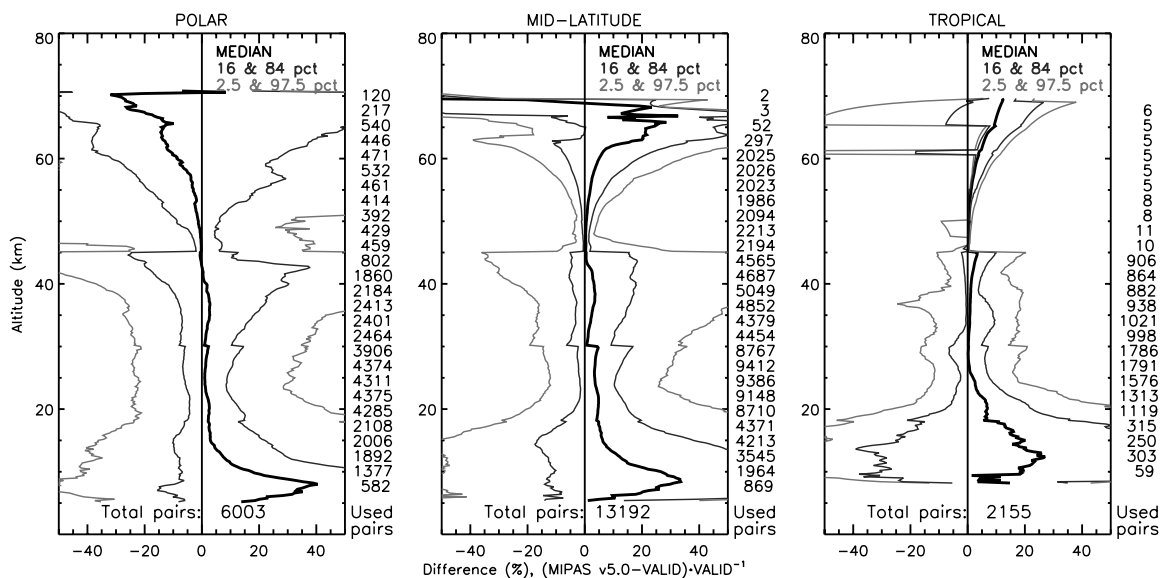


Figure 6-2. First validation results for MIPAS v5.04, covering the years since 2005 (optimised resolution acquisition mode) as for Figure 6-1. Note that sonde data have been smoothed here to a resolution of 3 km.

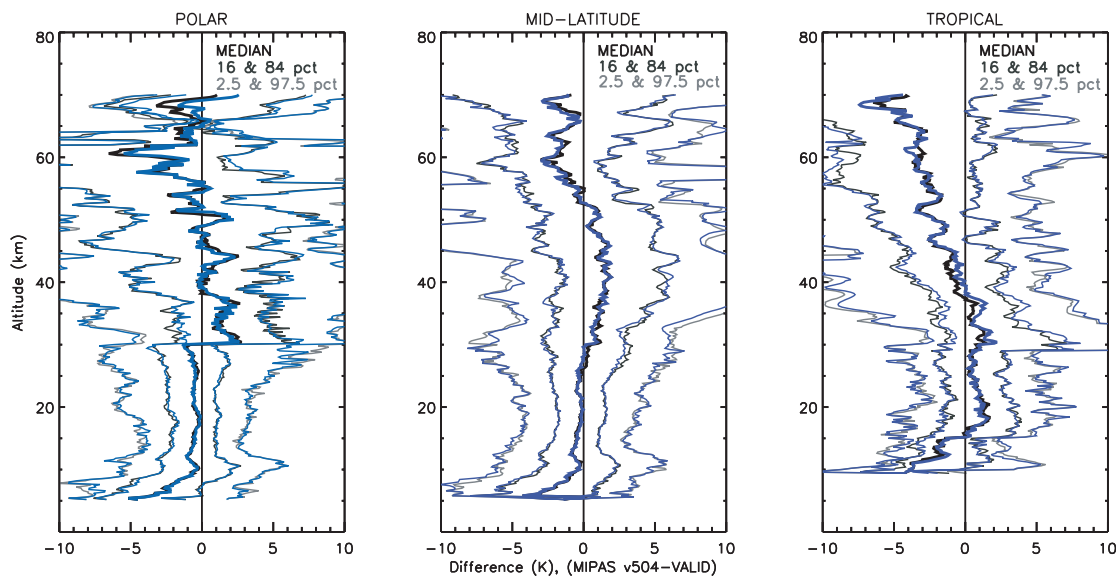


Figure 6-3. Verification results for MIPAS ORM v1 temperature based on the engineering altitudes (black) and corrected altitudes (blue) for the three latitude regions; from left to right: polar, mid-latitudes and tropics. Shown are the differences (percentiles corresponding to the median and the mean plus minus 1 and 2 sigma for a normal distribution) with respect to the verification data (lidar and sonde) as a function of altitude. The number of cases is not shown as they differ between altitude groups, although they are similar. Note that the subscript of the middle panel erroneously states MIPAS v504 (this is ORM 1).

The observed bias in the MIPAS ORM temperature data with respect to the verification instruments is within the -6 K to +2 K extremes and mostly within 1 to 2 K from lidar. No best altitude axis (engineering/corrected) can be identified from the verification results. Although the numbers of pairs used in the comparison are not equal, no obvious differences are found between the two ORM versions. An altitude shift seems to exist in comparison to the lidar data, but this is not visible in the comparison with the sonde data. With the full dataset becoming available after completion of the reprocessing in the beginning of 2011, a more detailed study can be devoted to the origins of these differences.

7 GOMOS

GOMOS ozone profiles (IPF 5.00) have shown an excellent agreement with lidar data with a bias within 5% between altitudes of 15–45 km. A large part of our activities focussed on the validation of GOMOS ozone profiles in preparation of two manuscripts for the special issue dedicated to GOMOS observations in Atmospheric Chemistry and Physics (Keckhut et al., 2010; van Gijssels et al., 2010b).

Ozone profiles from the GOMOS prototype processor (GOPR) versions 6.0cf and 7.0de have been compared with ground-based measurements within 800 km and 20 hours (5 hours above 50 km). Several data filters were tested:

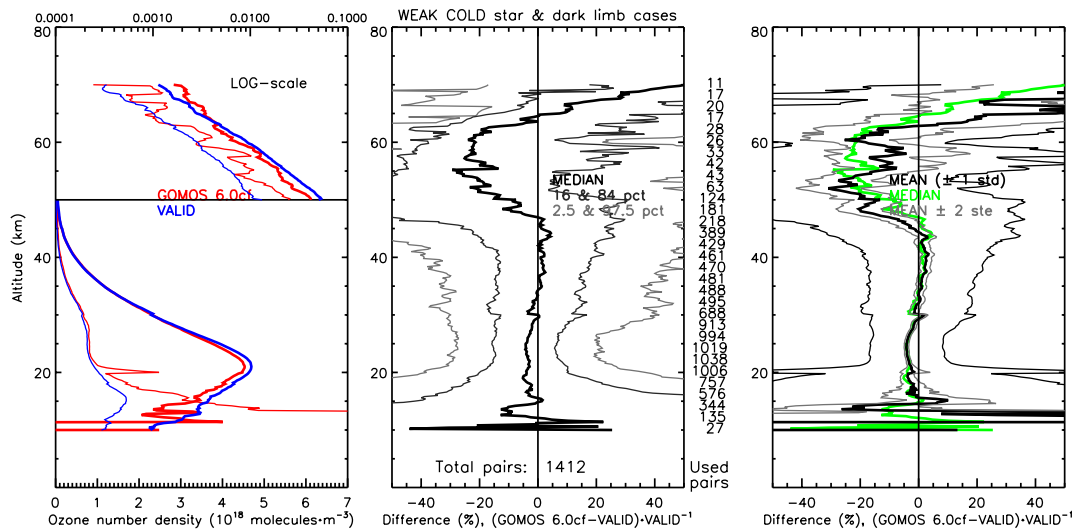
- maximum error of 30% or 100%.

in combination with

- all ozone values allowed (including extreme and also negative values)
- values limited to positive values below 10^{19} molecules/m³. Only the parts of the profile outside this range are removed (not the full profile will be rejected).

Data are in most cases limited to those having a solar zenith angle $> 107^\circ$, which we refer to as ‘dark’ measurements. These measurements may have an illumination flag that is not equal to 0 (so, indicating possible twilight and/or straylight contamination). In all cases, the processing flag has been considered, i.e. the ozone retrieval flag should be equal to 0.

When matched against microwave radiometer data, the GOMOS data have been smoothed to a resolution of 10 km. Balloon borne measurements on the other hand are smoothed using a running mean to a resolution of 2 km to match the GOMOS resolution.



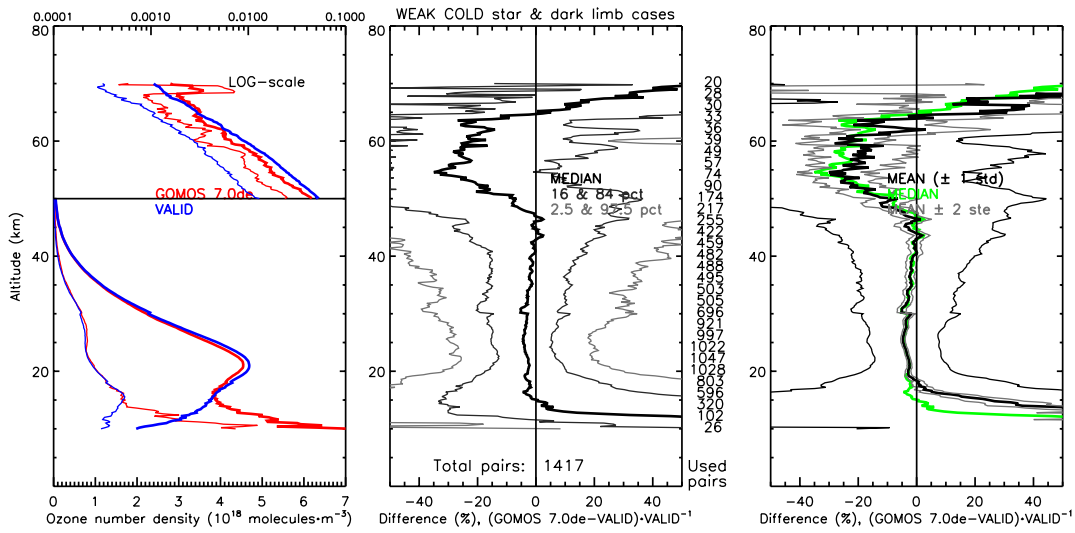
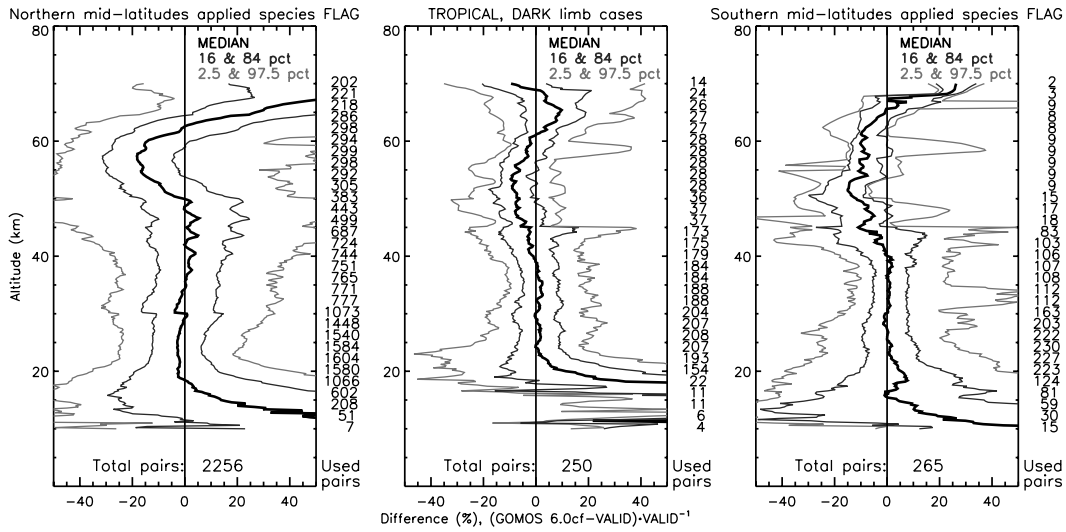


Figure 7-1. Retrievals using weak, cold stars compared to validation data for version 6.0cf (top) and 7.0de (bottom). Both cases are filtered to have a maximum error of 30%, but no restrictions are placed on the allowed ozone range. Left panels show the mean ozone number density as a function of altitude as thick lines for GOMOS in red and VALID in blue with the corresponding standard deviations as thin lines in the same colours. The middle panels show the 2.5, 16, 50 (=median), 86 and 97.5 percentile differences with respect to the validation data. On the right side the number of collocating pairs is given for the corresponding altitudes and the total number of available, usable pairs is given at the bottom of the plots. The right panels show the median difference as a green line (equal to the thick black line of the middle panels) together with the mean (thick black line) plus/minus 1 standard deviation (thin black lines) and 2 standard errors (thin grey lines) of the differences.



GOPR versions 6.0cf and 7.0de were found to compare similarly to the ground-based data, with differences mainly visible in outlier profiles (Figure 7-1 and Figure 7-2). Both versions therefore match the lidar, sonde and microwave radiometer data within a few percent between 20 and 50 km. The largest deviations (up to 20%) occurred in the polar region. Most of these observations are flagged as twilight and/or straylight contaminated profiles however, and a large spatial heterogeneity exists in this area. Too few data are available to see which variable affect the results most.

Increasing the error limit from 30% to 100% is sometimes beneficial (through increase of number of available profiles) and other times disadvantageous (through the inclusion of outlier profiles), see the example for weak, cold stars in Figure 7-3. Limiting the ozone profiles to values that are positive and below 10^{19} molecules affects the mean and standard deviation profiles through the removal of extremes, but less extreme positive spikes at high altitudes where ozone concentration is lower can still occur.

High Resolution Temperature Profiles (HRTTP)

The HRTTP product coming with version 5.00 was found to have several issues: data are often missing, not provided with a processing flag (validity of the retrieval) and temperature data are often provided for duplicated altitudes (the same altitude is repeatedly reported).

The maximum allowed error between 1K and 5K for the validation dataset was varied and between 1% and 5% for the GOMOS HRTTP. The choice for a different range for the GOMOS HRTTP is based on the warning in the disclaimer [http://envisat.esa.int/handbooks/availability/disclaimers/GOM_NL_2P_Disclaimers.pdf page 12] that the provided errors in the HRTTP product are “largely overestimated”. With an average temperature of 220K 5% would allow for a maximum estimated error of 11K. Be reminded that the error is estimated for each altitude of each retrieved profile. All GOMOS HRTTP furthermore had to be taken with a solar zenith angle larger than 107° .

When comparing this last restriction with the selection based on the limb condition flag (0 = dark), the overall shape of the differences is very similar, but the number of collocations is strongly reduced.

All GOMOS temperature profiles have been compared with balloon sonde and lidar temperature profiles. Collocated data were required to be within 300 km and 5 hours of each other. Profiles were only considered if they resulted in useful data over at least 3 km. Data were splined to a common altitude grid of 50 m ranging between a minimum altitude of 10 and maximum of 40 km.

Most notable is the difference between observations with cold and hot weak stars. Whereas the temperatures retrieved using weak cold stars (Figure 7-4) slowly change from an underestimation of about -2K at 20 km towards an overestimation of 1.5K at 29 km, the difference in temperature for the weak hot stars (Figure 7-5) only slightly varies between -3K and -2 K at these altitudes.

Overall, the HRTTP are mostly negatively biased except below 19 km in the tropics and below 16 km in the mid-latitudes. For the polar regions (Figure 7-6, left panel), we see a negative bias with a maximum deviation of around -4K that is decreasing to zero around 28 km and then increases again. In the mid-latitudes (Figure 7-6, middle panel), differences in temperatures range between 0 at 16 km to -3.5K at 19 km to + 0.5K around 28 km to -4K at 35 km. In the tropics (Figure 7-6 right panel), differences between GOMOS and the validation data are 0 at 19 km rapidly increasing to -1.5K at 28 km. A relatively large spread in the found differences for all cases is seen (2.5 and 97.5 percentiles often “off-plot”).

The data disclaimer (specifically, on page 5) furthermore warns to consider the azimuth angle of the observation: “*For vertical occultations, the altitude range for validity is 18 km - 35 km. The upper limit depends on the scintillation strength. For oblique occultations, the altitude range for validity is 20 km - 30 km. Data outside this altitude range should be considered with caution.*”

For altitudes above 30 km, data taken using a backward line of sight have a smaller negative bias than those with a slant or sideward line of sight. The negative bias is increasing in magnitude with altitude in all cases. Note that very few points are available for the sideward direction (95 in total, only 30 at 30 km and less than half of that above), also because of the filtering on error.

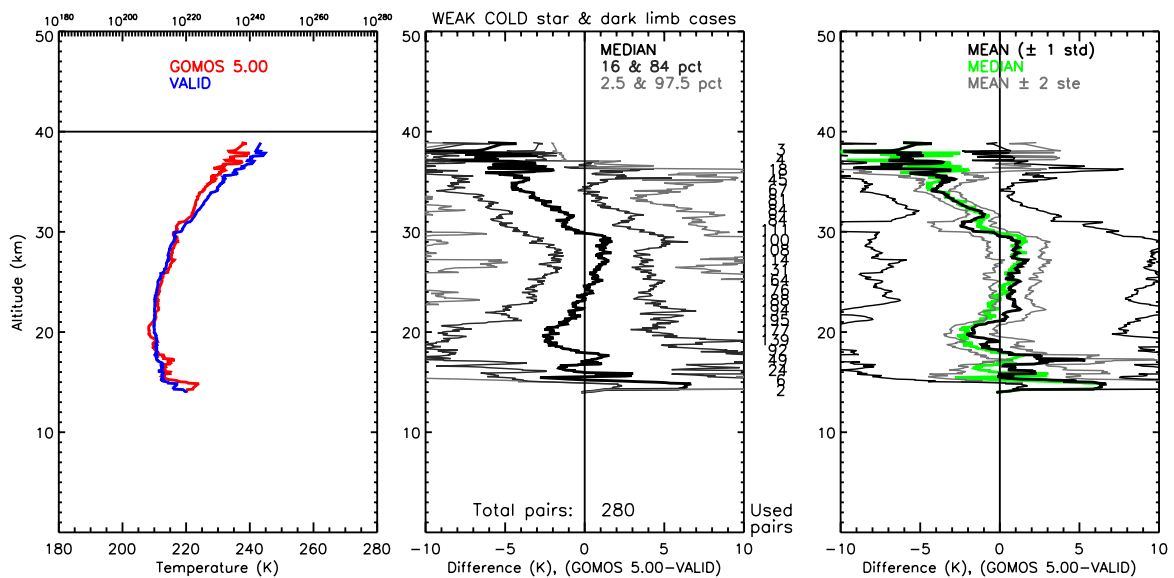


Figure 7-4: All collocations with weak cold stars for a maximum error of 5% for GOMOS and 1K for the validation data.

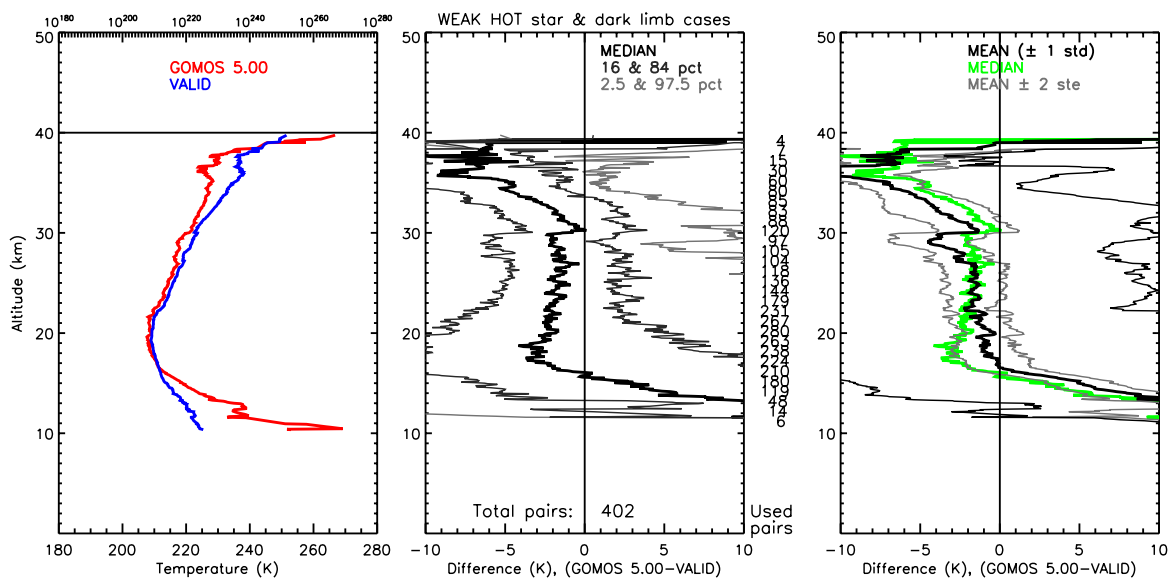


Figure 7-5: All collocations with weak hot stars for a maximum error of 5% for GOMOS and 1K for the validation data.

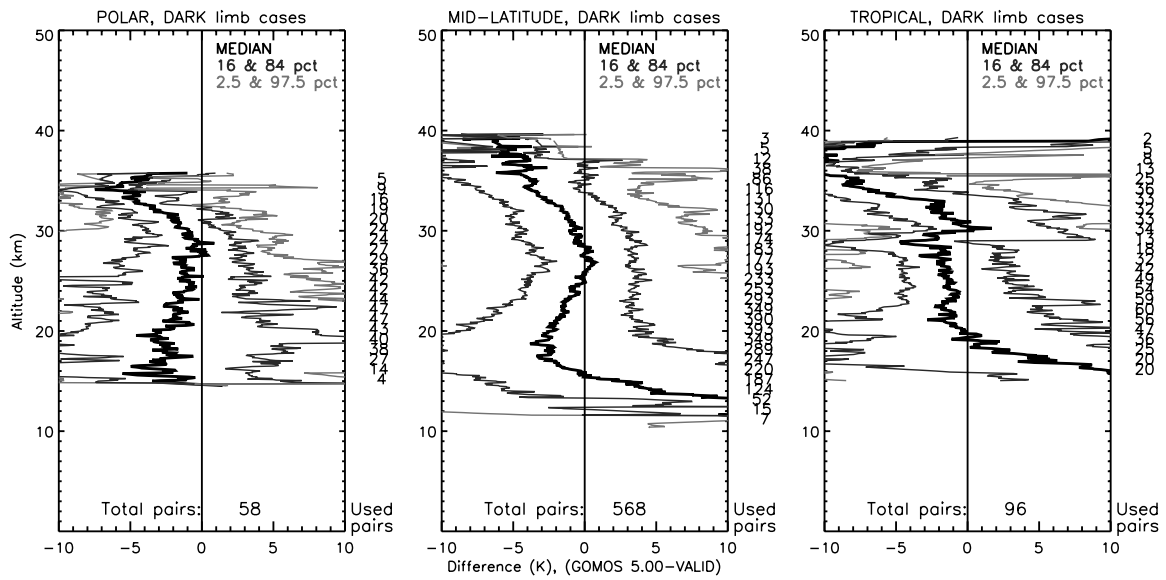


Figure 7-6: Validation results for the polar regions (left), mid-latitudes (middle) and tropics (left). Panels are as the middle panel of the previous figures.

More details can be found in the full analysis in Appendix 4: Validation of GOMOS high resolution temperature profiles using sonde and lidar measurements.

8 ACE FTS

ACE FTS is onboard the third-party mission SCI-SAT and provides, amongst other constituents, ozone profiles together with the MAESTRO instrument. Through ESA, in 2010 only version 2.2 profiles were accessible.

ACE-FTS version 2.2 (updated) ozone and temperature profiles have been compared with balloon sonde, lidar and microwave radiometer (ozone only) profiles.

Used collocation criteria were 20 hours (5 hours) and 800 km (300 km) for ozone (temperature) profiles. Above an altitude of 50 km, collocations are required to be within 5 hours. Sonde profiles have been cut off at an altitude of 30 km. Lidar profiles are used in the altitude range 18 (15) to 45 (70) km for ozone (temperature) comparisons. Lidar profiles are further more restricted to a maximum error of 30%. Microwave radiometer data are used starting at 30 km altitude. Similar to the lidar profiles, the microwave radiometer data are constrained to those data where the error is 30% at most.

ACE-FTS data have been limited to an error of 100% for the comparison regarding ozone profiles and 1 K for temperature.

In a previous validation study, Dupuy et al. (2009) have shown that the ozone profiles from the ACE FTS version 2.2 ozone update data have a positive bias ranging from +1 to +8% between 16 and 44 km. At higher altitudes (up to 60 km), the bias is increasing to an average of about 20% (40% at most). No systematic difference was found between ACE-FTS sunset and sunrise observations. Figure 8-1 shows that we also find a small positive bias (mostly within 5%), which increases from 30 km to reach a maximum around 52 km for sunrise measurements and from about 40 km reaching a maximum at 50 km for sunset observations after which the bias starts to reduce becoming negative at 60 km for sunrise measurements and at 55 km for sunset measurements. These observations do have to be seen considering the low number of collocation pairs available at these altitudes. At low altitudes (below 15 km), the sunrise measurements still seem to provide relatively good profiles (median error within 10% above 6 km) whereas the sunset measurements also give reasonable values (median error within 20% above 6 km). Outlier profiles can be seen for both modes, resulting in larger mean errors for these low altitudes.

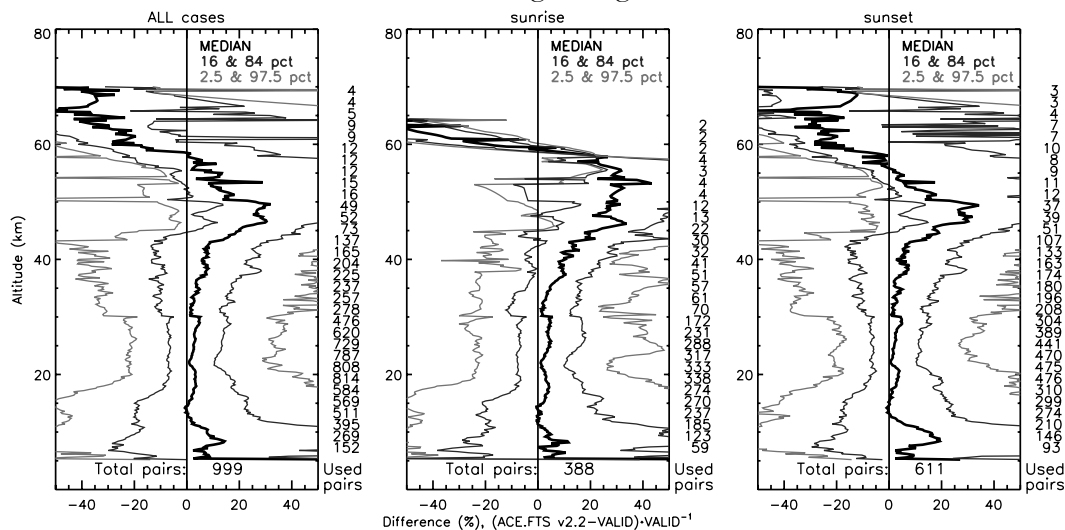


Figure 8-1. Validation results for all cases together (left panel) and split into FTS sunrise (middle panel) and sunset (right panel) observations. Plotted quantities are percentile differences with respect to the validation data. Note that all data above 45 km are from the northern hemisphere.

Most observations are available for sunset measurements, outside the tropics, and for absolute beta angles ranging between 0 and 60°. No significant differences between the different groups (consisting of 30 degree bins from -90 to 90°) could be identified. Figure 8-2 shows the location of the available measurements with colours indicating the beta angle. Collocations with values close to 0 do not occur in the tropics. Positive angles are not found in the Southern polar area.

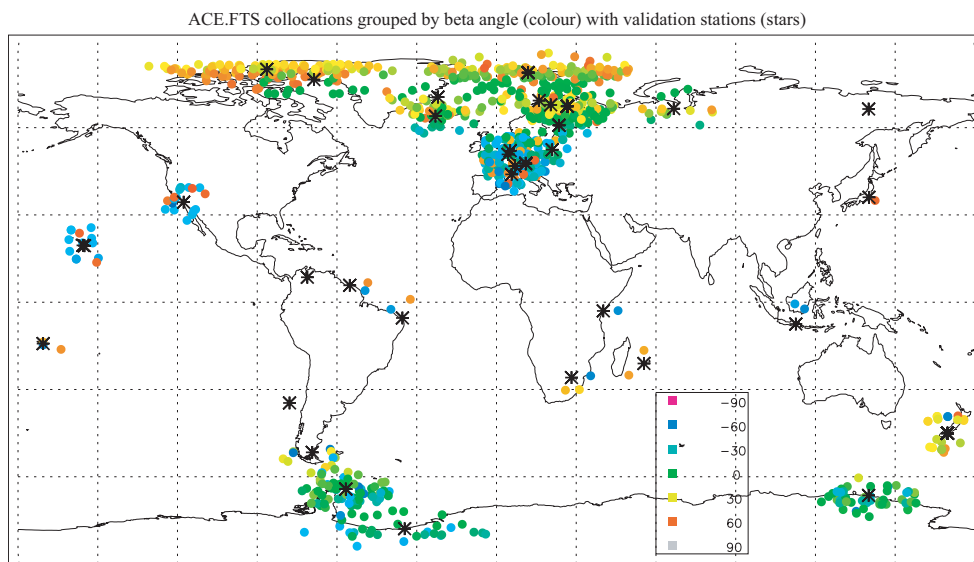


Figure 8-2. Location of validation sites (black asterisks) and ACE-FTS collocated measurements with colours indicating the beta angle of the FTS-observation.

Very few collocations are found in the tropics, partially as a consequence of the lower coverage of this region resulting from the satellite path and observation strategy, and differences with the other regions are therefore not significant (Figure 8-3). Most collocations are located on the northern hemisphere where there are more ground-based and balloon-borne measurements available. For instance, no collocations with microwave radiometer data were available for the southern hemisphere. Nevertheless, the behaviour seems to be the same for both hemispheres. The best match between FTS and the validation data is seen in the polar regions for altitudes between 10 and 42 km.

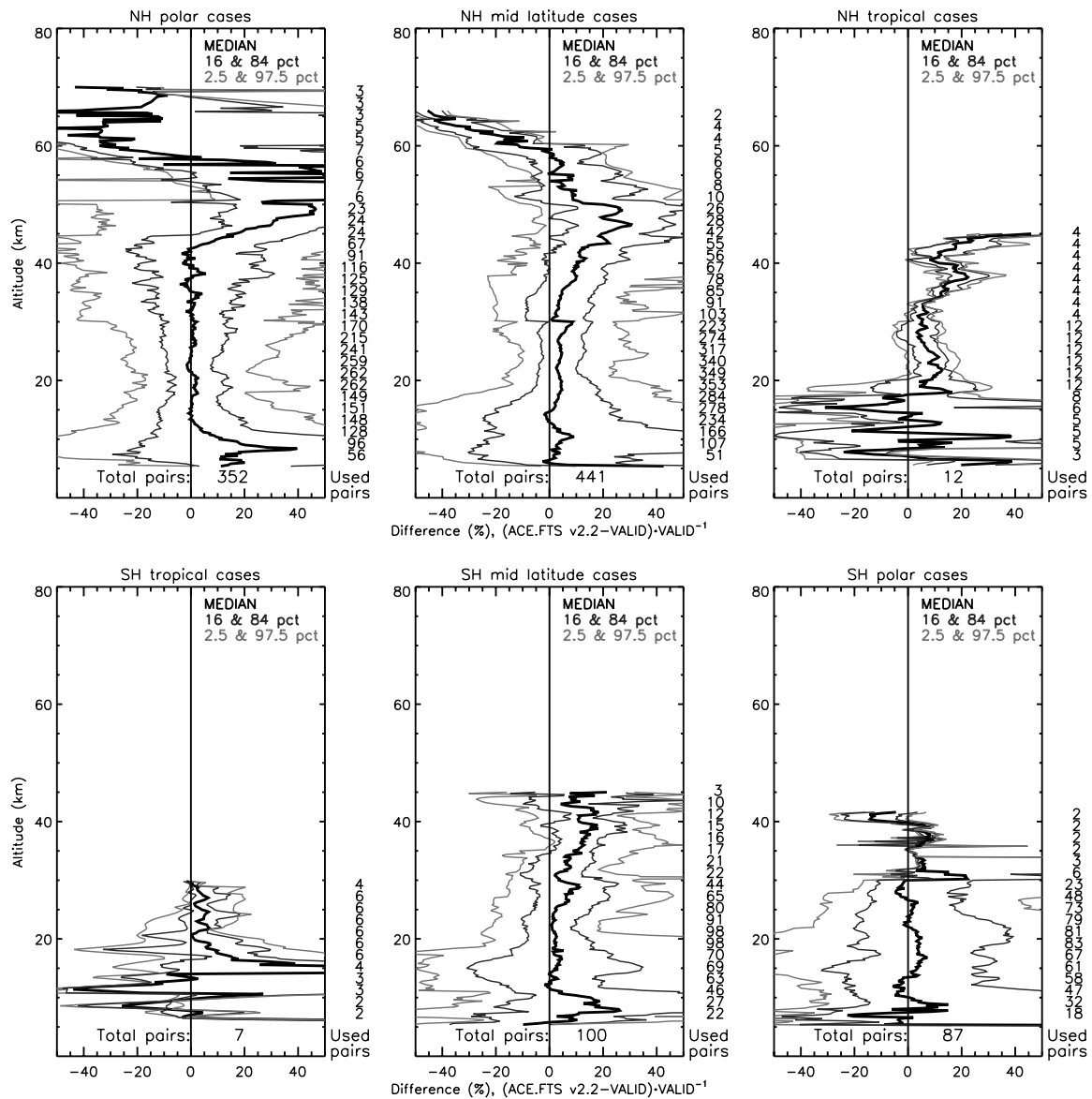


Figure 8-3. Top: Validation results for the northern hemisphere with the left panel: northern polar region; middle panel: northern mid-latitudes; right panel: northern tropics. Bottom: southern hemisphere. Left panel: southern tropics; middle panel: southern mid-latitudes; right panel: southern polar region.

Figure 8-4 shows the results for the temperature validation. Very few profiles are available above 30 km (where the sonde data end). For the altitude region between 5 and 30 km deviations are between -2 and +2K for sunrise observations. For sunset observations, the temperature profiles match the validation data within 1 K (ranging between -1 to +1K) up to 29 km. These differences again have to be considered taking into account the low amount of data available.

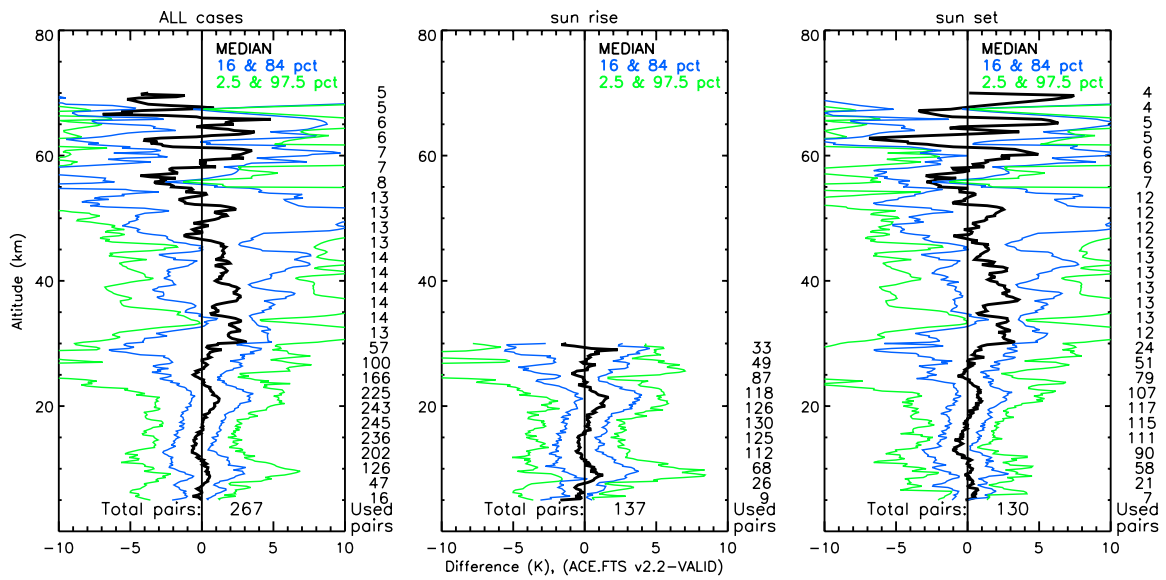


Figure 8-4. Validation results for ACE FTS v2.2 temperature profiles. Left panel: all cases together. Middle panel: sunrise observations. Right panel: sunset observations. Median differences are given in black, 16 and 84 percentiles in blue and 2.5 and 97.5 percentiles in green. Note that if there are fewer than 2 pairs available, results are not plotted (a single sunrise observation is available above 30 km, which is considered for all cases together).

9 CALIPSO

EARLINET ground based lidars as reference points are necessary to increase and validate the accuracy of aerosol optical properties retrieved from CALIPSO. In particular EARLINET Raman station's data are important to validate and improve the aerosol retrievals from the pure backscatter lidar on board CALIPSO. With EARLINET, Raman lidars we can investigate intensive optical parameters (like lidar ratios and Ångström exponents) and their dependences on the specific aerosol and cloud types, information needed for the development and optimisation of space-borne lidar algorithms. Already before the launch of CALIPSO, a strategy for correlative measurements had been developed within EARLINET. Based on the experience of the first 18 months of correlative observations we have consolidated this strategy in the frame of a dedicated ESA study (ESA-EARLINET-CALIPSO project) aiming at a long-term aerosol and cloud data base from ground-based and satellite-borne lidars which started on April 1, 2008. The main goal is to obtain a statistically significant data set from network observations with ground-based lidars to correlate it to CALIPSO observations for validation purposes and also for a possible use of integrated lidar measurements from satellite and from ground for studying aerosol and cloud variability in space and time.

Since CALIPSO related EARLINET activities are carried out in the frame of an ESA project, here we shortly report some results.

Before comparing vertical profiles of the aerosol optical properties, a previous assessment of the accuracy of CALIPSO raw signals (namely level 1 data) was performed. Comparing EARLINET ground-based measurements with the CALIPSO Level 1 data products, potential problems and biases already contained in the calibrated CALIPSO lidar signals can be distinguished from any errors and uncertainties due to assumptions needed for the inversion. A methodology for the comparison was presented and discussed in detail by Mona et al. (2009). A first systematic comparison between EARLINET and CALIPSO data in terms of Level 1 data has been carried out on the base of almost 18 months of EARLINET and CALIPSO correlative measurements performed in the June 2006 - November 2007 period before the change of CALIPSO pointing angle from 0.3° to 3° off nadir. Following the criteria established in the CALIPSO validation plan (<http://calipsovalidation.hamptonu.edu>), a horizontal radius of 100 km is established as maximum distance between EARLINET ground-based and CALIOP satellite-borne measurements to be compared for validation study. Measurements as close in time as possible are requested to EARLINET stations, typically EARLINET measurements are obtained with a temporal integration centered around the CALIPSO overpass time, so measurements can be considered as coincident in time. v2.01 data are considered in the Pappalardo et al. (2010b) publication, as this version was available for the June 2006 to September 2008 period. Apart from the planetary boundary layer, where CALIPSO signals seems to have strange behaviors, results from these studies are encouraging, demonstrating the good performance of CALIPSO and the absence of evident biases in the CALIPSO raw signals, with a relative mean difference of 4.6%, a relative standard deviation of 50% and a relative median value of 0.6%.

A major Saharan dust outbreak has been used as a case study for showing first results in terms of comparison with CALIPSO level 2 data (aerosol extinction and backscatter profiles). Comparisons are good in some cases, but in other cases CALIPSO classifies most of the plume as cloud. For example, on 30 May, EARLINET observations detected dust plume up to 5 km a.s.l. at Maisach, and up to 8 km a.s.l. at Hamburg and Leipzig, around 12:00UT. CALIPSO signals show the presence of intense layers over Germany in correspondence to the EARLINET observed dust plume. However, moving toward North (Leipzig and Hamburg) the dust plume is identified as cloud. Obviously, this is a misclassification caused by the high backscatter and depolarization values of dust at relatively high latitudes. North of 50°N , outside of the so called dust belt, the CALIPSO cloud-aerosol discrimination algorithm forces the identification of polar ice clouds instead of dust.

After 3 years of CALIPSO related activities, some issues are highlighted concerning CALIPSO data/retrieval. First of all, it is clear that cloud/aerosol discrimination is a critical issue and the multi-parameter probability distribution functions (PDF) used in version 2 are insufficiently accurate and needs further improvement. Moreover, multiple scattering, considered already for cloud cases, came out to be important also for high aerosol load such as for dust cases. The comparison with EARLINET Raman measurements showed that the lidar ratio assumptions, based on AERONET database, are often not appropriate and could be significantly improved on the base of the EARLINET long term lidar ratio database. In addition other aerosol types should be added as well.

Some of the points reported above are addressed in the new release of the data, version 3 released in June 2010. The PDF used in the version 2 data release are 3D, including as attributes (dimensions): the mean attenuated backscatter at 532 nm, the 1064/532 layer-integrated attenuated backscatter ratio, and the mid-layer altitude. By adding dimensions of volume depolarization ratio (VDR) and latitude, a new set of 5D PDFs has been developed. These improvements are particularly noticeable for very dense dust layers, which were frequently misclassified as cloud by the 3D algorithm in the version 2 data release (Liu et al., 2010).

Another important change is related to the horizontal resolution of the aerosol profile products, that is now 5 km, rather than the 40 km used in the version 2 data products. As of version 3, the cloud and aerosol profile products are reported at identical spatial resolutions. With the change to a 5 km resolution for the aerosol profile products, all profile products are now produced on the same horizontal grid used by the 5 km layer products. In addition, a new procedure is included in this version to improve the profiling in the PBL through adjustment of PBL altitude.

Figure 9-1 reports the comparison between ground-based lidar measurements of aerosol backscatter at 532 and 1064 nm performed at the EARLINET Potenza station and CALIPSO version 2 and version 3 corresponding profiles. Version 3 backscatter profiles look more realistic than version 2 profile (strongly increasing in the lowest altitudes) and some points are added close to the surface in the profiles. Between 4 and 1.5 km a.s.l., profiles in version 3 are significantly changed with respect to version 2, but with different behaviours for the 2 wavelengths: the profile is higher for the IR and lower for the backscatter at 532 nm in this new version. However at both wavelengths and for both versions, CALIPSO retrievals are significantly higher than correspondingly EARLINET profiles. For both versions, also the extinction profiles are higher than ones measured by EARLINET. Differences are probably related to the difference between the CALIPSO's assumed lidar ratio (around 50 sr) and the EARLINET measured one (about 70 sr in the 3.5-1.5 km a.s.l. altitude range).

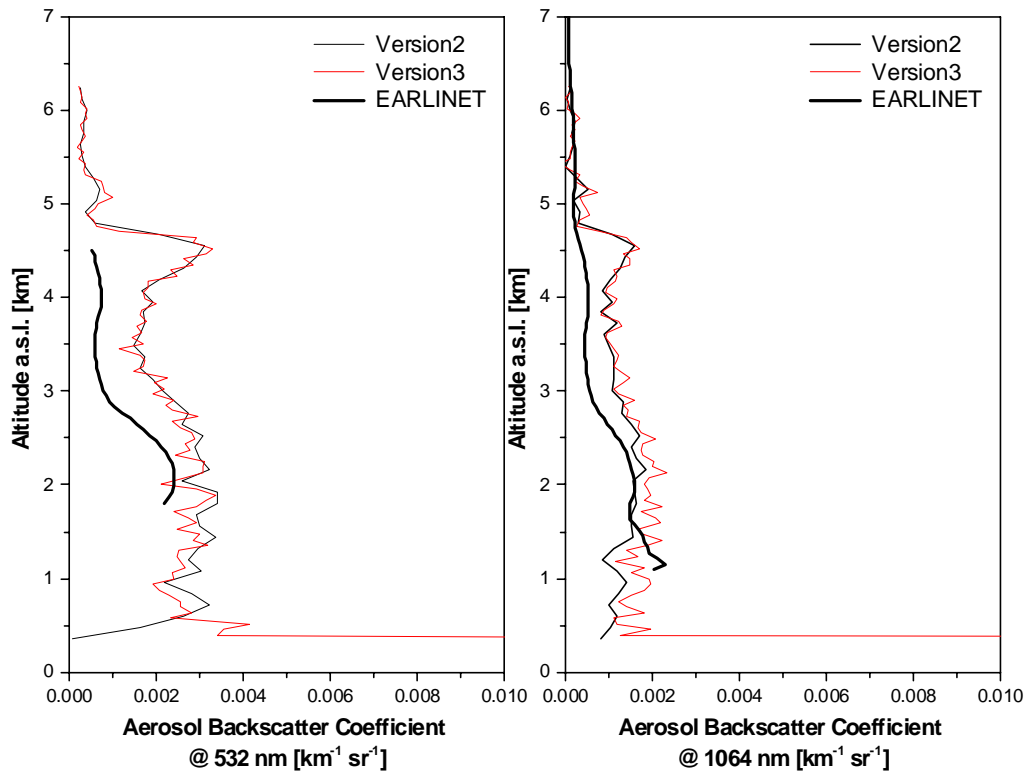


Figure 9-1. Comparison of aerosol vertical profiles as measured by Potenza EARLINET station (40.6 N, 15.72 E, 24 August 2007, 00:04-02:04 UT) and CALIPSO (01:05 UT) with both versions 2 (black) and 3 (red). Aerosol backscatter at 532 nm and 1064 nm are reported on left and right panel, respectively.

10 MODIS

In this section, all AOD measurements obtained with EARLINET Raman stations reported in Table 2-1 are compared to the measurements of AOD obtained with MODIS at 550 nm. As reported above MODIS data are averaged on $1^\circ \times 1^\circ$ area, as indicated in Table 10-1.

Results reported in the following paragraph are an update of those reported in 2009: a detailed study was performed in order to identify the main cause of the discrepancies observed between MODIS and the EARLINET Thessaloniki station. It came out that a modification of the instrument set-up strongly affected the overlap function. Therefore Thessaloniki data are appropriately corrected. In the following results are updated with the new calculation for Thessaloniki AOD from ground-based lidar data.

Table 10-1. EARLINET site location and corresponding MODIS area averaged around each EARLINET site

Station	ID	Station Coordinates	Averaging Area
Aberystwith, UK	ab	51.86°N, 4.25°W	51.36÷52.36 N ; -4.75÷-3.75E
Athens, Greece	at	37.96°N, 23.78°E	37.46 ÷ 38.46 N; 23.28÷24.28 E
Hamburg, Germany	hh	53.57°N, 9.97°E	53.07÷54.07 N; 9.47 ÷ 10.47 E
L'Aquila, Italy	la	42.38°N, 13.32°E	41.88 ÷ 42.88 N; 12.82÷13.82 E
Lecce, Italy	lc	40.30°N, 18.10°E	39.80÷40.80 N; 17.6 ÷18.6 E
Leipzig, Germany	le	51.35°N, 12.44°E	50.85 ÷ 51.85 N; 11.94 ÷ 12.94 E
Napoli, Italy	na	40.84°N, 14.18°E	40.34 ÷ 41.34 N; 13.68÷14.68
Potenza, Italy	po	40.60°N, 15.72°E	40.10 ÷ 41.10 N; 15.22÷16.22 E
Thessaloniki, Greece	th	40.63°N, 22.95°E	40.13 ÷ 41.13 N; 22.45 ÷ 23.45

Considering a $1^\circ \times 1^\circ$ averaging area around each EARLINET site for MODIS data, a maximum distance between EARLINET and MODIS measurements of about 90 km is obtained, comparable to the limit established for the CALIPSO validation purposes on the base of variability of aerosol fields.

For MODIS (and OMI and MISR) measurements, collocation perfectly matching in time is not possible, since these satellite sensors provide measurements during daytime, while extinction (and therefore AOD) measurements are available from ground-based EARLINET stations mainly during night-time. Measurements performed on the same day are compared for the validation purposes of this report. Because of the large temporal difference, we could attend also large differences in a one-to-one comparison and a large number of comparisons is needed in order to average in some sense the smaller scale variability. Comparisons reported in the following are performed both in terms of climatologic analysis and of coincident measurements.

For the climatological comparisons, only climatological EARLINET measurements are considered in order to avoid possible biases due to intense measurement periods related to special events observations. For this kind of comparisons, yearly mean AOD are calculated for the two instruments. Seasonal averages are also calculated considering for the MODIS mean the time period of EARLINET data availability as reported in Table 2-1.

For a quantitative comparison between EARLINET and MODIS measurements, MODIS data are scaled to the EARLINET measurement wavelength using the mean Ångström exponent measured at the closest AERONET station. In particular, EARLINET and AERONET instruments are co-located for Athens, Hamburg, Lecce, Leipzig, Potenza and Thessaloniki, while Mace-Head, Rome, and Potenza AERONET values are considered for Aberystwith, L'Aquila and Napoli, respectively.

Figure 10-1 reports the monthly averages of AOD at 355 nm as measured by EARLINET Raman stations during climatological measurements and as obtained by MODIS AOD measurements at 550 nm in the corresponding area (see Table 10-1) scaled to 355 nm using the

mean Ångström exponent provided by the closest AERONET station. Seasonal behaviour is typically seen by both lidar and spectrometer measurements with maximum during spring-summer and minimum during the coldest seasons. In general there is a good agreement between EARLINET and MODIS measurements. Differences are observed for Aberystwith in the May 2000 – December 2001 period and for some values measured at Thessaloniki and Athens. However it has to be considered that, following the EARLINET schedule for climatological measurements, a maximum of 8 Raman measurements for month could be provided by each station, but low clouds and bad weather conditions limit this number to an average of 3 measurements per month. Larger and more significant statistics are achieved considering the annual averages.

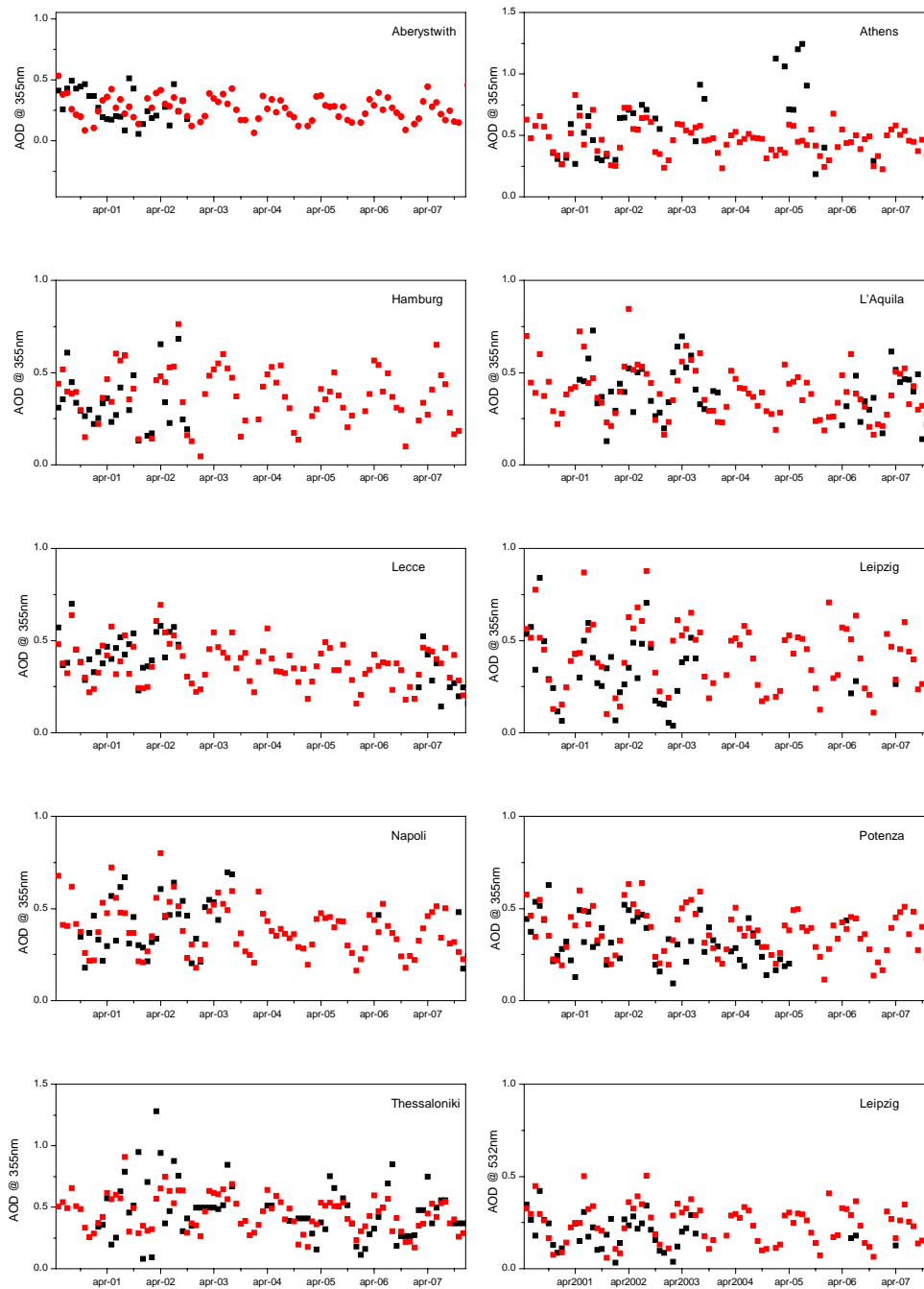


Figure 10-1. Monthly mean AOD at 355 nm as measured by EARLINET stations (black) and obtained by scaling MODIS measurements (red) at 550 nm to 355 nm using the mean Ångström exponent provided by the closest AERONET stations.

Figure 10-2 shows the annual mean of AOD at 355 nm measured at EARLINET stations together with annually averaged AOD measured at 550 nm by MODIS and scaled to 355 nm using the mean Ångström exponent measured at the closest AERONET station. For the Leipzig station, the comparison for AOD at 532 nm is also reported. In this case, and in particular for coincident measurements, there is a lower uncertainty in the validation since the lidar measurements are closer in wavelength to the MODIS wavelength.

On average there is a good agreement between lidar and MODIS spectrometer measurements. For almost all stations, AOD in 2002 and 2003 is significantly higher than in the following years when the aerosol content decreases reaching a minimum around 2005/2006. Even though within the errors, MODIS AOD is typically slightly higher than AOD measured by EARLINET stations. This could be related to a MODIS overestimation of AOD over land, but there could be other reasons for this difference. A small underestimation of AOD in EARLINET measurements could be due to the overlap function (see Appendix 2), but the largest uncertainty in this kind of comparison originates in the wavelength scaling through a mean Ångström exponent value. This is confirmed by the better agreement obtained for Leipzig comparison at 532 nm rather than at 355 nm.

A different behaviour is observed for the Napoli, Athens and Thessaloniki measurements. At Napoli, MODIS mean values are, although within the error bar, lower than EARLINET AOD. Regarding this station it has to be considered that mean Ångström value used is measured by AERONET Sun-photometer located in Potenza. Since Napoli is a mega-city, more polluted and industrial than Potenza, a higher Ångström exponent, corresponding to smaller anthropogenic particles, should be more reasonable and would explain the observed differences between MODIS and EARLINET data. Finally, EARLINET AOD mean values for Greek stations in 2002, 2003, 2005 and 2006, are considerably higher than those measured by MODIS. This could be related to the extremely high aerosol load due to local fires occurring in Greece that could be identified by MODIS as clouds. A possible confirmation of this can be provided by the comparison for coincident measurements for these stations.

Seasonal behaviour is studied considering for both MODIS and EARLINET data all measurements performed in the time period reported in Table 2-1 for each season. Some of the comments related to annual averages also apply to seasonal averages even if the agreement, averaging over a large number of measurements, is typically improved. Apart from Aberystwith, that is a maritime station, for all the considered stations Spring and Summer values are higher than in cold seasons.

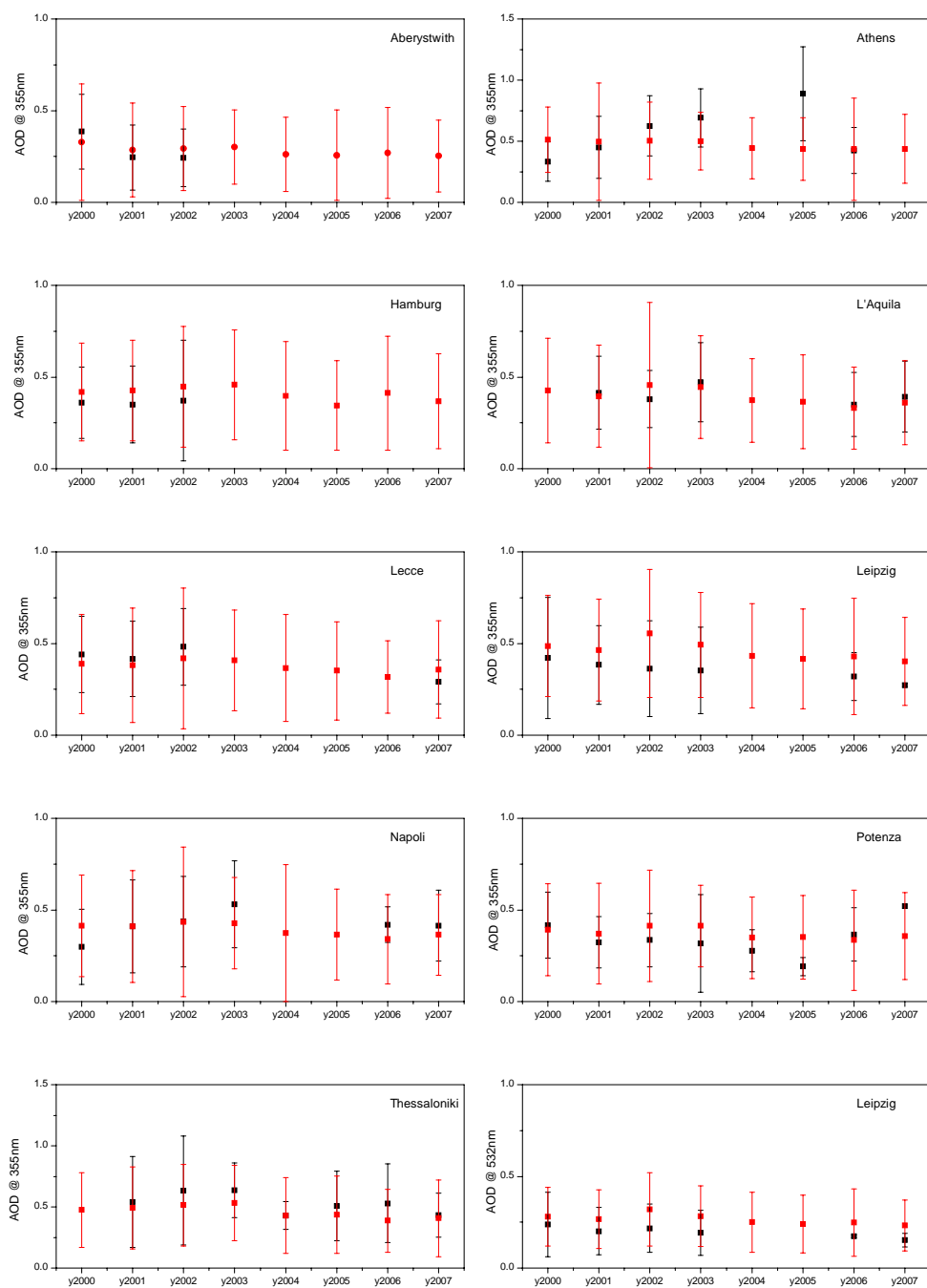


Figure 10-2. Yearly mean AOD at 355 nm as measured by EARLINET stations (black) and obtained by scaling MODIS measurements (red) at 550 nm to 355 nm using the mean Ångström exponent provided by the closest AERONET stations. Standard deviations are reported as error bars.

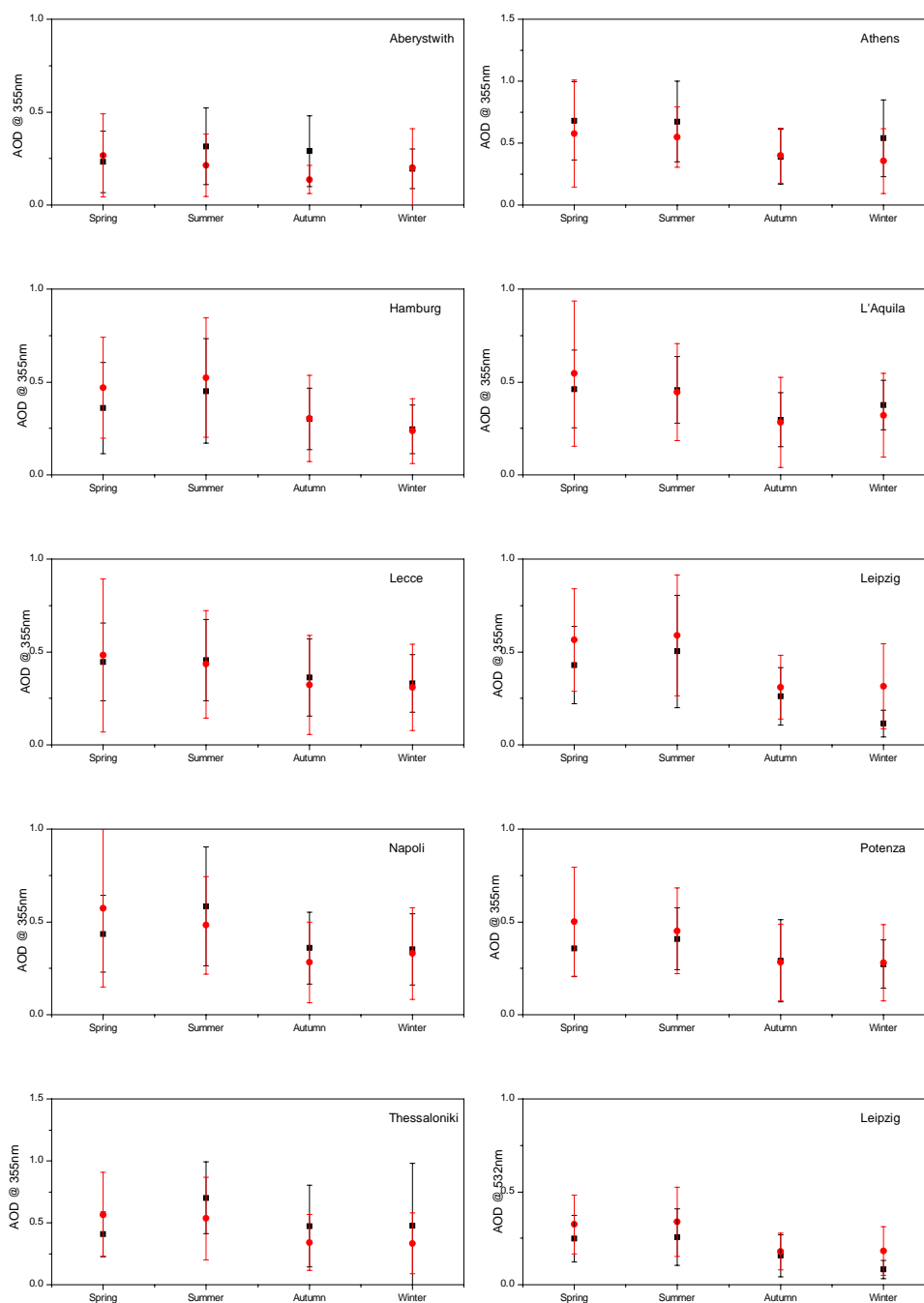


Figure 10-3. Seasonal averages of AOD at 355 nm as measured by EARLINET (black) stations and obtained by scaling MODIS measurements (red) at 550 nm to 355 nm using the mean Ångström exponent provided by the closest AERONET stations. Standard deviations are reported as error bars.

Differences between EARLINET and MODIS AOD measured on the same day are calculated for each station. All available EARLINET data are considered independently from the observation category. If more EARLINET profiles are available for the same day, the mean AOD is considered for the comparison. In this comparison, it is important to consider that MODIS measurements are performed during the day while lidar measurements are performed mostly during night-time.

The free troposphere (FT) contribution is calculated starting from the Planetary Boundary Layer (PBL) top height, which represents the layer closest to the surface where most of the aerosol content is usually confined and is here retrieved, according to EARLINET definition, as the first minimum of the backscattered range-corrected lidar signal (Matthias et al., 2004b). The FT contribution is calculated as the fraction of AOD above the PBL with respect to the total AOD, expressed in percentage. This quantity helps to separate between cases in which the aerosol is

confined to the PBL (low FT contribution) and cases in which there is significant aerosol load in the free troposphere (high FT contribution). This parameter also helps to identify large scale processes, which are characterized by a high FT contribution.

Figure 10-4 and Figure 10-5 show for each station the difference in AOD as measured by EARLINET and MODIS as a function of the FT contribution to the total columnar aerosol load (left) and the probability distribution function of the EARLINET-MODIS differences (right). Mean differences and standard deviation are reported in Table 10-2 together with the number of compared measurements.

For all the stations, the mean differences are zero within the error. The count distributions are typically well fitted by a Gaussian distribution (correlation coefficient higher than 0.9). Parameters of Gaussian fitting curves are reported in Table 10-2.

Table 10-2. Mean differences between EARLINET and MODIS AOD. Standard deviations and number of compared cases are also reported. Parameters of the Gaussian distribution fitting curve are also reported.

ID	$AOD_{EAR} - AOD_{MOD}$	Number of cases	Correlation coefficient	Center of fitting curve	Half-width of fitting curve
ab	0.02 ± 0.22	47	0.954	-0.04	0.12
at	0.13 ± 0.40	110	0.989	0.12	0.26
hh	0.06 ± 0.28	84	0.922	0.02	0.16
la	0.04 ± 0.22	194	0.997	0.06	0.17
lc	0.03 ± 0.25	201	0.978	0.07	0.17
le	0.003 ± 0.26	87	0.905	-0.012	0.16
na	0.02 ± 0.30	234	0.978	0.04	0.18
po	-0.05 ± 0.23	185	0.972	-0.018	0.16
th	0.03 ± 0.42	136	0.977	0.02	0.26
le 532nm	-0.01 ± 0.16	86	0.984	-0.018	0.11

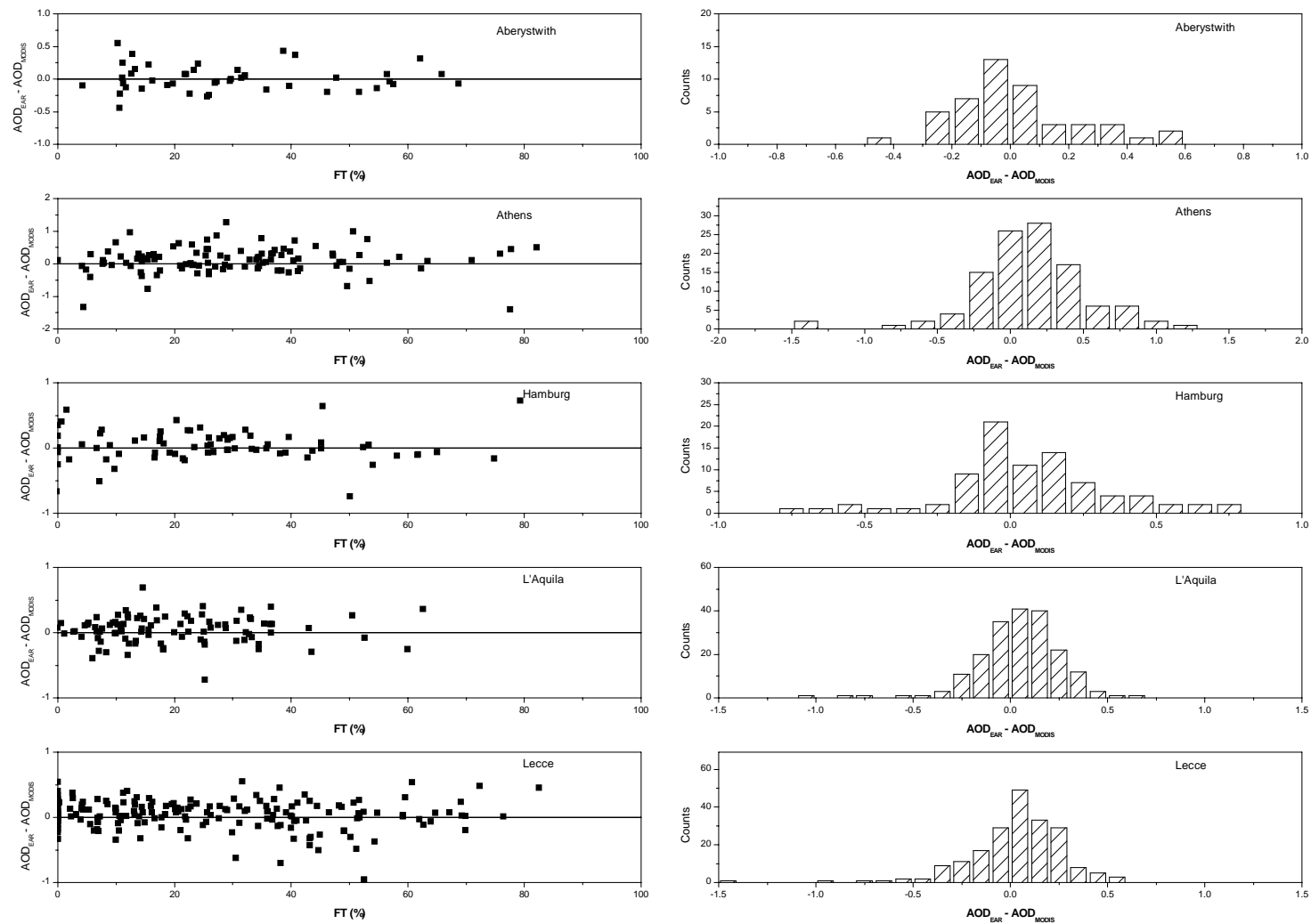


Figure 10-4. Differences between EARLINET and MODIS AOD as a function of the FT contribution (left) and frequency distribution of the differences (right).

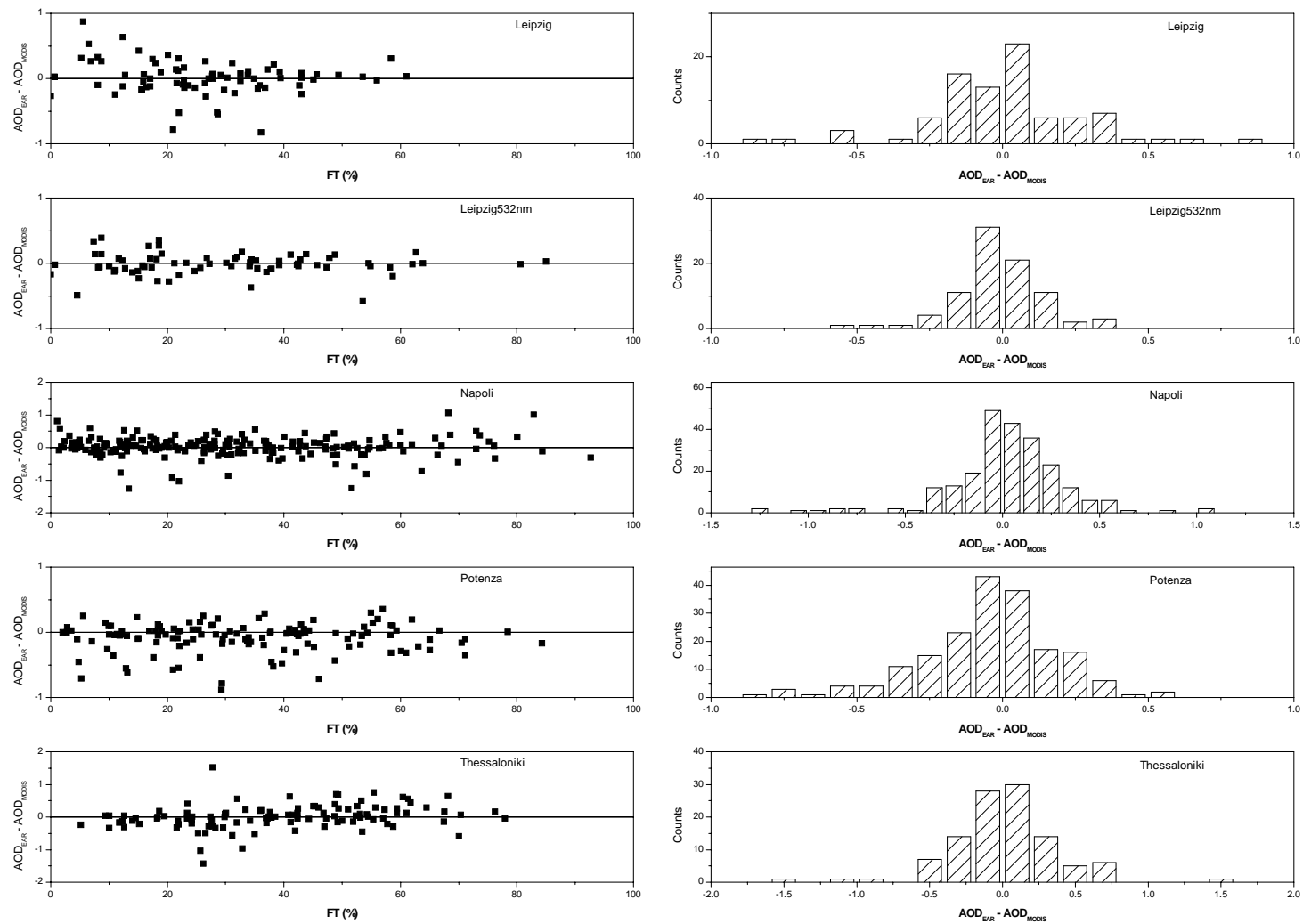


Figure 10-5. Differences between EARLINET and MODIS AOD as a function of the FT contribution (left) with corresponding histogram of the differences (right).

Figure 10-6 shows the differences in AOD as a function of the FT (left) and in terms of the frequency distribution (right) for all considered sites together. Differences are always around zero for all FT values, but for cases with a large FT contribution differences are more spread over a large range. On the whole, the differences distribution is well approximated by a Gaussian distribution centred around 0.04 with a standard deviation of 0.2. Therefore in cases of coincident measurements no biases are evidenced. However the observed differences range over a large interval extending between -1.5 and 2 . In order to better quantify the influence of long range transport of these differences, we studied the probability distribution function of the EARLINET-MODIS differences for two classes defined by the FT contribution, lower and higher than 30% following results obtained for Potenza EARLINET station (see the VALID annual report of 2008).

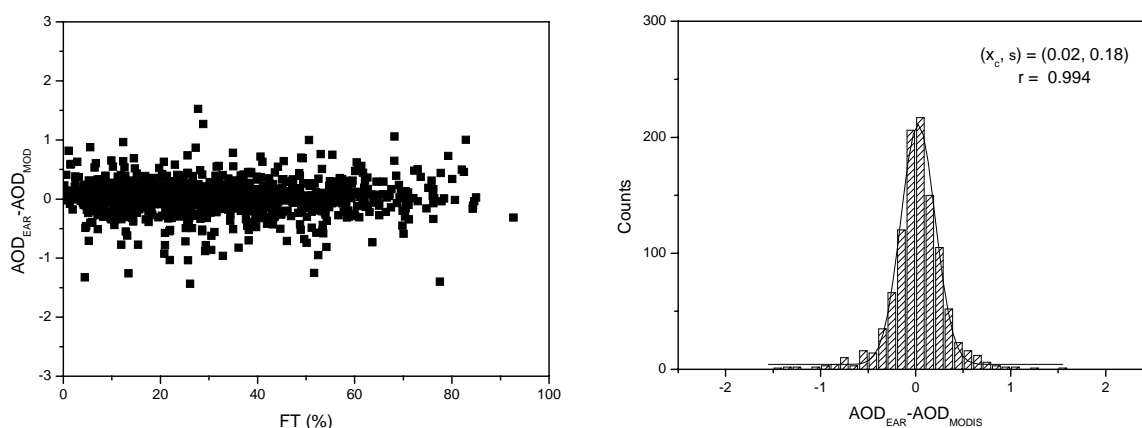


Figure 10-6. Differences between EARLINET and MODIS AOD as a function of the FT contribution (left) with a histogram of the differences (right). Data collected at all sites are considered all together.

Figure 10-7 reports the probability distribution function of the EARLINET-MODIS differences in the two classes defined by the FT contribution. Both distributions are well fitted by a Gaussian distribution with a mean value around 0, but the standard deviation of the fitting curve for cases with high FT aerosol load is slightly higher than for the other class. Therefore there is an indication that in the presence of lofted aerosol up to the FT, which typically indicates large scale processes, differences between satellites $1^\circ \times 1^\circ$ measurements and punctual measurements of the AOD are typically more spread than for small FT contributions.

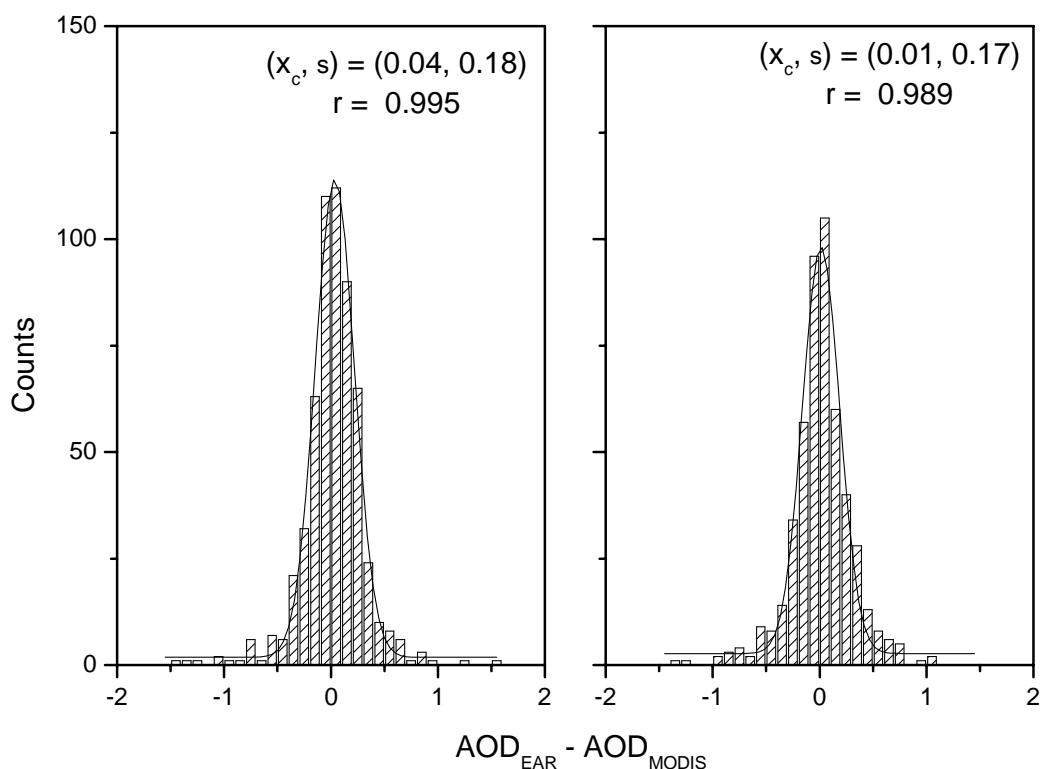


Figure 10-7. Histogram of the differences between EARLINET and MODIS AOD for FT contribution lower than 30% (left) and higher than 30% (right).

11 MISR

The first comparisons of MISR aerosol products versus Potenza reference EARLINET station's data, performed last year, showed the good agreement of MISR AOD measurements with the ground-based measurements and a typical underestimation of MISR data respect to MODIS, in agreement with previous studies in which has been shown that MODIS overestimates the MISR aerosol optical depth data (Abdou et al., 2005). On the basis of last year results, the comparison has been enlarged to the whole network in the last year of the project.

As for MODIS, all coincident (i.e. same day) EARLINET and MISR AOD measurements are considered disregarding about the EARLINET observation's category and considering the mean AOD if more EARLINET profiles are available for the same day.

For each station the difference in AOD as measured by EARLINET and MISR is investigated in terms of the probability distribution function of the EARLINET-MISR differences. Mean differences and standard deviation are reported in Table 11-1 together with the number of compared measurements.

For all the stations, the mean differences are zero within the error. On average the mean difference is 0.1, but 2 "outliers" are evident: the apparent 0.1 overestimation of MISR in Lecce case and the large mean difference observed for Thessaloniki. However, these anomalous behaviours are at least decreased when probably density functions are investigated. The count distributions are typically well fitted by a Gaussian distribution (correlation coefficient higher than 0.9). Parameters of Gaussian fitting curves are reported in Table 11-1.

Table 11-1: Mean differences between EARLINET and MISR AOD. Standard deviations and number of compared cases are also reported. Parameters of the Gaussian distribution fitting curve are also reported.

ID	AODEAR– AODMISR	Number of cases	Correlation coefficient	Center of fitting curve	Half-width of fitting curve
ab	0.11 ± 0.26	7	n/a	n/a	n/a
at	0.13 ± 0.19	45	0.980	0.12	0.2
hh	0.11 ± 0.18	18	0.995	0.06	0.13
la	0.14 ± 0.14	53	0.999	0.16	0.14
lc	-0.10 ± 0.19	60	0.994	-0.01	0.17
le	0.16 ± 0.22	21	0.988	0.17	0.17
na	0.07 ± 0.22	58	0.984	0.08	0.11
po	0.05 ± 0.20	44	0.994	0.06	0.19
th	0.23 ± 0.46	38	0.721	-0.1	0.11
le 532nm	0.07 ± 0.12	20	0.998	0.07	0.14

The differences in AOD for the whole network are shown in Figure 11-1 as a function of the FT contribution (left) and in terms of the frequency distribution (right). No dependence of differences on FT contribution is observed. A mean difference of 0.10 ± 0.26 is obtained for MISR, confirming its good performances. The Gaussian fitting for the frequency distribution of MISR differences is almost perfect with a correlation coefficient higher than 0.99 and centred around 0.08 with a standard deviation of 0.17. Comparing these results to MODIS, it is clear that a slight underestimation of MISR data exists with respect to MODIS and EARLINET.

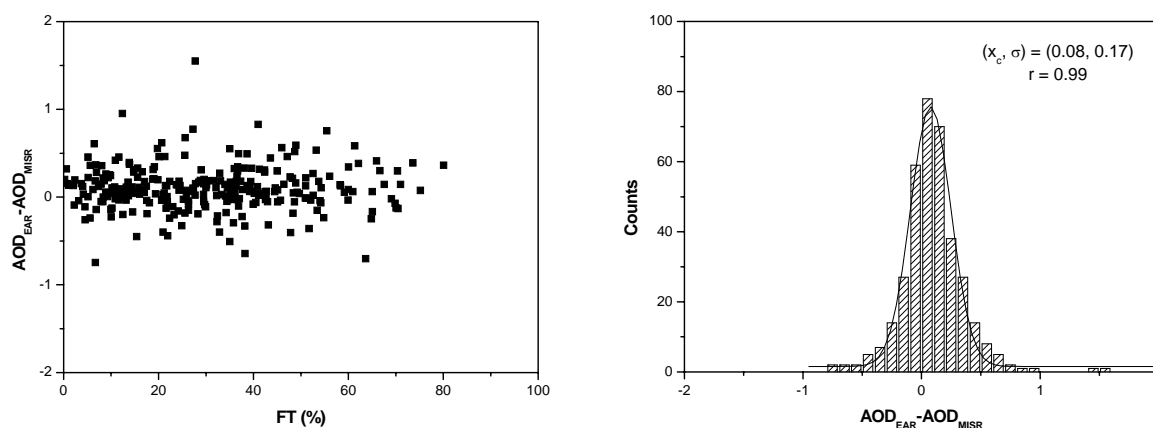


Figure 11-1. Differences between EARLINET and MISR AOD as a function of the FT contribution (left) with a histogram of the differences (right). Data collected at all sites are considered all together.

12 OMI

In the following the same kind of analysis performed for both MODIS and MISR AOD data is applied to OMI, in order to allow a comparison of the mean performances of all these satellite instruments.

As for MODIS, all coincident (i.e. same day) ground-based and satellite AOD measurements are considered disregarding about the EARLINET observation's category and considering the mean AOD if more EARLINET profiles are available for the same day.

For each station, mean difference and standard deviation are reported in Table 12-1 together with the number of compared measurements. Moreover, AOD differences are investigated in terms of the probability distribution function of the EARLINET-OMI differences. Apart from Athens, mean differences are negative indicating an overestimation of the AOD respect to the direct EARLINET measurements. For this sensor, the correlation with the Gaussian fitting curve for the pdf is significantly lower than those obtained for MODIS and MISR. This could be the signature of anomalous behaviour of retrieved OMI AOD for specific situations that would need further investigations. The centres of resulting fitting curve are still negative even if lower in absolute values and in any cases zero within the errors (half-width of fitting curve).

Table 12-1. Mean differences between EARLINET and MISR AOD. Standard deviations and number of compared cases are also reported. Parameters of the Gaussian distribution fitting curve are also reported. No comparisons are available for Aberystwith and Hamburg.

ID	$AOD_{EAR} - AOD_{MISR}$	Number of cases	Correlation coefficient	Centre of fitting curve	Half-width of fitting curve
at	0.11 ± 0.51	34	0.85	0.02	0.21
la	-0.26 ± 0.62	100	0.95	-0.002	0.28
lc	-0.20 ± 0.35	78	0.96	-0.06	0.18
le	-0.58 ± 0.97	20	0.91	-0.04	0.19
na	-0.43 ± 0.82	23	0.98	-0.18	0.18
po	-0.28 ± 0.48	39	0.96	-0.14	0.25
th	-0.08 ± 0.48	57	0.95	-0.05	0.36

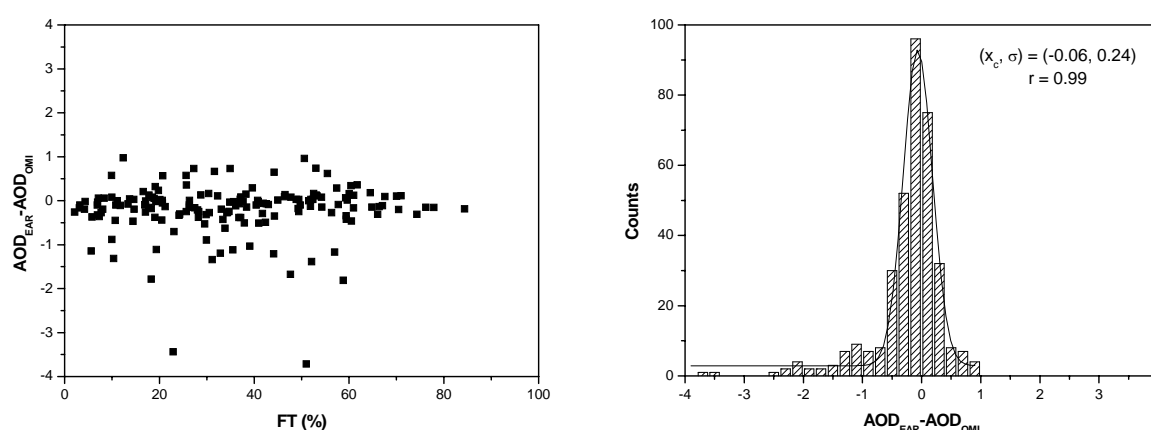


Figure 12-1. Differences between EARLINET and OMI AOD as a function of the FT contribution (left) with a histogram of the differences (right). Data collected at all sites are considered all together.

The typical overestimation in OMI is quantified by the whole network comparison. Figure 12-1 reports the differences as a function of the FT contribution (left) and in terms of the frequency distribution (right). No clear dependence on differences of FT contribution is observed. The Gaussian fitting for the frequency distribution of MISR differences is almost perfect with a correlation coefficient higher than 0.99 and centred around -0.06 with a standard deviation of 0.24. A long tail of negative values is present in the pdf (Figure 12-1), that is probably the main cause of small correlation coefficient for the single station evaluations (Table 12-1).

13 SYNAER

Daily aerosol optical depth evaluated by the SYNAER/ENV method are available for Europe, Africa and North America from 2003 until now in the current updated version 2.2. Data in hdf format have been downloaded by the World Data Center for Remote Sensing of the Atmosphere (<http://wdc.dlr.de>).

The EARLINET stations with the largest amount of AOD data available from 2003 are selected for this comparison: L'Aquila, Napoli and Potenza. For each day on which are available AOD measurements for these stations, SYNAER files were inspected to identify cases with overpass within $1^\circ \times 1^\circ$ over the three selected EARLINET stations. A total of 123 coincident measurements are identified. A mean difference of 0.16 ± 0.12 is obtained, revealing a possible small underestimation in the SYNAER algorithm. The pdf of the observed differences is reported in Figure 13-1. The Gaussian fit confirms the small bias of 0.15 ± 0.09 in the SYNAER analysis. However, it is clear that the database available for the comparison is far from being sufficient for an assessment of the SYNAER aerosol load characterization capability.

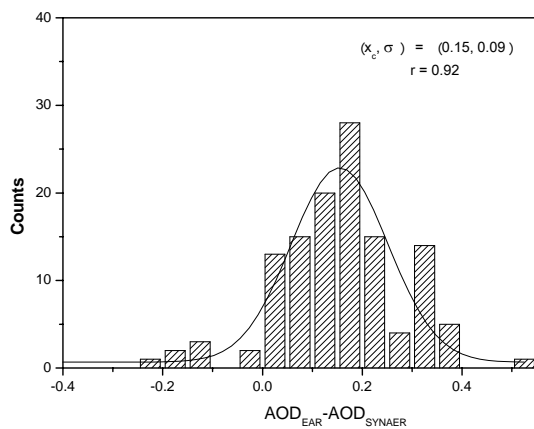


Figure 13-1. Histogram of the differences between EARLINET and SYNAER AOD. Data collected at the three selected sites (L'Aquila, Napoli, Potenza) are considered all together.

14 VALID-related presentations and publications

Several papers and presentations have been created reporting on the activities of the VALID project.

Two contributions that were prepared for the special issue on 25 years of the Montreal protocol have been published in the International Journal of Remote Sensing (Steinbrecht et al., 2009; van Gijssel et al., 2009b).

Results of the validation of CALIPSO have been published in ACP (Mona et al., 2009) and JGR (Pappalardo et al., 2010b).

Two papers on the validation of the GOMOS ozone data from the operational processor were published in the special issue on GOMOS in ACP (Keckhut et al., 2010; van Gijssel et al., 2010b).

Work was presented at the following conferences:

- * Quadrennial ozone symposium (Bovensmann et al., 2008a; Steinbrecht et al., 2008a; van Gijssel et al., 2008)
- * 24th International laser radar conference (Mona et al., 2008; Pappalardo et al., 2008)
- * 37th Committee on space research (Bovensmann et al., 2008b)
- * AGU Fall meeting (Hauchecorne et al., 2008; Steinbrecht et al., 2008b)
- * 5th Atmospheric limb conference (Kyrölä et al., 2009a)
- * Atmospheric science conference (Kwiatkowska et al., 2009; Kyrölä et al., 2009b; van Gijssel et al., 2009c)
- * NDACC lidar working group meeting (van Gijssel, 2009; van Gijssel et al., 2009a)
- * SPIE (Pappalardo et al., 2009a)
- * the EarthCARE workshop (Pappalardo et al., 2009b)
- * EARLINET-ASOS symposium (Mona et al., 2010a)
- * 25th International Laser Radar Conference (Pappalardo et al., 2010a)
- * European Geo-sciences Union general assembly (van Gijssel et al., 2010a)
- * ESA Living planet symposium (Kwiatkowska et al., 2010; van Gijssel et al., 2010c)

Also a document describing the possibilities for validating other kinds of atmospheric parameters with lidar was created (Swart et al., 2010).

Representing ESA as a large NDACC data user and further involved as data producer and coordinators of the VALID project partners and EARLINET, we are participating in the NDACC lidar working subgroup meeting on standardisation hosted by ISSI. This group will try to homogenise the used terminology, standardise the reported errors and its propagation and create a tool to determine vertical resolutions using the same approach. The first meeting was held end of November/beginning of December 2010. Two additional meetings are to be planned in 2011 and a full implementation of the recommendations should take place in 2012.

15 Conclusions

One of the aims of this project has been to assess the quality of ENVISAT's ozone and temperature profiles with lidar data, and check for possible dependencies on certain parameters. One of the main objectives was to make lidar ozone and temperature profiles available for validation activities. Currently over 10000 ozone and temperature lidar profiles are stored in HDF-format in the correlative database at NILU. These profiles are covering the period July 2002 until the end of 2010, and are located in several different regions.

The current status of the validation activities is that an extensive analysis of ENVISAT data has been performed for various versions of the GOMOS ozone profiles, SCIAMACHY ozone profiles and MIPAS ozone and temperature profiles. The GOMOS HRTP and bright limb ozone data have been validated on a limited data set. A complete overview of the validation status of each instrument is provided in Table 15-1 and Table 15-2. Additionally, ozone and temperature

data from ACE FTS (version 2.2 including the “ozone update”) were compared to ground-based observations.

Table 15-1: Validation status of ENVISAT Data from IPF Processor				
Legend: = complete assessment, = initial assessment				
Instrument	Ozone version		Temperature version	
GOMOS	GOPR 6.0cf, IPF 5.0	GOPR 7.0ab-de	H RTP from GOPR 6.0cf, IPF 5.0	
MIPAS FR	IPF 4.61/4.62	IPF 5.04	IPF 4.61/4.62	IPF 5.04
MIPAS OR	IPF 4.61/4.62	IPF 5.04	IPF 4.61/4.62	IPF 5.04
SCIAMACHY	IPF 3.01,	IPF 5.01	not applicable	

Table 15-2: Validation status of ENVISAT Data from ‘Scientific’ Processing		
Legend: = complete assessment, = initial assessment, = no assessment.		
Instrument	Ozone version	Temperature version
GOMOS	FMI GOMOS Bright limb 2.0	Only from prototype
MIPAS FR + OR	University of Oxford MORSE 1.00, 1.01 and 1.02	University of Oxford MORSE 1.00, 1.01 and 1.02
SCIAMACHY	Stratozone 2.2	not applicable

In the second part of VALID project, CNR-IMAA carried out dedicated studies to aerosol and cloud satellite products, involving lidar measurements from EARLINET. In the third year of this project, large differences observed in the MODIS-EARLINET comparison for Thessaloniki station were investigated and the corresponding Thessaloniki data were corrected. The MODIS comparison has been updated. In 2010 a new version of CALIPSO data was released and the software for the almost automatic EARLINET-CALIPSO comparison was updated taking into account the new parameters and the new vertical extension of the aerosol products within version 3 CALIPSO data. An example of version 2 versus version 3 comparison is reported. The comparison with OMI and MISR data at one reference station was extended to all the other Raman lidar stations of EARLINET. Finally, EARLINET Raman lidar data are used for the validation of SYNAER/ENV aerosol optical depth data.

16 References

- Ansmann, A. and Müller, D., 2005. *Lidar and atmospheric aerosol particles*. In: C. Weitkamp (Editor), *Lidar: range-resolved optical remote sensing of the atmosphere*. Springer, New York, pp. 105-141.
- Ansmann, A., Riebesell, M. and Weitkamp, C., 1990. *Measurement of atmospheric aerosol extinction profiles with a Raman lidar*. *Optics Letters*, 15 (13):746-748.
- Ansmann, A., Riebesell, M., Wandinger, U., Weitkamp, C., Voss, E., Lahmann, W. and Michaelis, W., 1992. *Combined raman elastic-backscatter LIDAR for vertical profiling of moisture, aerosol extinction, backscatter, and LIDAR ratio*. *Applied Physics B Photophysics and Laser Chemistry*, 55 (1):18-28.
- Barnes, W.L., Pagano, T.S. and Salomonson, V.V., 1998. *Prelaunch Characteristics of the Moderate Resolution Imaging Spectroradiometer (MODIS) on EOS-AM1*. *IEEE Transactions on Geoscience and Remote Sensing*, 36 (4):1088-1100.
- Böckmann, C., Miranova, D., Müller, D., Scheidenbach, L. and Nessler, R., 2005. *Microphysical aerosol parameters from multiwavelength lidar*. *Journal of the optical society of America*, 22 (3):518-528.
- Böckmann, C., Wandinger, U., Ansmann, A., Bösenberg, J., Amiridis, V., Boselli, A., Delaval, A., de Tomasi, F., Frioud, M., Grigorov, I.V., Hagard, A., Horvat, M., Iarlori, M., Komguem, L., Kreipl, S., Larchevêque, G., Matthias, V., Papayannis, A., Pappalardo, G., Rocadenbosch, F., Rodriguez, J.A., Schneider, J., Shcherbakov, V. and Wiegner, M., 2004. *Aerosol lidar intercomparison in the framework of the EARLINET project 2. Aerosol backscatter algorithms*. *Applied Optics*, 43 (4):977-989.
- Bovensmann, H., Rozanov, A., von Savigny, C., Eichmann, K.-U., Bramstedt, K., Amekudzi, L.K., Burrows, J.P., A., D., Lichtenberg, G., Gottwald, M., van Gijssel, J.A.E. and Fehr, T., 2008a. *Monitoring of stratospheric O₃ and NO₂ profiles with SCLAMACHY/ENVISAT*. Quadrennial ozone symposium, Tromso (Norway).
- Bovensmann, H., Rozanov, A., von Savigny, C., Eichmann, K.-U., Bramstedt, K., Amekudzi, L.K., Burrows, J.P., Doicu A., Lichtenberg, G., Gottwald, M., van Gijssel, J.A.E. and Fehr, T., 2008b. *Monitoring of stratospheric O₃ and NO₂ profiles with SCLAMACHY/ENVISAT*, 37th Committee on Space Research (COSPAR) Scientific Assembly., Montréal (Canada).
- di Girolamo, P., Ambrico, P.F., Amodeo, A., Boselli, A., Pappalardo, G. and Spinelli, N., 1999. *Aerosol observations by lidar in the nocturnal boundary layer*. *Applied Optics*, 38 (21):4585-4595.
- Diner, D.J., Abdou, W.A., Ackerman, T.P., Crean, K.A., Gordon, H.R., Kahn, R.A., Martonchik, J.V., McMuldroy, S., Paradise, S.R., Pinty, B., Verstraete, M.M., Wang, M. and West, R.A., 1999. *MISR level 2 aerosol retrieval algorithm theoretical basis*, Jet Propulsion Laboratory - California Institute of Technology.
- Dupuy, E., Walker, K.A., Kar, J., Boone, C.D., McElroy, C.T., Bernath, P.F., Drummond, J.R., Skelton, R., McLeod, S.D., Hughes, R.C., Nowlan, C.R., Dufour, D.G., Zou, J., Nichitiu, F., Strong, K., Baron, P., Bevilacqua, R.M., Blumenstock, T., Bodeker, G.E., Borsdorff, T., Bourassa, A.E., Bovensmann, H., Boyd, I.S., Bracher, A., Brogniez, C., Burrows, J.P., Catoire, V., Ceccherini, S., Chabrilat, S., Christensen, T., Coffey, M.T., Cortesi, U., Davies, J., De Clercq, C., Degenstein, D.A., De Mazière, M., Demoulin, P., Diodion, J., Firanski, B., Fischer, H., Forbes, G., Froidevaux, L., Fussen, D., Gerard, P., Godin-Beekmann, S., Goutail, F., Granville, J., Griffith, D., Haley, C.S., Hannigan, J.W., Höpfner, M., Jin, J.J., Jones, A., Jones, N.B., Jucks, K., Kagawa, A., Kasai, Y., Kerzenmacher, T.E., Kleinböhl, A., Klekociuk, A.R., Kramer, I., Küllmann, H., Kuttippurath, J., Kyrölä, E., Lambert, J.C., Livesey, N.J., Llewellyn, E.J., Lloyd, N.D., Mahieu, E., Manney, G.L., Marshall, B.T., McConnell, J.C., McCormick, M.P., McDermid, I.S., McHugh, M., McLinden, C.A., Mellqvist, J., Mizutani, K., Murayama, Y., Murtagh, D.P., Oelhaf, H., Parrish, A., Petelina, S.V., Piccolo, C., Pommereau, J.-P., Randall, C.E., Robert, C., Roth, C., Schneider, M., Senten, C., Steck, T., Strandberg, A., Strawbridge, K.B., Sussmann, R., Swart, D.P.J., Tarasick, D.W., Taylor, J.R., Tétard, C., Thomason, L.W., Thompson, A.M., Tully, M.B., Urban, J., Vanhellefont, F., Vigouroux,

- C., von Clarmann, T., von der Gathen, P., von Savigny, C., Waters, J.W., Witte, J.C., Wolff, M. and Zawodny, J.M., 2009. *Validation of ozone measurements from the Atmospheric Chemistry Experiment (ACE)*. Atmospheric Chemistry and Physics, 9 (2):287-343.
- Esselborn, M., Wirth, M., Fix, A., Tesche, M. and Ehret, G., 2008. *Airborne high spectral resolution lidar for measuring aerosol extinction and backscatter coefficients*. Applied Optics, 47 (3):346-358.
- Fernald, F.G., 1984. *Analysis of atmospheric lidar observations: some comments*. Applied Optics, 23 (5):652-653.
- Forster, P., Ramaswamy, V., Artaxo, P., Bernsten, T., Betts, R., Fahey, D.W., Haywood, J., Lean, J., Lowe, D.C., Myhre, G., Nganga, J., Prinn, R., Raga, G., Schulz, M. and van Dorland, R., 2007. *Changes in Atmospheric Constituents and in Radiative Forcing*. In: S. Solomon, D. Qin, M. Manning, Z. Chen, M. Marquis, K.B. Averyt, M. Tignor and H.L. Miller (Editors), Climate Change 2007: The physical science basis. Contribution of working group I to the Fourth assessment report of the Intergovernmental Panel on Climate Change. Cambridge University Press, Cambridge (United Kingdom) and New York (United States of America).
- Hassinen, S., Verronen, P., van Gijssel, J.A.E. and Pijters, A.J.M., 2010. *GOMOS Bright Limb Project - validation report*.
- Hauchecorne, A., Bertaux, J.L., Dalaudier, F., Kyrölä, E., Tamminen, J., Sofieva, V., Fussen, D., Vanhellemont, F., De Clercq, C., Lambert, J.-C., Fanton d'Andon, O., Barrot, G., Guirlet, M., Fehr, T., Saavedra de Miguel, L. and van Gijssel, A., 2008. *Highlights of six-year GOMOS observations*, AGU Fall Meeting Atmospheric Sciences [A] 0340 Middle atmosphere: composition and chemistry, 2008, San Francisco, USA.
- Hess, M., Köpke, P. and Schult, I., 1998. *Optical properties of aerosols and clouds: the software package OPAC*. Bulletin of the American Meteorological Society, 79:831-844.
- Holzer-Popp, T., Schroedter, M. and Gesell, G., 2000. *High Resolution Aerosol Maps Exploiting the Synergy of ATSR-2 and GOME*. Earth observation quarterly, 65:19-24.
- Holzer-Popp, T., Schroedter, M. and Gesell, G., 2002a. *Retrieving aerosol optical depth and type in the boundary layer over land and ocean from simultaneous GOME spectrometer and ATSR-2 radiometer measurements, 2. Case study application and validation*. Journal of geophysical research, 107 (D24).
- Holzer-Popp, T., Schroedter, M. and Gesell, G., 2002b. *Retrieving aerosol optical depth and type in the boundary layer over land and ocean from simultaneous GOME spectrometer and ATSR-2 radiometer measurements, 1. Method description*. Journal of geophysical research, 107 (D24).
- Holzer-Popp, T., Schroedter-Homscheidt, M., Breitkreuz, H., Martynenko, D. and Klüser, L., 2008. *Improvements of synergetic aerosol retrieval for ENVISAT*. Atmospheric Chemistry and Physics, 8 (24):7651-7672.
- Keckhut, P., Hauchecorne, A., Blanot, L., Hocke, K., Godin-Beekmann, S., Bertaux, J.L., Barrot, G., Kyrölä, E., van Gijssel, J.A.E. and Pazmino, A., 2010. *Mid-latitude ozone monitoring with the GOMOS-ENVISAT experiment version 5: the noise issue*. Atmospheric Chemistry and Physics, 10 (23):11839-11849.
- King, M.D., Herring, D.D. and Diner, D.J., 1995. *Earth observing system: a space-based program for assessing mankind's impact on the global environment*. Optics and Photonics News, 6 (1):34-39.
- King, M.D., Kaufman, Y.J., Menzel, W.P. and Tanré, D., 1992. *Remote sensing of cloud, aerosol, and water vapor properties from the Moderate Resolution Imaging Spectrometer (MODIS)*. IEEE Transactions on Geoscience and Remote Sensing, 30 (1):2-27.
- Klett, J.D., 1985. *Lidar inversion with variable backscatter/extinction ratios*. Applied Optics, 24 (11):1638-1643.
- Kwiatkowska, E., Fehr, T., Gessner, R., van Gijssel, A., Lambert, J.-C., Weber, M., Kirchengast, G. and van Roozendaal, M., 2010. *QA4EO for atmospheric composition measurements*, ESA living planet symposium, Bergen (Norway).
- Kwiatkowska, E., Fehr, T., van Gijssel, A., Lambert, J.-C., Oelhaf, H., Kirchengast, G., van Roozendaal, M., Lecomte, P. and Ottaviani, G., 2009. *ESA's operational atmospheric*

- validation strategy and results*, Atmospheric Science Conference. ESA SP-676. ESA, Barcelona (Spain), pp. 8.
- Kyrölä, E., Tamminen, J., Sofieva, V., Bertaux, J.L., Hauchecorne, A., Dalaudier, F., Fussen, D., Vanhellefont, F., Fanton d'Andon, O., Barrot, G., Fehr, T., Saavedra de Miguel, L., van Gijssel, J.A.E. and Fraisse, R., 2009a. *GOMOS overview 2009*, 5th Atmospheric limb conference, Helsinki (Finland).
- Kyrölä, E., Tamminen, J., Sofieva, V., Bertaux, J.L., Hauchecorne, A., Dalaudier, F., Fussen, D., Vanhellefont, F., de Clerq, C., Lambert, J.-C., Fanton d'Andon, O., Barrot, G., Guirlet, M., Fehr, T., Saavedra de Miguel, L. and van Gijssel, J.A.E., 2009b. *GOMOS/ENVISAT overview*, Atmospheric Science Conference, Barcelona (Spain).
- Liu, Z., Kuehn, R., Vaughan, M., Winker, D., Omar, A., Powell, K., Treppe, C., Hu, Y. and Hostetler, C., 2010. *The CALIPSO cloud and aerosol discrimination: version 3 algorithm and test results*, 25th International laser radar conference, St. Petersburg (Russia).
- Martonchik, J.V., Diner, D.J., Crean, K.A. and Bull, M.A., 2002. *Regional aerosol retrieval results from MISR*. IEEE transactions on geoscience and remote sensing, 40 (7):1520-1531.
- Martonchik, J.V., Diner, D.J., Kahn, R.A., Verstraete, M.M., Pinty, B., Gordon, H.R. and Ackerman, T.P., 1998. *Techniques for the retrieval of aerosol properties over land and ocean using multi-angle imaging*. IEEE transactions on geoscience and remote sensing, 36 (4):1212-1227.
- Matthias, V., Balis, D., Bösenberg, J., Eixmann, R., Iarlori, M., Komguem, L., Mattis, I., Papayannis, A., Pappalardo, G., Perrone, M.R. and Wang, X., 2004a. *Vertical aerosol distribution over Europe: Statistical analysis of Raman lidar data from 10 European aerosol research lidar network (EARLINET) stations*. J. Geophys. Res., 109 (D18201):doi:10.1029/2004JD004638.
- Matthias, V., Balis, D., Bösenberg, J., Eixmann, R., Iarlori, M., Komguem, L., Mattis, I., Papayannis, A., Pappalardo, G., Perrone, M.R. and Wang, X., 2004b. *Vertical aerosol distribution over Europe: Statistical analysis of Raman lidar data from 10 European Aerosol Research Lidar Network (EARLINET) stations*. Journal of Geophysical Research D: Atmospheres, 109 (18):D18201 18201-18212.
- Meijer, Y.J. and Swart, D.P.J., 2005a. *Envisat Quality Assessment with Lidar: Annual report 2004*, RIVM, Bilthoven.
- Meijer, Y.J., Lolkema, D.E. and Swart, D.P.J., 2005b. *Overview of EQUAL Analysis Results (in support of ESL processor upgrade verification)*, RIVM, Bilthoven.
- Meijer, Y.J., Swart, D.P.J., Allaart, M., Andersen, S.B., Bodeker, G., Boyd, I., Braathen, G., Calisesi, Y., Claude, H., Dorokhov, V., von der Gathen, P., Gil, M., Godin-Beekmann, S., Goutail, F., Hansen, G., Karpetchko, A., Keckhut, P., Kelder, H.M., Koelemeijer, R., Kois, B., Koopman, R.M., Kopp, G., Lambert, J.-C., Leblanc, T., McDermid, I.S., Pal, S., Schets, H., Stubi, R., Suortti, T., Visconti, G. and Yela, M., 2004. *Pole-to-pole validation of Envisat GOMOS ozone profiles using data from ground-based and balloon sonde measurements*. Journal of Geophysical Research, 109 (D23305):doi:10.1029/2004JD004834.
- Mona, L., Amodeo, A., Boselli, A., d'Amico, G., Madonna, F. and Pappalardo, G., 2008. *Systematic multi-wavelength Raman measurements: a reference for aerosol study*, 24th international laser radar conference, Boulder, Colorado (USA).
- Mona, L., Pappalardo, G., Amodeo, A., d'Amico, G., Madonna, F., Boselli, A., Giunta, A., Russo, F. and Cuomo, V., 2009. *One year of CNR-IMAA multi-wavelength Raman lidar measurements in coincidence with CALIPSO overpasses: Level 1 products comparison*. Atmospheric Chemistry and Physics, 9 (18):7213-7228.
- Mona, L., Balis, D., Iarlori, M., Kinne, S., Linné, H., Madonna, F., Mattis, I., Papayannis, A., Perrone, M.R., Spinelli, N. and Pappalardo, G., 2010a. *EARLINET climatology*, EARLINET-ASOS Symposium, Geneva (Switzerland), pp. in press.
- Mona, L., Balis, D., Goloub, P., Iarlori, M., Kinne, S., Li, Z., Linné, H., Madonna, F., Mattis, I., Papayannis, A., Perrone, M.R., Spinelli, N. and Pappalardo, G., 2010b. *EARLINET and AERONET: first comparison and integrated study*, 25th International Laser Radar Conference, St. Petersburg, Russia, pp. 879-882.

- Müller, D., Wandinger, U. and Ansmann, A., 1999. *Microphysical particle parameters from extinction and backscatter lidar data by inversion with regularization: theory*. Applied Optics, 38 (12):2346-2357.
- National aeronautics and space administration (NASA), 2007. *OMAERUV readme file* (http://daac.gsfc.nasa.gov/documents/OMAERUV_README_File_v3.doc).
- Pappalardo, G., Amodeo, A., Pandolfi, M., Wandinger, U., Ansmann, A., Bösenberg, J., Matthias, V., Amiridis, V., de Tomasi, F., Frioud, M., Iarlori, M., Komguem, L., Papayannis, A., Rocadenbosch, F. and Wang, X., 2004. *Aerosol lidar intercomparison in the framework of the EARLINET project. 3. Raman lidar algorithm for aerosol extinction, backscatter, and lidar ratio*. Applied Optics, 43 (28):5370-5385.
- Pappalardo, G., Wandinger, U., Mona, L., Hiebsch, A., Mattis, I., Linné, H., Apituley, A., Arboledas, L.A., Balis, D., Comeron, A., Freudenthaler, V., Giannakaki, E., Giunta, A., Rascado, J.L.G., Madonna, F., Mamouri, R.-E., Molero, F., Papayannis, A., Pujadas, M., Rocadenbosch, F., Spinelli, N., Wang, X. and Wiegner, M., 2010a. *Representativeness of aerosol measurements: EARLINET-CALIPSO correlative study*, 25th International Laser Radar Conference, St. Petersburg (Russia), pp. 883-886.
- Pappalardo, G., Mona, L., Wandinger, U., Mattis, I., Linné, H., Amodeo, A., Ansmann, A., Apituley, A., Alados Arboledas, L., Balis, D., Chaikovsky, A., Comeron, A., d'Amico, G., Freudenthaler, V., Giunta, A., Grigorov, I., Müller, D., Papayannis, A., Perrone, M.R., Pietruczuk, A., Pujadas, M., Rizi, V., Spinelli, N. and Wiegner, M., 2009a. *Analysis of the EARLINET correlative measurements for CALIPSO*, Lidar Technologies, Techniques, and Measurements for Atmospheric Remote Sensing V, SPIE meeting. proceedings of SPIE, Berlin.
- Pappalardo, G., Bösenberg, J., Amodeo, A., Ansmann, A., Apituley, A., Arboledas, L.A., Balis, D., Bockman, C., Comeron, A., d'Amico, G., Freudenthaler, V., Grigorov, I., Hansen, G., Linné, H., Mattis, I., Mona, L., Müller, D., Mitev, V., Nicolae, D., Papayannis, A., Perrone, M.R., Pietruczuk, A., Pujadas, M., Putaud, J.-P., Ravetta, F., Rizi, V., Simeonov, V., Spinelli, N., Trickl, T., Wandinger, U. and Wiegner, M., 2008. *EARLINET for long term observations of aerosol over Europe*, 24th international laser radar conference, Boulder, Colorado (USA).
- Pappalardo, G., Wandinger, U., Mona, L., Mattis, I., Hiebsch, A., Amodeo, A., Ansmann, A., Linné, H., Apituley, A., Alados Arboledas, L., Balis, D., Chaikovsky, A., d'Amico, G., de Tomasi, F., Freudenthaler, V., Giannakaki, E., Giunta, A., Grigorov, I., Iarlori, M., Madonna, F., Mamouri, R.-E., Molero, F., Papayannis, A., Perrone, M.R., Pietruczuk, A., Rizi, V., Rocadenbosch, F., Schnell, F., Spinelli, N., Wang, X. and Wiegner, M., 2009b. *The EARLINET contribution to the EARTHCARE mission*, The EarthCARE workshop, Kyoto.
- Pappalardo, G., Wandinger, U., Mona, L., Hiebsch, A., Mattis, I., Amodeo, A., Ansmann, A., Seifert, P., Linne, H., Apituley, A., Arboledas, L.A., Balis, D., Chaikovsky, A., d'Amico, G., de Tomasi, F., Freudenthaler, V., Giannakaki, E., Giunta, A., Grigorov, I., Iarlori, M., Madonna, F., Mamouri, R.-E., Nasti, L., Papayannis, A., Pietruczuk, A., Pujadas, M., Rizi, V., Rocadenbosch, F., Russo, F., Schnell, F., Spinelli, N., Wang, X. and Wiegner, M., 2010b. *EARLINET correlative measurements for CALIPSO: first intercomparison results*. Journal of geophysical research, 115 (D00H19):doi:10.1029/2009JD012147.
- Steinbrecht, W., Claude, H., Schönenborn, F., McDermid, I.S., Leblanc, T., Godin, S., Keckhut, P., van Gijsel, J.A.E., Swart, D.P.J., Bodeker, G.E., Parrish, A., Boyd, I.S., Kämpfer, N., Hocke, C., Stolarski, R.S., Frith, S.M., Thomason, L.W., Remsberg, E.E., von Savigny, C. and Burrows, J.P., 2009. *Ozone and temperature trends in the upper stratosphere at five stations of the Network for the Detection of Atmospheric Composition Change*. International Journal of Remote Sensing, 30 (15):3875-3886.
- Steinbrecht, W., Claude, H., Schönenborn, F., McDermid, I.S., Leblanc, T., Godin-Beekmann, S., Keckhut, P., Hauchecorne, A., van Gijsel, J.A.E., Swart, D.P.J., Bodeker, G., Parrish, A., Boyd, I.S., Kämpfer, N., Hocke, K., Stolarski, R.S., Frith, S.M., Thomason, L.W., Remsberg, E.E., von Savigny, C., Burrows, J.P., Eyring, V. and Shepherd, T.G., 2008a.

- Ozone and temperature trends in the upper stratosphere at five stations of the Network for the detection of atmospheric composition change*, Quadrennial ozone symposium, Tromso (Norway).
- Steinbrecht, W., Claude, H., Schöenborn, F., McDermid, S., Leblanc, T., Godin-Beekmann, S., Keckhut, P., Hauchecorne, A., van Gijssel, J.A., Swart, D.P., Bodeker, G.E., Parrish, A., Boyd, I.S., Kämpfer, N., Hocke, K., Stolarski, R.S., Frith, S., Thomason, L.W., Remsberg, E.E., von Savigny, C., Burrows, J.P., Eyring, V. and Shepherd, T.G., 2008b. *Ozone and temperature trends in the upper stratosphere at five stations of the Network for the detection of atmospheric composition change*, AGU Fall Meeting Atmospheric Sciences [A] 0340 Middle atmosphere: composition and chemistry / 0394 Instruments and techniques / 1610 Atmosphere (0315, 0325) / 1616 Climate variability (1635, 3305, 3309, 4215, 4513), San Francisco (USA).
- Swart, D.P.J. and van Gijssel, J.A.E., 2010. *Review of possibilities for satellite validation by groundbased lidar systems*, RIVM, Bilthoven.
- Tukiainen, S., Kyrölä, E., Verronen, P.T., Fussen, D., Blanot, L., Barrot, G., Hauchecorne, A. and Lloyd, N., 2010. *Retrieval of ozone profiles from GOMOS limb scattered measurements*. Atmospheric measurement techniques discussions, 3 (5):4355-4382.
- van Gijssel, J.A.E., 2009. *GOMOS versus NDACC*, NDACC lidar working group meeting 2009, Nottawasaga (Canada).
- van Gijssel, J.A.E. and Swart, D.P.J., 2009a. *VALID: satellite validation with lidar*, NDACC lidar working group meeting 2009, Nottawasaga (Canada).
- van Gijssel, J.A.E., Swart, D.P.J. and the VALID team, 2010a. *Validation of GOMOS, SCLAMACHY and MIPAS ozone and temperature profiles with lidar measurements*, European Geosciences Union general assembly 2010, Vienna (Austria).
- van Gijssel, J.A.E., Swart, D.P.J., Baray, J.-L., Claude, H., Fehr, T., von der Gathen, P., Godin-Beekmann, S., Hansen, G.H., Leblanc, T., McDermid, I.S., Nakane, H., Quel, E., Steinbrecht, W., Strawbridge, K.B. and Wolfram, E., 2008. *Pole-to-pole validation of ENVISAT ozone profiles using data from lidar measurements*, Quadrennial ozone symposium, Tromso (Norway).
- van Gijssel, J.A.E., Swart, D.P.J., Baray, J.-L., Claude, H., Fehr, T., von der Gathen, P., Godin-Beekmann, S., Hansen, G., Leblanc, T., McDermid, I.S., Meijer, Y.J., Nakane, H., Quel, E., Steinbrecht, W., Strawbridge, K.B., Tatarov, B. and Wolfram, E., 2009b. *Global validation of ENVISAT ozone profiles using lidar measurements*. International Journal of Remote Sensing, 30 (15):3987-3994.
- van Gijssel, J.A.E., Swart, D.P.J., Baray, J.-L., Bencherif, H., Claude, H., Dudhia, A., Fehr, T., Godin-Beekmann, S., Hansen, G.H., Leblanc, T., McDermid, I.S., Nakane, H., Quel, E., Stebel, K., Steinbrecht, W., Strawbridge, K.B. and Tatarov, B., 2009c. *Satellite validation with lidar*, Atmospheric Science Conference. ESA SP-676, Barcelona (Spain), pp. 4.
- van Gijssel, J.A.E., Swart, D.P.J., Baray, J.L., Bencherif, H., Claude, H., Fehr, T., Godin-Beekmann, S., Hansen, G.H., Keckhut, P., Leblanc, T., McDermid, I.S., Meijer, Y.J., Nakane, H., Quel, E.J., Stebel, K., Steinbrecht, W., Strawbridge, K.B., Tatarov, B.I. and Wolfram, E.A., 2010b. *GOMOS ozone profile validation using ground-based and balloon sonde measurements*. Atmospheric Chemistry and Physics, 10 (21):10473-10488.
- van Gijssel, J.A.E., Swart, D.P.J., Baray, J.-L., Claude, H., Fehr, T., Gathen, P.v.d., Godin-Beekmann, S., Gumbel, J., Hansen, G.H., Keckhut, P., Kwiatkowska, E., Leblanc, T., Bellevue, J.L.d., Maturilli, M., McDermid, I.S., Nakane, H., Quel, E.J., Steinbrecht, W., Strawbridge, K.B., Tatarov, B. and Wolfram, E.A., 2010c. *Long-term multi-mission validation of ozone and temperature profiles by the Validation with Lidar (VALID) project*, ESA living planet symposium, Bergen (Norway).
- Veihelmann, B. and Veeffkind, J.P., 2009. *OMAERO README File 2009*, available at http://disc.sci.gsfc.nasa.gov/Aura/data-holdings/OMI/omaero_v003.shtml.
- Veselovskii, I., Kolgotin, A., Griaznov, V., Müller, D., Wandinger, U. and Whiteman, D.N., 2002. *Inversion with regularization for the retrieval of tropospheric aerosol parameters from multiwavelength lidar sounding*. Applied Optics, 41 (18):3685-3699.

- Wandinger, U. and Ansmann, A., 2002. *Experimental determination of the lidar overlap profile with Raman lidar*. Applied Optics, 41 (3):511-514.
- Winker, D.M., Hunt, W.H. and McGill, M.J., 2007. *Initial performance assessment of CALIOP*. Geophysical research letters, 34 (L19803):doi:10.1029/2007GL030135.

17 Appendix 1: Overview of submission statistics - tables

In this section we give an overview of the lidar data submitted to the ENVISAT Cal/Val database at NILU in table format. In Table 17-1 we present the number of days (661) with measurements during the Commissioning Phase of ENVISAT, and most of these data have been submitted prior to the VALID project. In Table 17-2 we present the statistics for the data measured in 2003. Although the VALID project formally started in January 2004, the project partners additionally contributed data of 2003 and hence filled the gap between the end of the Commissioning Phase and the start of the project, which is a bonus for the project and amounts in total an extra 1259 days with measurements. In Table 17-3 we present the data measured in 2004, which come to a total of 1385 days. In Table 17-4 we present the data measured in 2005, which come to a total of 1287 days with measurements. In Table 17-5 we present the data measured in 2006, which now come to a total of 1331 days with measurements submitted to the database and Table 17-6 presents the data from 2007 with a total of 1226 measurements. In Table 17-7, the data for 2008 is presented with a total of 1234 measurements and for 2009 825 profiles have been submitted so far (Table 17-8).

Note that not all data has been submitted yet and that some differences for previous years can be found when comparing with the annual reports (2004-2006 and 2008) and EQUAL final report (2007) due to new submissions and re-processing.

Station	System	Jul.	Aug.	Sept.	Oct.	Nov.	Dec.	Total
ALO	NILU001	0	0	7	11	13	8	39
ALO	NILU002	0	0	4	6	10	9	29
ESR	UBONN003	10	19	0	0	0	0	29
HOH	DWD001	5	7	8	4	6	3	33
HOH	DWD002	5	8	8	4	6	3	34
LAR	LPA001	0	0	2	0	0	0	2
LAR	LPA002	7	5	8	7	0	0	27
LAU	RIVM002	10	13	9	8	6	2	48
LAU	RIVM003	0	0	0	0	0	0	0
MLO	CNRS.SA004	9	15	15	3	10	9	61
MLO	CNRS.SA005	14	15	15	3	10	9	66
NYA	AWI001	0	0	0	11	6	11	28
NYA	AWI002	0	0	0	5	3	12	20
OHP	l_CNRS.SA001	13	15	14	10	11	6	69
OHP	r_CNRS.SA001	7	0	3	9	12	9	40
TMF	CNRS.SA003	13	16	2	9	11	10	61
TMF	CNRS.SA002	13	17	2	9	13	16	70
TOR	MSC001	2	0	1	2	0	0	5
TOTAL all systems		108	130	98	101	117	107	661

Note that submission of data for Lauder (temperature) is still foreseen after completion of the temperature retrieval scripts. The system in Toronto broke down in 2002 and has not been submitting measurements beyond 2002.

Table 17-2. Data submission statistics, 2003 (in grey temperature lidar systems)

Station	System	Jan.	Feb.	Mar.	Apr.	May	Jun.	Jul.	Aug.	Sept.	Oct.	Nov.	Dec.	Total
ALO	NILU001	4	5	11	12	0	0	0	0	3	6	1	4	50
ALO	NILU002	4	3	7	12	0	0	0	1	3	5	1	4	32
ESR	UBONN003	9	1	0	0	0	0	4	0	1	1	0	0	32
HOH	DWD001	3	7	10	10	8	6	9	9	8	9	4	10	108
HOH	DWD002	4	7	10	10	8	6	9	9	8	9	4	10	111
LAR	LPA001	0	0	0	0	0	2	5	0	3	0	1	1	0
LAR	LPA002	2	8	11	11	7	15	6	5	14	12	9	5	90
LAU	RIVM002	7	8	7	9	5	5	11	8	9	11	3	2	59
LAU	RIVM003	0	0	0	0	0	0	0	0	0	0	0	0	0
MLO	CNRS.SA004	16	10	13	5	End	-	-	-	-	-	-	-	44
MLO	NASA.JPL001	-	-	-	Start	12	15	13	11	13	0	11	8	83
MLO	CNRS.SA005	16	10	14	5	End	-	-	-	-	-	-	-	45
MLO	NASA.JPL002	-	-	Start	1	14	15	13	11	16	8	11	8	97
NYA	AWI001	0	0	0	0	0	0	0	0	0	0	8	6	35
NYA	AWI002	13	9	0	0	0	0	0	0	0	0	3	2	41
OHP	l_CNRS.SA001	11	11	15	10	12	5	11	14	17	2	11	7	84
OHP	r_CNRS.SA001	3	9	17	13	12	15	15	0	11	8	14	7	111
TMF	CNRS.SA003	10	5	13	7	End	-	-	-	-	-	-	-	35
TMF	NASA.JPL003	-	-	-	Start	9	12	1	5	9	13	7	7	63
TMF	CNRS.SA002	14	5	13	8	End	-	-	-	-	-	-	-	40
TMF	NASA.JPL004	-	-	Start	1	10	13	3	5	9	14	9	8	72
TSU	NIES001	3	5	3	2	0	0	0	0	0	0	0	2	15
TSU	NIES002	3	4	1	2	0	0	0	0	0	0	0	2	12
TOTAL all systems		172	138	115	65	79	90	75	92	110	97	114	112	1259

Table 17-3. Data submission statistics, 2004 (in grey temperature lidar systems)														
Station	System	Jan.	Feb.	Mar.	Apr.	May	Jun.	Jul.	Aug.	Sept.	Oct.	Nov.	Dec.	Total
ALO	NILU001	4	5	11	12	0	0	0	0	3	6	1	4	46
ALO	NILU002	4	3	7	12	0	0	0	1	3	5	1	4	40
ESR	UBONN003	9	1	0	0	0	0	4	0	1	1	0	0	16
EUR	MSC003	0	9	5	0	0	0	0	0	0	0	0	0	14
EUR	MSC004	0	9	5	0	0	0	0	0	0	0	0	0	14
HOH	DWD001	3	7	10	10	8	6	9	9	8	9	4	10	93
HOH	DWD002	4	7	10	10	8	6	9	9	8	9	4	10	94
LAR	LPA001	0	0	0	0	0	2	5	0	3	0	1	1	12
LAR	LPA002	2	8	11	11	7	15	6	5	14	12	9	5	105
LAU	RIVM002	7	8	7	9	5	5	11	8	9	11	5	3	88
LAU	RIVM003	0	0	0	0	0	0	0	0	0	0	0	0	0
MLO	NASA.JPL001	10	11	7	12	11	14	14	15	15	9	10	9	137
MLO	NASA.JPL002	10	11	7	12	11	14	14	15	15	9	10	9	137
NYA	AWI001	0	0	0	0	0	0	0	0	0	0	8	6	14
NYA	AWI002	13	9	0	0	0	0	0	0	0	0	3	2	27
OHP	l_CNRS.SA001	11	11	15	10	12	5	11	14	17	2	11	7	126
OHP	r_CNRS.SA001	3	9	17	13	12	15	15	0	11	8	14	7	124
TMF	NASA.JPL003	8	8	14	7	8	10	11	2	10	5	7	6	96
TMF	NASA.JPL004	12	8	14	13	13	17	12	4	11	9	10	10	133
TSU	NIES001	4	3	2	4	4	2	3	3	4	6	3	4	42
TSU	NIES002	2	0	1	3	1	2	2	3	3	5	1	4	27
TOTAL	all systems	106	127	143	138	100	113	126	88	135	106	102	101	1385

Table 17-4: Data submission statistics, 2005 (in grey temperature lidar systems)

Station	System	Jan.	Feb.	Mar.	Apr.	May	Jun.	Jul.	Aug.	Sept.	Oct.	Nov.	Dec.	Total
ALO	NILU001	6	6	1	4	1	0	2	1	1	3	8	9	42
ALO	NILU002	6	6	1	2	0	0	0	0	1	3	7	8	34
DDU	CNRS.SA007	0	0	0	0	0	0	0	0	0	0	0	0	0
DDU	RMR_CNRS.SA002	0	0	0	0	0	0	0	0	0	0	0	0	0
ESR	UBONN003	7	0	0	0	0	0	14	1	0	0	0	0	22
EUR	MSC003	0	5	4	0	0	0	0	0	0	0	0	0	9
EUR	MSC004	0	5	4	0	0	0	0	0	0	0	0	0	9
HOH	DWD001	8	3	8	8	6	6	9	7	9	16	5	6	91
HOH	DWD002	8	3	8	8	6	6	9	7	9	17	5	6	92
LAR	LPA001	0	2	2	1	0	0	0	0	0	0	2	3	10
LAR	LPA002	5	11	5	6	16	17	6	10	16	11	4	1	108
LAU	RIVM002	5	5	5	5	2	4	6	5	5	5	6	3	56
LAU	RIVM003	0	0	0	0	0	0	0	0	0	0	0	0	0
MLO	NASA.JPL001	13	9	12	11	13	10	5	16	14	16	8	10	137
MLO	NASA.JPL002	13	9	13	11	13	10	5	16	14	16	8	10	138
NYA	AWI001	0	0	3	0	0	0	0	0	0	0	0	0	3
NYA	AWI002	4	2	3	0	0	0	0	0	0	0	0	0	9
OHP	l_CNRS.SA001	17	17	4	4	8	10	11	9	10	3	9	11	113
OHP	r_CNRS.SA001	18	18	16	17	9	9	15	15	20	6	14	16	173
RGa	CEILAP001	0	0	0	0	0	0	0	9	10	6	4	0	29
TMF	NASA.JPL003	5	4	9	1	5	12	7	3	8	14	12	4	84
TMF	NASA.JPL004	6	8	12	2	10	14	8	3	10	14	12	7	106
TSU	NIES001	4	0	2	0	1	0	1	2	2	1	0	0	13
TSU	NIES002	4	0	1	0	0	0	1	1	1	1	0	0	9
TOTAL	all systems	129	113	113	80	90	98	99	105	130	132	104	94	1287

Table 17-5: Data submission statistics, 2006 (in grey temperature lidar systems)

Station	System	Jan.	Feb.	Mar.	Apr.	May	Jun.	Jul.	Aug.	Sept.	Oct.	Nov.	Dec.	Total
ALO	NILU001	3	4	10	2	0	0	0	2	5	8	2	2	38
ALO	NILU002	3	4	9	1	0	0	0	2	5	8	1	1	34
DDU	CNRS.SA007	0	0	0	0	0	0	0	0	0	0	0	0	0
DDU	RMR_CNRS.SA002	0	0	0	0	0	0	0	0	0	0	0	0	0
ESR	UBONN003	9	0	0	0	0	0	0	12	0	0	0	0	21
EUR	CARE.EC.STB001	0	5	0	0	0	0	0	0	0	0	0	0	5
EUR	CARE.EC.STB002	0	5	0	0	0	0	0	0	0	0	0	0	5
HOH	DWD001	10	4	5	5	9	8	12	4	8	11	5	10	91
HOH	DWD002	10	4	7	5	9	8	12	4	8	11	5	10	93
LAR	LPA001	1	1	5	4	5	2	0	0	0	0	0	1	19
LAR	LPA002	0	7	1	0	5	16	9	13	15	18	12	3	99
LAU	RIVM002	6	5	5	5	6	6	6	6	4	6	5	4	64
LAU	RIVM003	0	0	0	0	0	0	0	0	0	0	0	0	0
MLO	NASA.JPL001	13	0	3	10	14	14	16	18	15	12	12	11	138
MLO	NASA.JPL002	14	0	3	10	14	14	16	18	15	12	12	11	139
NYA	AWI001	0	0	0	0	0	0	0	0	0	0	0	0	0
NYA	AWI002	0	0	0	0	0	0	0	0	0	0	0	0	0
OHP	l_CNRS.SA001	12	7	9	12	11	14	9	14	15	10	14	11	138
OHP	r_CNRS.SA001	15	13	13	15	13	17	12	18	17	15	14	13	175
RGH	CEILAP001	1	1	3	5	5	3	1	8	6	12	3	3	51
TMF	NASA.JPL003	8	8	3	6	10	6	9	13	11	8	7	0	89
TMF	NASA.JPL004	9	9	6	8	12	6	9	13	11	9	11	0	103
TSU	NIES001	1	1	1	2	0	0	0	0	0	4	5	4	18
TSU	NIES002	1	0	1	0	0	0	0	0	0	2	4	2	4
TOTAL	all systems	116	78	84	90	113	114	111	145	135	146	112	86	1331

Table 17-6: Data submission statistics, 2007 (in gray temperature lidar systems)

Station	System	Jan.	Feb.	Mar.	Apr.	May	Jun.	Jul.	Aug.	Sept.	Oct.	Nov.	Dec.	Total
ALO	NILU001	3	10	3	2	0	0	0	0	0	1	3	3	25
ALO	NILU002	2	10	2	1	0	0	0	0	0	0	3	2	20
DDU	CNRS.SA007	0	0	0	0	0	0	0	0	0	0	0	0	0
DDU	RMR_CNRS.SA002	0	0	0	0	0	0	0	0	0	0	0	0	0
ESR	UBONN003	0	2	6	0	0	0	1	5	0	0	0	0	14
EUR	CARE.EC.STB001	0	5	3	0	0	0	0	0	0	0	0	0	8
EUR	CARE.EC.STB002	0	5	3	0	0	0	0	0	0	0	0	0	8
HOH	DWD001	6	7	7	16	9	3	8	10	7	7	8	10	98
HOH	DWD002	6	7	8	16	9	3	8	10	8	7	8	10	100
LAR	LPA001	0	0	0	0	0	0	0	0	0	0	0	0	0
LAR	LPA002	3	8	17	15	19	20	21	24	15	14	20	15	191
LAU	RIVM002	6	4	6	5	6	5	5	6	3	4	6	4	60
LAU	RIVM003	0	0	0	0	0	0	0	0	0	0	0	0	0
MLO	NASA.JPL001	8	8	9	11	10	10	14	14	9	11	8	1	113
MLO	NASA.JPL002	8	8	9	12	10	11	14	14	9	11	8	2	116
NYA	AWI001	0	0	0	0	0	0	0	0	0	0	0	0	0
NYA	AWI002	0	0	0	0	0	0	0	0	0	0	0	0	0
OHP	l_CNRS.SA001	15	14	6	6	2	0	8	10	8	11	10	13	103
OHP	r_CNRS.SA001	6	17	16	15	17	16	1	0	18	20	16	10	152
RGH	CEILAP001	2	2	3	0	0	0	1	6	4	6	3	2	29
TMF	NASA.JPL003	2	2	4	8	10	5	4	10	1	7	5	7	65
TMF	NASA.JPL004	2	2	4	8	10	8	0	10	4	10	10	7	75
TSU	NIES001	3	7	4	1	0	0	0	1	0	2	4	4	26
TSU	NIES002	3	6	3	1	0	0	0	1	0	2	4	3	23
TOTAL	all systems	75	124	113	117	102	81	85	121	86	113	116	93	1226

Table 17-7: Data submission statistics, 2008 (in gray temperature lidar systems)														
Station	System	Jan.	Feb.	Mar.	Apr.	May	Jun.	Jul.	Aug.	Sept.	Oct.	Nov.	Dec.	Total
ALO	NILU001	9	4	6	5	0	0	0	0	5	2	0	1	32
ALO	NILU002	2	0	2	4	0	0	0	0	4	1	0	1	14
DDU	CNRS.SA007	0	0	9	11	11	18	10	7	13	16	0	0	95
DDU	RMR_CNRS.SA002	0	7	9	13	11	18	11	8	13	16	0	0	106
ESR	MISU001	11	0	0	0	0	2	5	0	0	4	0	0	22
EUR	CARE.EC.STB001	0	7	4	0	0	0	0	0	0	0	0	0	11
EUR	CARE.EC.STB002	0	7	4	0	0	0	0	0	0	0	0	0	11
HOH	DWD001	9	9	5	7	8	8	7	9	5	10	8	6	91
HOH	DWD002	9	9	5	7	8	8	7	9	5	10	8	6	91
LAR	LPA001	0	0	0	0	0	0	0	0	0	0	0	0	0
LAR	LPA002	5	13	0	6	17	8	0	7	16	11	24	14	121
LAU	RIVM002	6	5	6	6	4	5	2	6	6	6	5	4	61
LAU	RIVM003	0	0	0	0	0	0	0	0	0	0	0	0	0
MLO	NASA.JPL001	10	7	15	10	14	12	12	14	13	7	8	10	132
MLO	NASA.JPL002	10	7	15	10	14	12	12	14	13	7	8	10	132
NYA	AWI002	2	2	1	0	0	0	0	0	0	1	0	0	6
OHP	l_CNRS.SA001	9	5	11	11	4	0	7	11	6	12	6	8	90
OHP	r_CNRS.SA001	8	17	12	4	0	0	0	8	13	12	0	4	78
RGA	CEILAP001	0	1	1	3	1	1	0	2	7	11	4	1	32
TMF	NASA.JPL003	7	11	7	16	9	4	10	10	7	4	3	6	94
TMF	NASA.JPL004	7	11	8	16	9	4	11	11	7	12	5	6	107
TSU	NIES001	2	5	1	1	1	0	0	0	0	2	0	2	14
TSU	NIES002	2	5	1	1	1	0	0	0	0	0	0	0	10
TOTAL all systems		108	132	122	131	112	100	94	116	133	144	79	79	1350

Table 17-8: Data submission statistics, 2009 (in gray temperature lidar systems)

Station	System	Jan.	Feb.	Mar.	Apr.	May	Jun.	Jul.	Aug.	Sept.	Oct.	Nov.	Dec.	Total
ALO	NILU001	7	2	2	0	0	0	0	0	1	2	9	2	25
ALO	NILU002	7	2	2	0	0	0	0	0	1	2	9	2	25
DDU	CNRS.SA007	0	0	6	11	4	0	5	3	7	15	0	0	51
DDU	RMR_CNRS.SA002	0	0	6	11	4	0	5	3	7	16	0	0	52
ESR	MISU001	5	0	0	0	0	0	0	0	0	6	0	0	11
EUR	CARE.EC.STB001	0	14	5	0	0	0	0	0	0	0	0	0	19
EUR	CARE.EC.STB002	0	14	5	0	0	0	0	0	0	0	0	0	19
HOH	DWD001	7	6	2	11	8	6	9	12	10	0	8	3	82
HOH	DWD002	7	6	2	12	8	6	10	12	10	5	8	3	89
LAR	LPA001	0	0	0	0	0	0	0	0	0	0	0	0	0
LAR	LPA002	8	6	0	7	0	0	4	14	0	0	0	0	39
LAU	RIVM002	6	5	6	5	2	4	5	4	3	4	5	1	50
LAU	RIVM003	0	0	0	0	0	0	0	0	0	0	0	0	0
MLO	NASA.JPL001	14	7	9	6	14	15	10	12	14	8	8	10	127
MLO	NASA.JPL002	14	7	9	6	14	15	10	12	14	8	8	10	127
NYA	AWI002	2	0	0	0	0	0	0	0	0	0	0	0	2
OHP	l_CNRS.SA001	11	12	3	12	9	10	11	16	11	9	5	4	113
OHP	r_CNRS.SA001	13	13	12	12	11	10	14	12	3	0	3	9	112
RGA	CEILAP001	1	1	6	2	1	3	4	4	7	8	7	2	46
TMF	NASA.JPL003	12	10	7	5	7	8	6	6	4	13	4	2	84
TMF	NASA.JPL004	13	10	7	5	7	8	6	7	2	13	4	3	85
TSU	NIES001	0	3	3	5	0	0	0	0	0	0	0	0	11
TSU	NIES002	0	0	0	0	0	0	0	0	0	0	0	0	0
TOTAL all systems		127	118	92	110	89	85	99	117	94	109	78	51	1169

Note that submissions of data for Lauder (temperature) and La Reunion (temperature) are still foreseen.

Table 17-9: Data submission statistics, 2010 (in gray temperature lidar systems)

Station	System	Jan.	Feb.	Mar.	Apr.	May	Jun.	Jul.	Aug.	Sept.	Oct.	Nov.	Dec.	Total
ALO	NILU001	6	8	5	1	0	0	0	0	1	0	2	4	27
ALO	NILU002	6	8	5	1	0	0	0	0	1	0	2	4	27
DDU	CNRS.SA007	0	2	9	11	11	5	3	0	0	0	0	0	41
DDU	RMR_CNRS.SA002	0	2	10	11	11	5	3	0	0	0	0	0	42
ESR	MISU001	7	0	2	0	0	0	0	0	0	0	0	0	9
EUR	CARE.EC.STB001	0	0	0	0	0	0	0	0	0	0	0	0	0
EUR	CARE.EC.STB002	0	0	0	0	0	0	0	0	0	0	0	0	0
HOH	DWD001	6	5	5	6	3	9	9	7	7	9	8	4	78
HOH	DWD002	6	4	5	6	2	8	9	5	6	8	7	4	70
LAR	LPA001	0	0	0	0	0	0	0	0	0	0	0	0	0
LAR	LPA002	0	0	0	0	0	0	0	0	0	0	0	0	0
LAU	RIVM002	4	4	4	5	4	3	4	4	1	3	3	2	41
LAU	RIVM003	0	0	0	0	0	0	0	0	0	0	0	0	0
MLO	NASA.JPL001	8	7	3	5	8	7	7	7	12	0	8	5	77
MLO	NASA.JPL002	8	7	3	5	8	7	7	7	12	0	8	5	77
NYA	AWI002	0	0	0	0	0	0	0	0	0	0	0	0	0
OHP	l_CNRS.SA001	9	9	8	13	14	8	14	15	8	7	0	7	112
OHP	r_CNRS.SA001	11	0	0	5	11	9	19	4	0	0	0	0	59
RGA	CEILAP001	0	4	7	3	5	1	0	2	1	6	5	0	34
TMF	NASA.JPL003	0	0	0	7	0	8	4	2	4	5	9	3	42
TMF	NASA.JPL004	0	0	2	7	0	8	4	2	4	5	9	3	44
TSU	NIES001	3	3	0	0	0	0	0	0	0	0	0	0	6
TSU	NIES002	0	0	0	0	0	0	0	0	0	0	0	0	0
TOTAL all systems		74	63	68	86	77	78	83	55	57	43	61	41	786

Note that submissions of data for Alomar (T & O₃) Lauder (temperature), OHP (ozone) and La Reunion (temperature) are still foreseen.

18 Appendix 2: EARLINET AOD data

The main products contained in the EARLINET database are the aerosol extinction and backscatter profiles. Together with these quantities, the top altitude of the PBL + residual layer is provided (Matthias et al., 2004) and the lidar ratio profile is reported when the aerosol extinction and backscatter profiles are obtained independently. Additional information, as depolarization ratio profiles, is provided when available.

Details about the backscatter coefficient determination in conjunction or without extinction measurements are beyond the aim of this report and can be found in literature (Klett 1985; Fernald 1984; Di Girolamo et al., 1989; Ansmann et al., 1992). The method for extinction calculation with Raman lidar techniques is instead here shortly reported for the sake of completeness.

The lidar signal detected at the wavelength corresponding to the N₂ Raman shifted wavelength for a monostatic lidar is:

$$P(z) = \frac{C}{z^2} N(z) \sigma_{Ram}(z) \exp \left\{ - \int_0^z [\alpha_{mol}(\lambda_0, z') + \alpha_{aer}(\lambda_0, z') + \alpha_{mol}(\lambda_R, z') + \alpha_{aer}(\lambda_R, z')] dz' \right\}$$

where $P(z)$ is the power received from distance z at the Raman wavelength λ_R if the laser pulse is transmitted at λ_0 , $N(z)$ is the atmospheric number density, α_{mol} and α_{aer} are the extinction coefficients due to absorption and Rayleigh scattering by atmospheric gases and by the atmospheric aerosol, respectively.

At each altitude, the only unknown of this equation is the particle extinction coefficient that can be obtained by a simple derivative computation (Ansmann et al., 1990):

$$\alpha_{aer}(\lambda_0, z) = \frac{\frac{d}{dz} \left\{ \ln \left[\frac{N(z)}{z^2 P(z)} \right] \right\} - \alpha_{mol}(\lambda_0, z) - \alpha_{mol}(\lambda_R, z)}{1 + \left(\frac{\lambda_0}{\lambda_R} \right)^k}$$

where particle scattering is assumed to be proportional to λ^{-k} .

Intercomparison among the different computational procedures for the aerosol extinction calculation was performed within EARLINET showing that these differences lead to a discrepancies in the retrieved aerosol extinction profiles lower than 15% in the PBL and however lower than $5 \cdot 10^{-5} \text{ m}^{-1}$ (Pappalardo et al., 2004a).

For collecting a database of AOD values, aerosol optical depth is calculated from each extinction profile of the EARLINET database, integrating the aerosol extinction profile over the whole column. In case of cirrus cloud presence (highlighted by the presence of corresponding file also in the cirrus EARLINET data category), the altitude range interested by the presence of the cirrus is discarded by the AOD computation because it is not representative of the aerosol content.

Finally, in the AOD calculation from lidar measurements it has to be taken into account that the first altitude range sounded by a lidar is limited by the altitude range where full overlap between laser beam and telescope field of view is reached. This altitude strongly depends on the specific details of the instrumental set-up and it largely varies within the EARLINET network (Matthias et al., 2004a) and can range between 400 m up to 2.5 km depending on the receiving system and laser beam divergence. In Raman system (all stations providing extinction profiles are necessary Raman stations), it is possible to find out a correction function for the overlap region which permits to extend extinction profiles into lower altitudes (Wandinger et al., 2002). It is

responsibility of each station to provide profiles to the EARLINET database, down to the lowest reliable altitude range. Aerosol extinction profiles typically start above the first hundreds of meters above the lidar station. For example, at Potenza station the full overlap between the transmitted laser beam and the telescope field of view is reached at about 0.8 km above the lidar station. Thanks to the Wandinger and Ansmann correction, the aerosol extinction coefficient can be calculated from 500 m above the lidar station.

For the calculation of the total column aerosol optical depth, it is considered that the aerosol extinction is constant in the lowest part of the atmosphere because of the well mixed conditions typically observed in the first night-time hours. In the following this approach is referred as Approach 1. The total columnar aerosol optical depth as calculated by aerosol extinction profiles is:

$$AOD = \alpha_{aer}(\lambda_o, z_0) \cdot (z_0 - z_{station}) + \int_{z_0}^z \alpha_{aer}(\lambda_o, z') dz'$$

where $z_{station}$ is the altitude above the sea level of the station and z_0 is the lowest height a.s.l. where extinction coefficient is retrieved.

The contribution of the overlap region to the evaluated columnar AOD is on average about 40% with the assumption of well mixed conditions below the lowest overlap altitude. This assumption is however unreliable if the first altitude range sounded by a lidar is high, i.e. if it is above the mixed+ residual layer top altitude.

This is what happened for the Thessaloniki data starting from July 2001, when an upgrade of the system in terms of optical interferential filters occurred. This upgrade caused a dramatic change in the overlap function of the Thessaloniki lidar system. In particular the first reliable data point in the aerosol extinction profile was at 1500 m. In cases like this, where the overlap causes the profile to start above the local planetary boundary layer (well mixed altitude range in night-time conditions), the standard assumption of constant extinction profile below the first available data-point (z_0) could be highly unreliable. The aerosol backscatter profile retrieved by elastic/Raman method permits to investigate lower altitude ranges beneath the overlap because it is retrieved by the ratio between 2 lidar signals. In this way, the appropriateness of mixed condition assumption is checked. Where unreliable, the extinction profile below (z_0) is obtained as the backscatter profile multiplied for the lowest in altitude reliable lidar ratio value down to the first available backscatter data-point. Below this point a mixed condition assumption is applied. In the following this approach is referred as Approach 2. The same approach is applied whenever overlap corrections are not available. If no lower in altitude data-points are available from the backscatter profile, the AOD can only be estimated by assuming a constant extinction profile down to the ground.

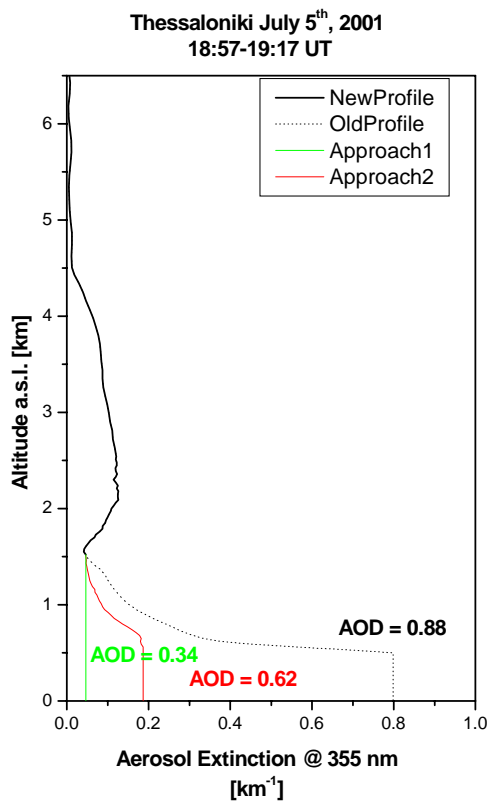


Figure A2-1: example of extinction profile and AOD calculation with the 2 described approaches. The case of July 5th 2001 is reported. The old profile (used for the previous report) where the altitude of complete overlap was underestimated is reported as dotted line. The new profile extending down to 1500 m is reported as solid black line. The red and green lines report the portion of extinction profile extended down to the ground with respectively the approach 1 and 2. Note that old and new profiles are coincident above 1500 m.

Figure A2-1 reports an example of the problem occurred with Thessaloniki data in the previous report. The wrong assumption on overlap function resulted in a columnar AOD of 0.88 and very high extinction values close to the ground. Whereas it is taken into account that the complete overlap is reached at 1500 m a.s.l., both approaches reported above could be applied. The aerosol vertical distribution reported in the simultaneous backscatter profile shows that there is a free troposphere layer (dust case) from 1700 m up to about 7000 m, while below 1550 m the typical mixed+residual layer is present. Even if backscatter profile is not reported here, the vertical layering can be inspected through the extinction profile resulting by the application of approach 2 (red line in Figure A2-1). The approach 2 results in an AOD of 0.62, which is in a better agreement with corresponding MODIS value of 0.51 at 355 nm. An unphysical result is obtained if approach 1 is applied, with very low values of extinction close to the ground and a low AOD value (0.34) if compared to MODIS and other Saharan dust cases over Thessaloniki.

For stations equipped with Sun-photometers, a comparison with closest in time AOD data is performed as an a-posteriori check. For the case under investigation (Thessaloniki data after July 2001) a good agreement with the AERONET data has been observed. The difference between EARLINET and daily mean AERONET AOD for the station of Thessaloniki is on average 8% with a median value of 4%. This result is similar to what obtained with other co-located EARLINET /AERONET stations characterized by lower overlap functions (Mona et al., 2010b). The residual differences are ascribed to the comparison of diurnal (AERONET) versus nocturnal (EARLINET) AOD values and AOD diurnal variability (Mona et al., 2010b).

19 Appendix 3: Comparison of Multi-TASTE and VALID validation strategies

As first steps towards harmonization of validation protocols, validation approaches used by the VALID and Multi-TASTE teams have been compared on MIPAS v5.05 ozone profiles. There can be several sources of differences between the two teams' approaches:

1. data selection criteria based on data validity (flags, manual check for unphysical values, etc.)
2. data selection based on data grouping (e.g. different latitude ranges used to define mid-latitudes)
3. maximum reported error allowed in the data
4. comparison attributes (altitude ranges used and selection criteria for the validation instruments)
5. maximum difference in time and space between two correlative measurements
6. metadata (e.g. original filenames that will allow identification of the correct profile and data version, site coordinates, usage of begin/mid/end of measurement properties, e.g. associated location and time)

Given that the metadata tracking is currently not implemented in the Multi-TASTE project, we have attempted to identify the collocated pairs used in VALID from the reported time, name of validation site and distance to station in the Multi-TASTE list of collocations. This did not result in unique identified pairs (issue 6 in the list above) and additional information is required. Additional feedback from the Multi-TASTE team is required with respect to issues 2 and 4. Nevertheless, a reconciliation of the used grouping criteria has been discussed and not much difference is foreseen to originate from issue 4 except extended altitude coverages. Issue 1 will not be considered in this section.

The analysis in this section will be carried out focussing on issues 3 and 5. This analysis will be called TASTE-sim.

The following criteria were originally used for the validation of the MIPAS v5.05 ozone profiles:

Parameter	VALID	Multi-TASTE
Maximum time diff.	20 hours	6 hours
Maximum distance diff.	800 km	500 km
Maximum allowed error	30%	~300%
Used altitude axis	Engineering/corrected altitude grid	Pressure grid
Used quantity	Molecules/m ³	ppmv

As VALID focuses on the validation using lidar data which are reported on an altitude grid and in number density, we have not used the pressure grid/volume mixing ratios and will report the results on the corrected altitude grid. The maximum error for the ground-based systems is kept at 30%, whereas the error in MIPAS is allowed to reach 300%. The collocation criteria are taken from Multi-TASTE. Contrarily to the Multi-TASTE approach, all lidar data are cut off at 45 km even if data are reported at higher altitudes. This does not affect the results here as we will only compare the results below 45 km.

The presented results are in both cases (original VALID and the TASTE-sim) without application of the MIPAS averaging kernels.

The first study evaluates the effect of using 30 or 300% for the maximum allowed error in the MIPAS data. Only 25 out of nearly 13000 collocations were removed when using the filtering of 30% in contrast to 300%. Thus, the validation result differences were negligible, which is shown in Figure A3- 1. In this case, the maximum collocation differences of 800 km and 20 hours were used.

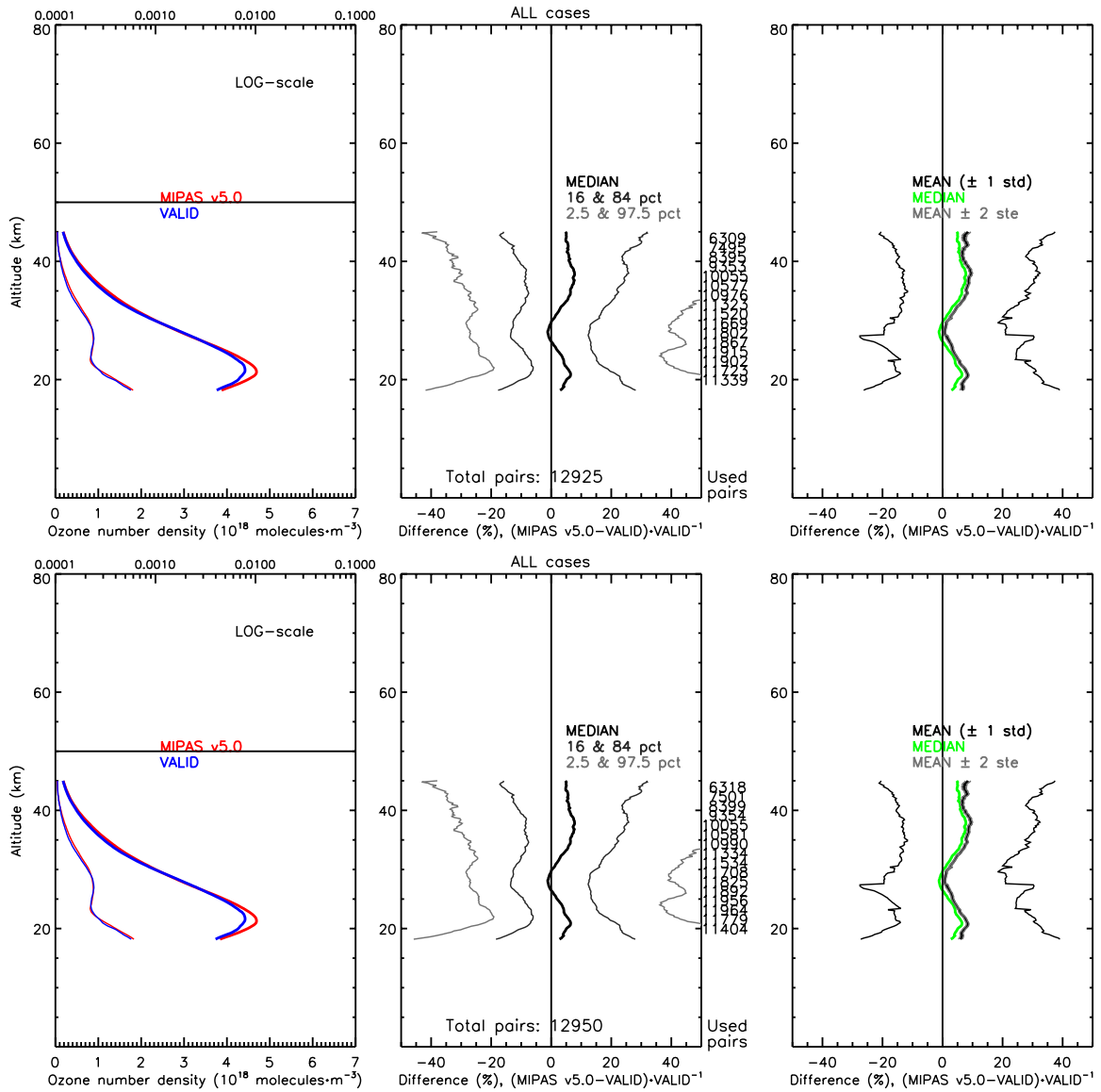


Figure A3- 1: Validation results for MIPAS v5.05 ozone profiles compared to lidar measurements using a maximum difference between collocations of 20 hours and 800 km and a maximum MIPAS error of 30% (top) and 300% (bottom).

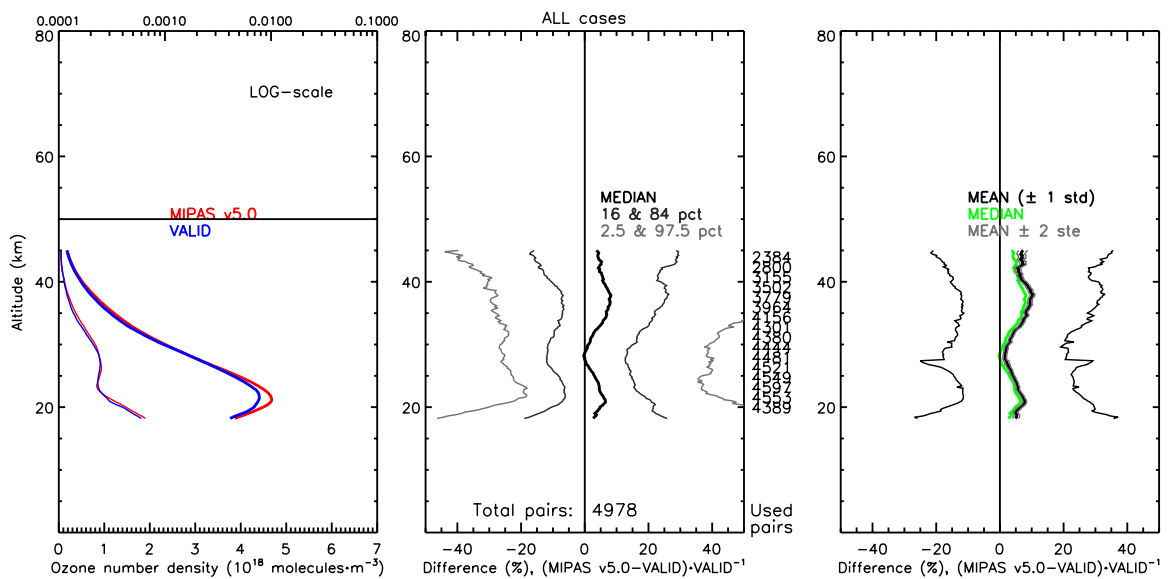


Figure A3- 2: As figure above, but with for collocations with a maximum difference of 6 hours and 500 km

The second study investigates the impact of temporal and spatial distance of the collocations (Figure A3- 2).

When comparing the full datasets for the two cases (800 km and 20 hours versus 500 km and 6 hours; both with a maximum error of 30%), the differences are in the order of 1 or 2 percent at most, but less than 40% of the original VALID dataset remains in the TASTE-sim (500 km and 6 hours).

When further narrowing down a selection, the effects can become out larger. For instance, when focussing at the tropics, which exhibit the most pronounced influence of time and space distances between these two cases, the validation differences below 30 km reach up to 2.5% (at 28 km). At the bottom of the profile (18 km), differences can be even larger, but these are not significant because of the concurrent increase in standard deviations and standard errors. The reduction in the number of collocated pairs is nearly a factor 3.

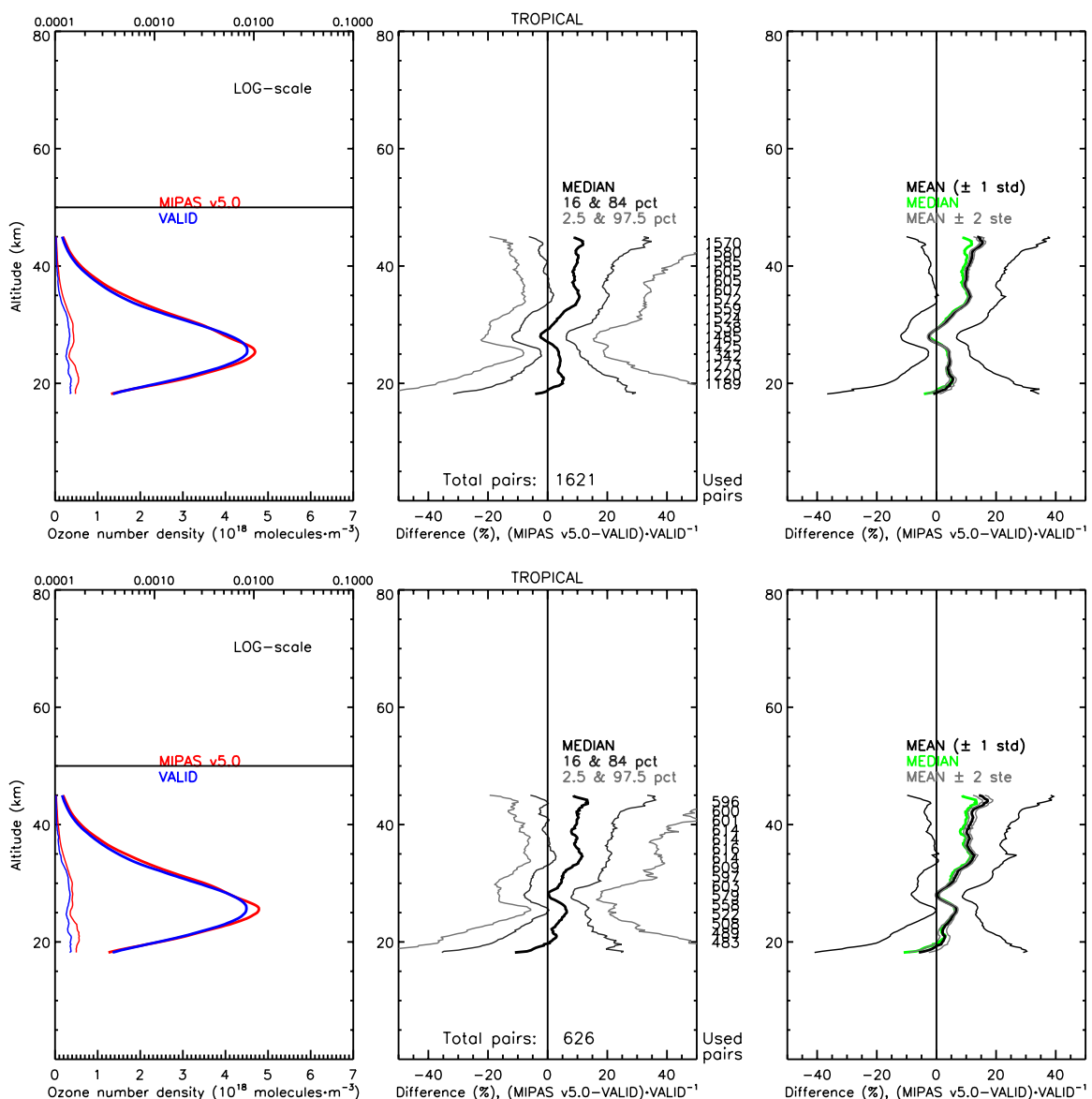


Figure A3- 3: Validation results for the tropics. Top: results using a maximum difference of 20 hours and 800 km; bottom: results using a maximum difference of 6 hours and 500 km.

Concluding, the differences in the validation results of MIPAS v5.05 ozone profiles due to the data error and spatial and temporal collocation criteria used by the VALID and Multi-TASTE teams are mostly in the order of 0 to 1-2 percent. The stricter data screening criteria cause a

reduction in the number of collocated data pairs which in turn can influence the validation results because of the decreased statistical significance acquired with smaller numbers of collocations and for instance, an increasing prevalence of specific sites (introducing e.g. a location or time bias as a large part of the data may originate from just a single location). In the case of MIPAS v5.05 ozone profiles, the effect of allowing a different maximum error was negligible, but this may not be the case for other datasets (e.g. GOMOS v5 ozone or temperature profiles).

20 Appendix 4: Validation of GOMOS high resolution temperature profiles using sonde and lidar measurements

In this appendix we provide more details to the validation results summarised in chapter 7 on the comparison of GOMOS high resolution temperature (HRTP) profiles with ground-based/balloon borne measurements.

Methodology

GOMOS HRTP have been compared with balloon sonde and lidar temperature profiles. The dataset corresponds to the data used for the analysis of the ozone profiles that was published in ACP (van Gijssels et al., 2010b) which is version 5.00 and currently the operational processor. Collocated data are required to be within 300 km and 5 hours of each other.

The associated errors in the GOMOS temperature profiles are an uncertainty estimate which are derived for each altitude of each retrieved profile. According to the disclaimer of the HRTP product, the errors provided in the GOMOS product are “largely overestimated” (see page 12 of http://envisat.esa.int/handbooks/availability/disclaimers/GOM_NL_2P_Disclaimers.pdf). If we for instance use the absolute error for GOMOS instead of the relative error, no collocating data are found that fulfil the requirement of a maximum error of 1K. Therefore we use here the relative error (error in percentage) for the HRTP. This is an arbitrary choice; we could also have used a large absolute error. Given an average temperature of 220K, 1% error in the HRTP would be equivalent to an error in K of 2.2 times larger (1% = 2.2K). The maximum allowed error for both the validation and the GOMOS datasets was varied between 1K(%), 3K(%) and 5K(%). Note that for the sonde data, no error is specified.

All GOMOS HRTP had to be taken with a solar zenith angle larger than 107°. We also compared analyses with and without considering the dark limb flag as provided in the product. Note that the profiles that are flagged dark in the ESA product are referred to as ‘Edark’ whereas those where only the solar zenith angle is larger than 107° are referred to as ‘dark’ in the figures.

Profiles are only considered if they result in useful data over at least 3 km. Data are splined to a common altitude grid of 50 m ranging between a minimum altitude of 10 and maximum of 40 km.

Effect of error

GOMOS HRTP are provided with an individual error estimate for each retrieval altitude and each measurement. If we compare the difference when only varying the maximum error in the validation dataset, we see this has a greater effect with increasing altitude. The number of collocations is naturally reduced when the error is more restricted, but it mainly affects the data between 29 and 35 km. At 35 km, allowing a maximum error for GOMOS of 5%, the median difference between GOMOS and the ground-based differs at most with 1K comparing with the validation data having an error of 5K or 1K (Figure A4- 1). At other altitudes differences are smaller. A similar effect is seen for limiting the maximum error of the validation data from 3K to 1K with a maximum error in the GOMOS data of 3% (not shown).

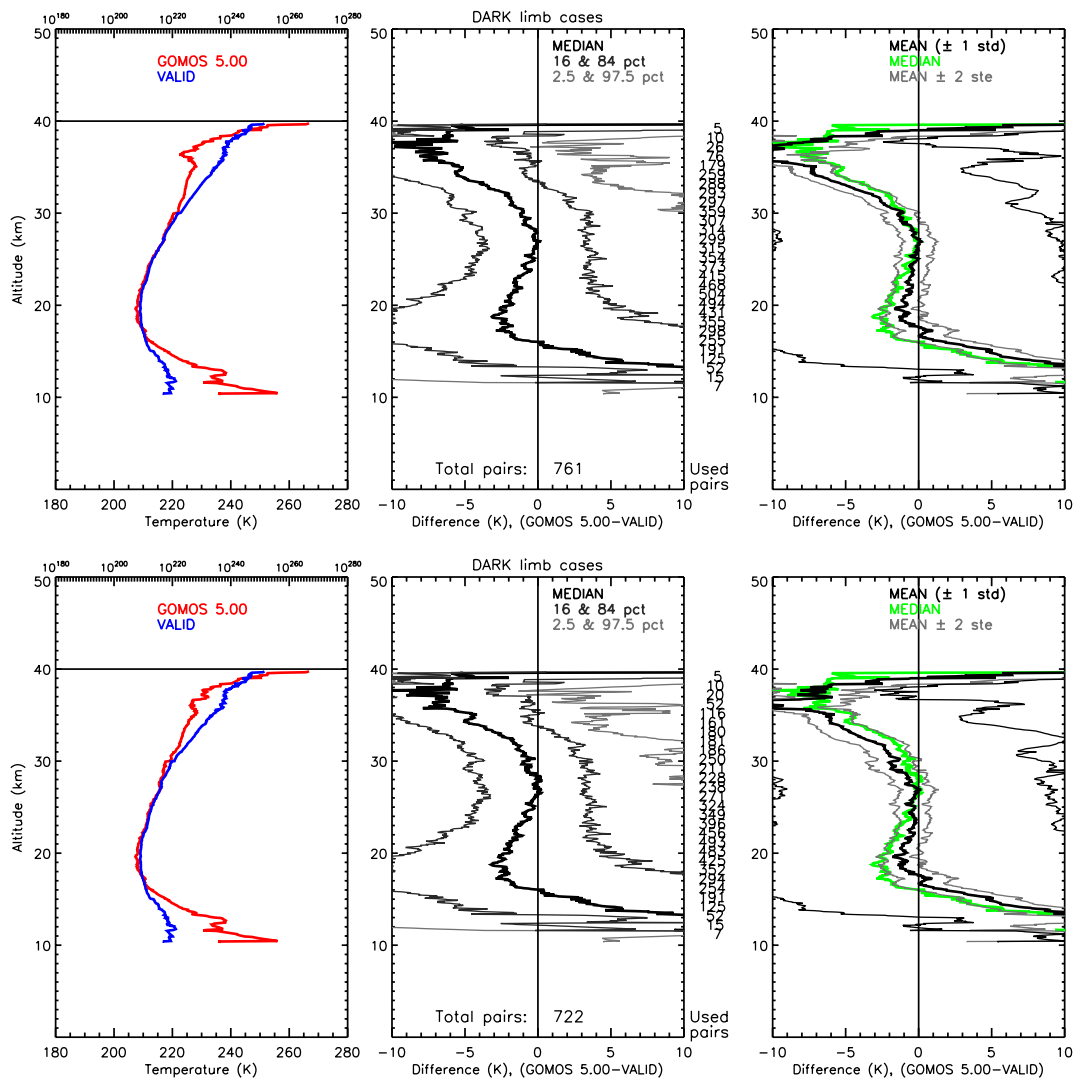


Figure A4- 1: Difference between a maximum error of 5K (top) and 1K (bottom) for the validation data. GOMOS data have a maximum error of 5K. Left panels show the mean temperature profiles for GOMOS (red) and the validation data (blue) as a function of altitude. The middle panel shows the difference in degrees Kelvin between GOMOS and the validation data as 2.5, 16, 50, 85 and 97.5 % quantiles (from left to right). Next to the right axis we display the number of collocated pairs for each altitude with the total number of pairs used at the bottom. The right panel shows the median difference in green, the mean difference in black together with the mean ± 1 standard deviation (thin black lines) and the mean ± 2 standard errors (thin grey lines).

Effect of applying dark limb flag

When limiting both datasets to a maximum error of 1K/1%, a total of 283 collocations are available with a solar zenith angle larger than 107° whereas those flagged dark result in 57 collocations (Figure A4- 2). For a maximum error of 3K/3% this is 627 versus 108 (flagged) and for 5K/5% this is 761 versus 144 (flagged), see Figure A4- 3.

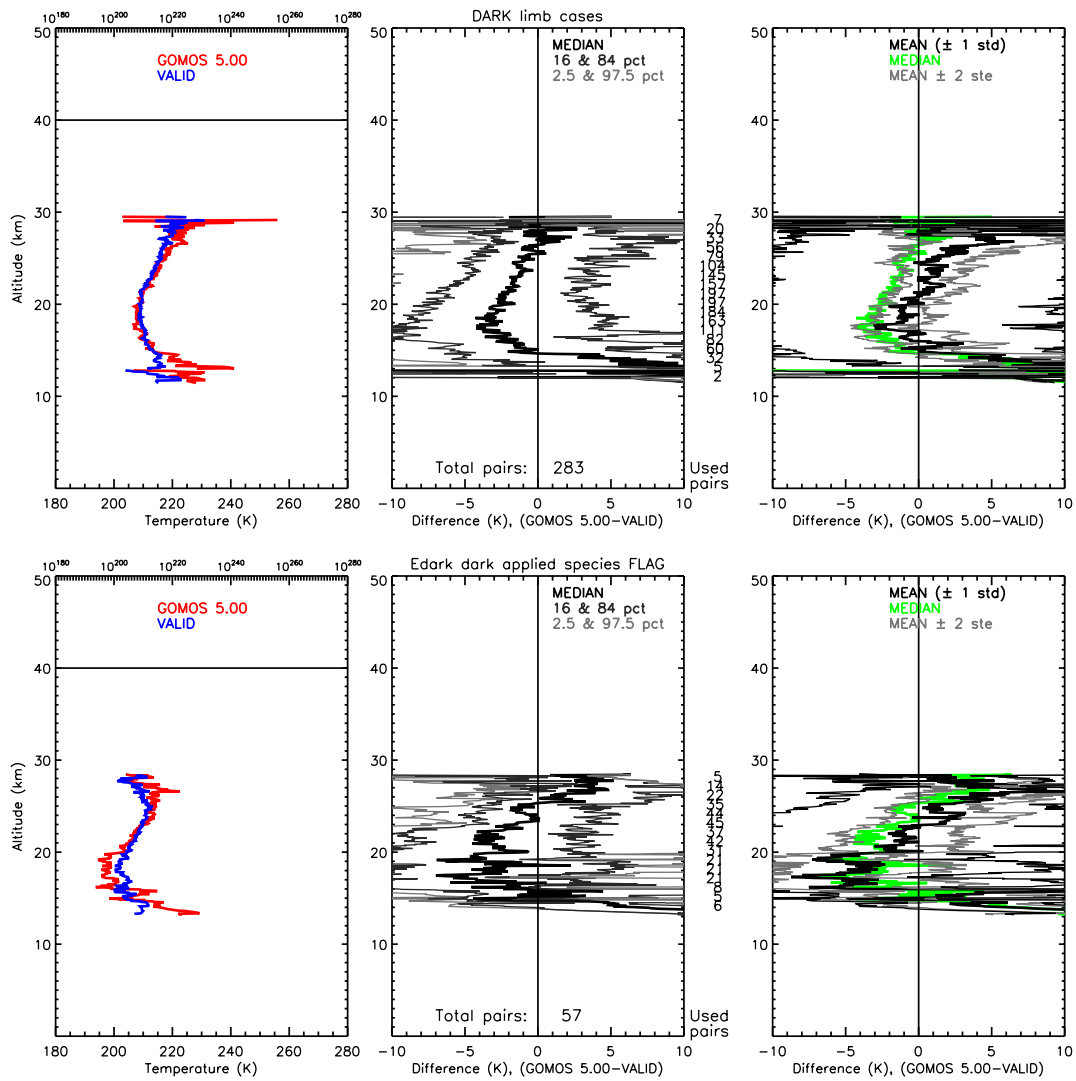


Figure A4- 2: Filtering dark limb observations based on solar zenith angle $> 107^\circ$ (top) or on the flag (flag = 0, bottom panel) for data with a maximum error of 1K (validation data) and 1% (GOMOS data).

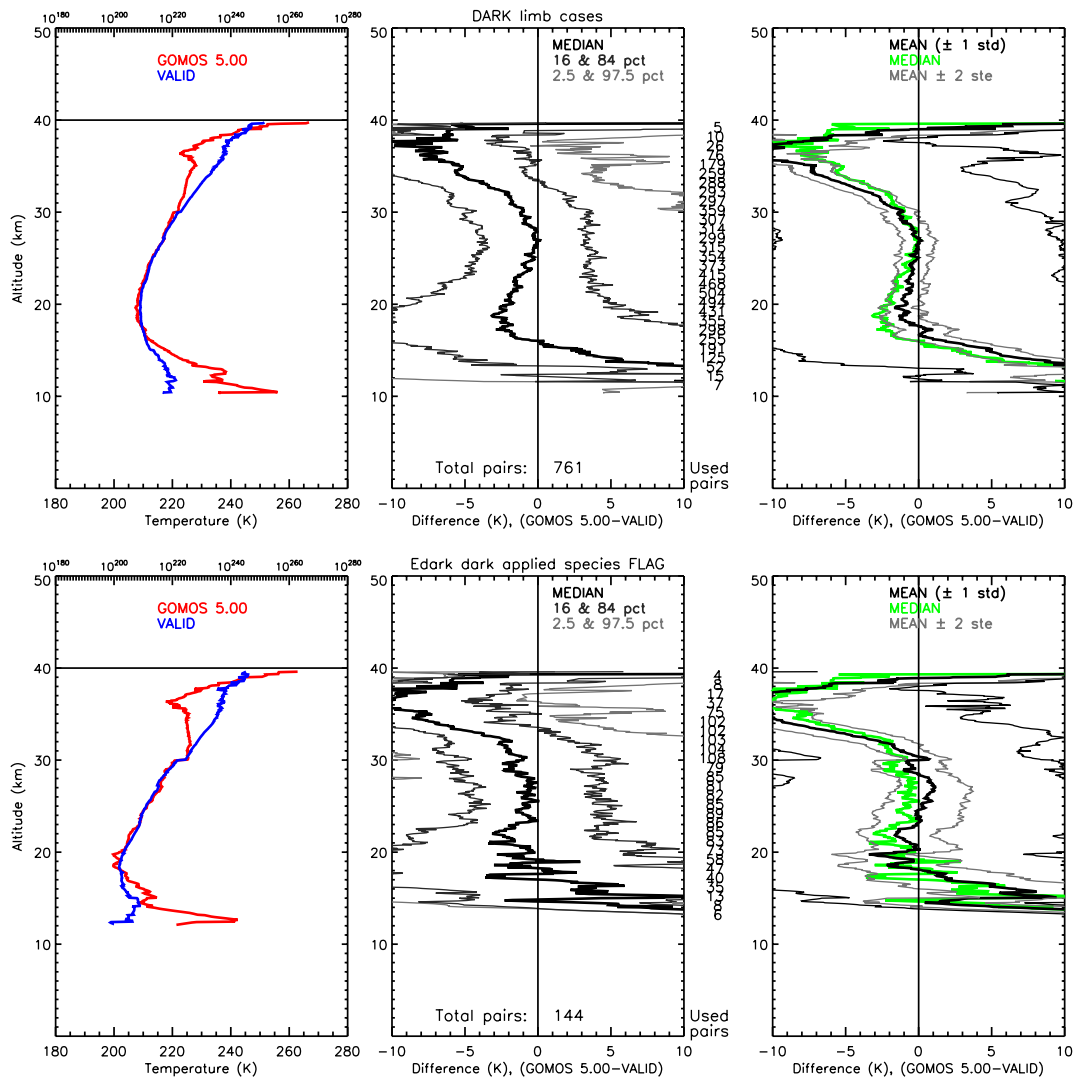


Figure A4- 3: Like Figure A4- 2 except data have a maximum error of 5K/5%.

Although the number of collocated cases is rather low for the ‘Edark’ cases, the shape of the differences is similar and the curves do not significantly deviate. Therefore we will use all data with a solar zenith angle larger than 107° . As the next largest reduction in the data is made by the error limit set for the GOMOS data and it is known that these values are overestimated, we will continue with a maximum estimated error of 5% ($\sim 11\text{K}$) for the HRTP data and a maximum error for the validation data of 1K.

Star characteristics

Most collocations are found with weak stars and only very few with strong stars (Figure A4- 4 and Figure A4- 5). These numbers are too low to state anything about possible differences.

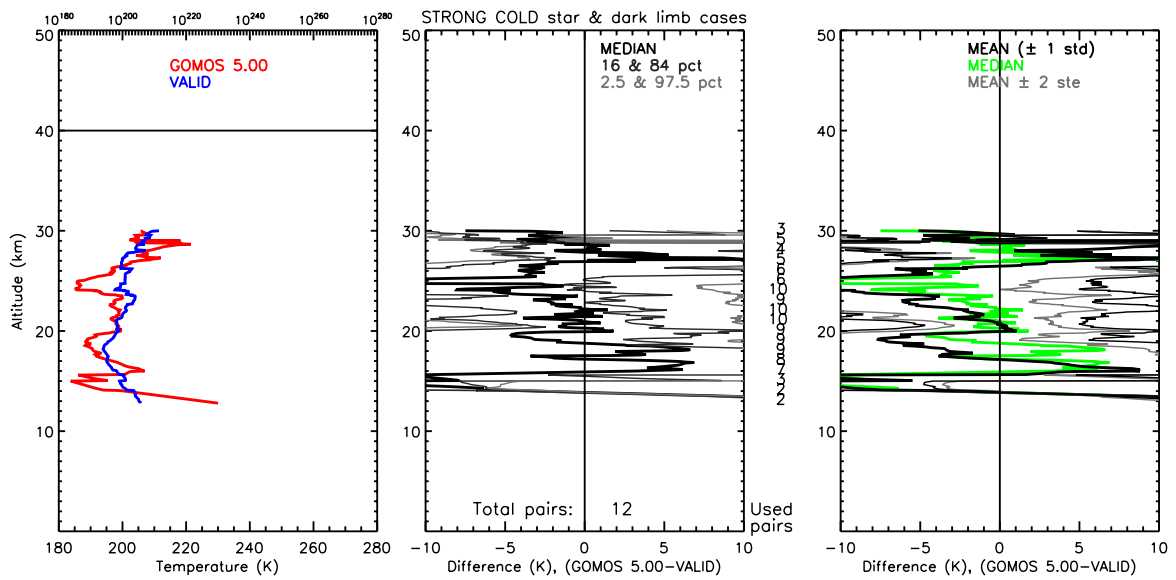


Figure A4- 4: All collocations with strong cold stars for a maximum error of 5% for GOMOS and 1K for the validation data.

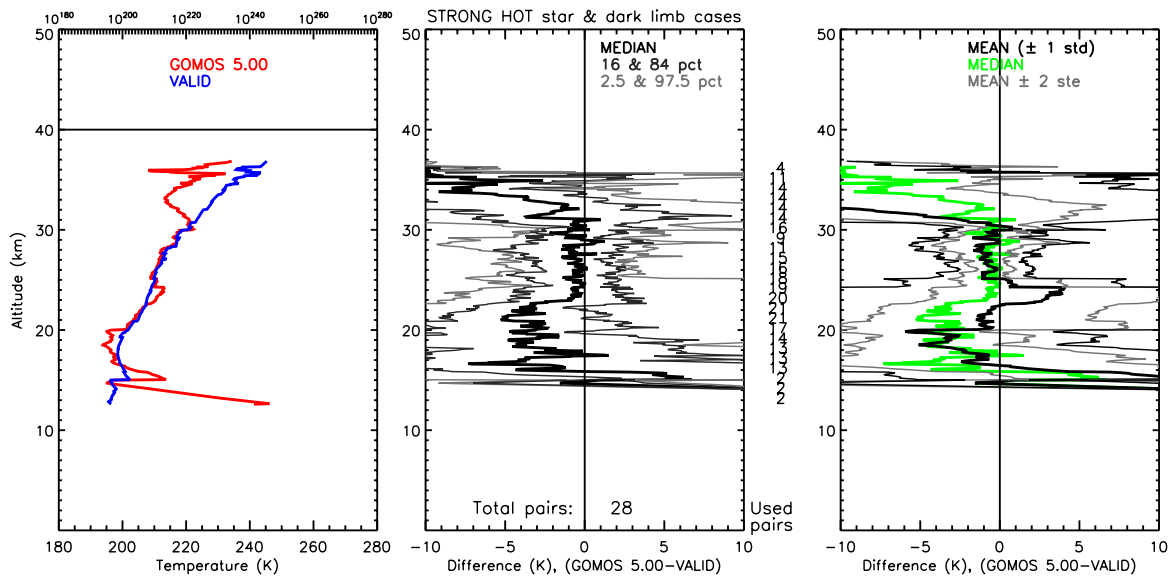


Figure A4- 5: All collocations with strong hot stars for a maximum error of 5% for GOMOS and 1K for the validation data.

Most notable is the difference between the cold and hot weak stars (Figure A4- 6 and Figure A4- 7). Whereas the weak cold stars slowly drift from a underestimation of about 2 degrees at 20 km towards an overestimation of 1.5K at 29 km, the difference in temperature for the weak hot stars ranges between -3K and -2 K at these altitudes.

In all cases, the deviation becomes very large towards the top of the profile.

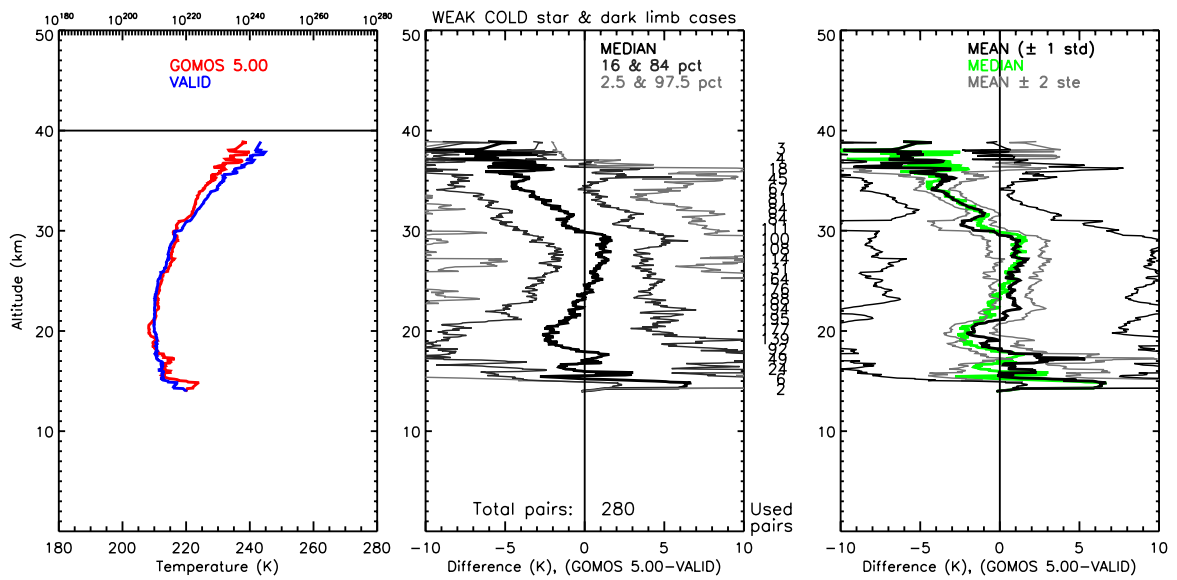


Figure A4- 6: All collocations with weak cold stars for a maximum error of 5% for GOMOS and 1K for the validation data. Same as Figure 7-4.

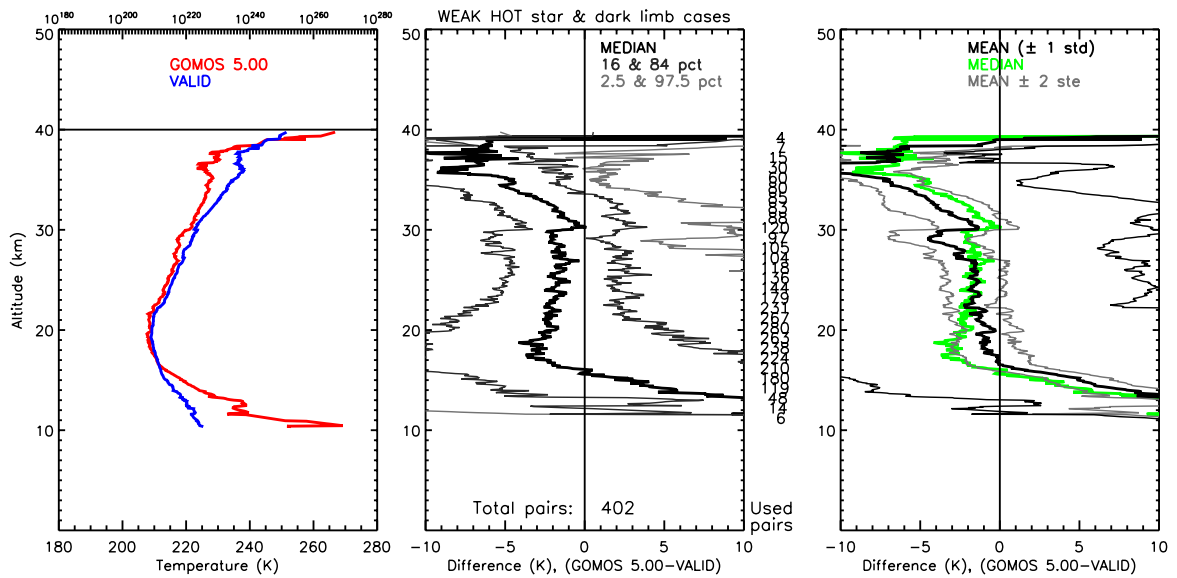


Figure A4- 7: All collocations with weak hot stars for a maximum error of 5% for GOMOS and 1K for the validation data. Same as Figure 7-5.

Latitude

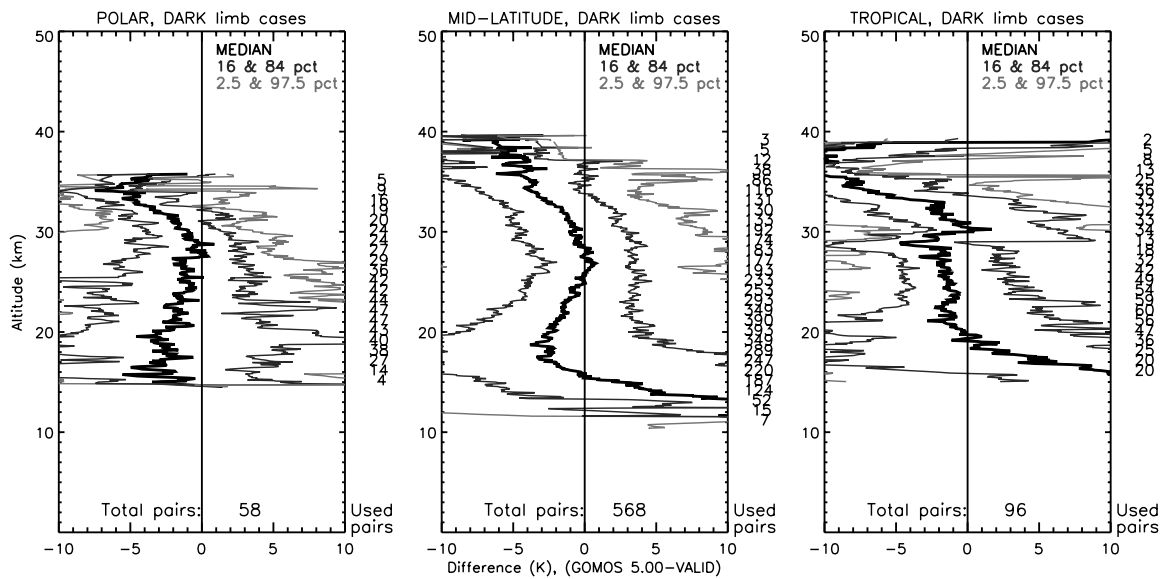


Figure A4- 8: Validation results for the polar regions (left), mid-latitudes (middle) and tropics (left). Panels are as the middle panel of the previous figures. Same as Figure 7-6.

For the polar regions, we see a negative bias with a maximum deviation of around -4K that is decreasing to zero around 28 km and then increases again (Figure A4- 8 left panel). The number of collocations is rather low.

In the mid-latitudes we find most collocations. The shape of the differences is similar to the polar region although the profiles extend further up- and downwards. At the lowest altitudes (below 18 km) the GOMOS HRTP are presenting increasingly higher temperatures than the validation data when descending – becoming positively biased below 16 km (Figure A4- 8 middle panel).

This warm bias is also seen in the tropics, where it occurs from around 19 km downwards (positive trending starts from ~21 km downwards). Contrarily to the polar and mid-latitude regions, in the tropics we see a small increase in the bias with altitude from 21 km upwards towards 29 km (Figure A4- 8 right panel). At that altitude there is a reduction of the number of collocations with is related to the selection of the allowed error for the validation data. Data are from the Paramaribo sonde (very few collocations, reaching up to 30 km), the Mauna Loa lidar (most data below 30 km) and the La Reunion lidar (starting at 30 km and presenting the largest part of the validation data for those altitudes). The number of high outliers with respect to the validation data increases (84th percentile further away from the 50th percentile than the 16th percentile).

Distance and time

When restricting the collocations criteria from 300 km and 5 hours to a maximum difference of 100 km and 1 hour we see a sharp reduction in the number of collocations (~factor 5 from 300 km & 5 h to 200 km & 3 h to nearly 1% at 100 km & 1 h). Too few collocations are thus available for the selection with 100 km and 1 hour, but the shape of median is very similar for the 200 km & 3 hours and the 300 km & 5 hours selection (Figure A4- 9).

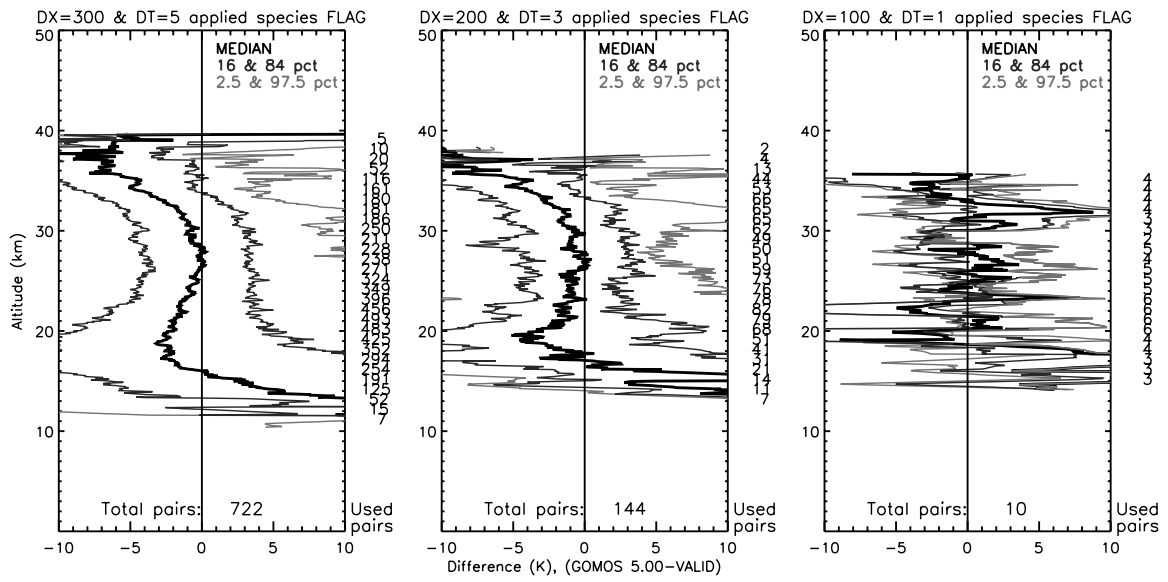


Figure A4- 9. Effect of restricting the collocation criteria from 300 km and 5 hours (left panel) to 200 km and 3 hours (middle panel) and 100 km and 1 hour (right panel).